The Chemical and Physical

Properties of Tourmaline

A Thesis presented for the Research Degree

of

DOCTOR OF PHILOSOPHY

of the

COUNCIL FOR NATIONAL ACADEMIC AWARDS

London

by

ERIC HENDERSON

Department of Chemistry,

Plymouth Polytechnic,

Plymouth,

Devon.

March 1971

ACKNOWLEDGEMENTS

The author wishes to thank:-

Dr. A. B. Meggy for the suggestion of the topic and for permission to work in these laboratories.

Mr. P. Roberts for supplying one of the tourmalines used.

Miss Margaret Sheppard for some valuable technical assistance.

The College Governors for the award of a research assistantship.

Summary.

The decomposition temperature of schorl was found to be 880 ± 10°C using X-ray and optical methods. The main crystalline product in decomposed schorl and dravite was found to be a boron containing mullite, the composition of this phase was found to become closer to that of mullite ($3Al_2O_3.2SiO_2$) as the decomposition temperature was increased. The size of these possibly slightly orientated needle shaped micro-crystals was approximately 25 ± 10μ by 3 ± 2μ by 3 ±2μ. The main decompostion products obtained in reducing conditions, in addition to the boron containing mullite, were hercynite ($FeO.Al_2O_3$) at low temperatures and α– iron at higher temperatures. The decomposition temperature of schorl in the presence of activated charcoal was found to be at least 60°C lower than that for air decomposed schorl. This decrease was thought to be associated with the formation of hercynite by a low temperature reaction between schorl and activated charcoal.

The boric oxide and iron oxide in air decomposed schorl were both extracted by dilute acid. The rate of extraction was found to increase as the original schorl decomposition temperature was increased. The activation energy for the extraction of boric oxide as a function of the schorl decomposition temperature was found to be equal to 19.2 ± 0.4 kcal/mole. This increase in the rate of extraction of boric oxide was suggested to be associated with the separation and growth of micro-regions of a boron rich phase within the silica-iron oxide amorphous matrix. The activation energy for the extraction of boric oxide as a function of the leaching temperature was found to be equal to 7.99 ± 0.19 kcal/mole, whilst the activation energy for the extraction of iron oxide from air decomposed schorl was found to be equal to 7.13 ± 1.06 kcal/mole. The similarity between these values and that of 6.8 kcal/mole for the activation energy of acid leaching of phase-separated borosilicate glass (138), was thought to provide further indirect evidence for the suggestion that the amorphous phase in decomposed schorl contains phase separated micro-regions. The rate of extraction of both boric oxide and iron from schorl decomposed in reducing conditions was found to be considerably faster than from air decomposed schorl. This increased extractability was thought to be connected with the presence of micro-crystals of iron in the decomposed reduced schorl.

The boric oxide present in both schorl and dravite was found to be extractable if water vapour was passed over the decomposed minerals at temperatures above 1000°C. The activation energy for the extraction of boric oxide by pyrohydrolysis from decomposed schorl was found to be equal to 85 ± 8 kcal/mole, whilst the activation energy for the extraction of boric oxide by pyrohydrolysis from both decomposed dravite and "pyrex" glass was found to be equal to 22 ±1 kcal/mole. The higher value was thought to be due to the incorporation of Fe^{2+} ions into the amorphous silica lattice in decomposed schorl. This process was suggested to lead to an increase in the energy barrier towards the diffusion of water vapour through the silica-iron oxide amorphous matrix to the boron rich reaction surface.

ACKNOWLEDGEMENTS

SUMMARY

CONTENTS

INTRODUCTION

CHAPTER I

Applied Boron Chemistry.

A large portion of this thesis will be concerned with the boron content in tourmaline. It was therefore thought useful to describe the chemistry of boron with special reference to its occurrence and extraction.

(1) Occurrence of Boron in nature.

Boron occurs as a trace element in most soils (1) and it is an essential constituent in a number of silicate minerals (2). It is present in sea water to the extent of about 4.6 parts per million (3) and is estimated to constitute approximately 0.001% of the earth's crust (4). Large deposits of commercially valuable boron minerals are found in only a few localities and these are primarily in areas of former intense volcanic activity.

(2) Geochemistry of Boron minerals.

The brief account given below of the formation of boron minerals was mainly taken from books edited by Samsonov (5) and by Adams (6).

Due to the overall low concentration of boron in the fused magma only a very small proportion would be precipitated during the early stages of the magma cooling. The major proportion is probably concentrated in the residual fusions, from which it can be crystallised as tourmaline in the pegmatites. However, a considerable quantity of boron still remains in solution and is only crystallised during the later hydrothermal cooling when tourmaline, axinite and datolite are formed. The remainder gives rise to the boron containing hot springs.

Most of the deposits of commercial interest may be traced back to former hot springs. These mineral containing waters are normally lost in the sea. However, in certain localities this removal may not occur due to the topography and the arid nature of the area. This situation occurred on a large scale during periods of intensive volcanic activity in Tertiary and Quaternary times.

The boron mineral deposited in greatest quantity was probably the double salt ulexite ($NaCaB_5O_9 8H_2O$) (7). However, in a few localities where the waters also contained appreciable amounts of carbonate ions, and were hence lacking in a sufficient calcium ion concentration to form ulexite, only sodium borate (borax) was formed on subsequent evaporation, as at Searles Lake (8) in California.

Some of the primary ulexite deposits were elevated during later geologic ages and were thus exposed to the weathering and leaching action of surface waters. This gradually removed much of the sodium borate (10) leaving a residue of the less soluble calcium borate mineral, colemanite ($Ca_2B_6O_{11} \cdot 5H_2O$). However, in a few localities it would seem that the resulting sodium borate leachings were caught, in turn, in other surface depressions to form secondary deposits of borax, which are relatively free of all other soluble substances.

In some instances, this secondary borax may have accumulated, layer upon layer, to considerable depths on shallow lake bottoms before ultimately being buried by alluvial material from surrounding elevations. It has been suggested that the Kramer deposits in California have been formed by this process (7), however other theories have been advanced by Gale (11).

(3) Boron Minerals.

At the present time about one hundred boron containing minerals are known. From the chemical point of view the principal boron minerals are salts of ortho- and meta- boric acid, the iso- and heteropolyacids, borosilicic and aluminoborosilicic acid, see Table 1.

The sodium borates kernite and borax have by far the greatest industrial significance. Other borate ores of industrial importance include colemanite, boracite, ludwigite and kotoite.

(4) Boron raw materials and their processing.

(4.1) Principal Sources in Western World.

The main suppliers of the western worlds boron requirements are the United States (6), Turkey (12) and Argentina (13). The major portion of the United States output is supplied from the following two sources in the Mojave Desert, California.

(4.1.1) Kramer deposits.

This sodium borate deposit is about one mile wide by four miles long, with an ore body varying from eighty to over one hundred and fifty feet in thickness (11). The ore body contains borax and kernite contaminated with clay shales and is covered by gravel beds, etc. In an area about twice as large as the borate beds colemanite and ulexite are found.

The borate deposits were worked by underground methods, but recently open pit mining has been developed (14,18). The shale content of these ores is a clay like material which tends to soften, swell and become peptised in contact with fresh water. These colloidal suspensions are difficult to settle or even to filter. In a typical crystallisation process the crushed ore is leached with heated mother liquor from a previous cycle without serious dispersal of the clay. The resulting hot concentrated borax solution may then be settled free of most of the insoluble residue and clarified by pressure filtration prior to cooling for the crystallisation of a crop of refined borax.

(4.1.2.) Searles lake deposits.

This deposit covers an area of between thirty and forty square miles and extends to a depth of fifty to one hundred and fifty feet (6). Many of the layers in the deposit are quite porous, the interstices being filled with a saturated brine, containing borax, halite (KCl), trona ($Na_2CO_3 \cdot NaHCO_3 \cdot 2H_2O$) and sodium sulphate.

This brine is pumped from wells drilled into the lake bed. The extraction of borax from this solution has proved a difficult problem; however, a process has been worked out involving the Carbonation of the brine for the recovery of both borax and soda ash without evaporation (15). This process has been in operation from the nineteen twenties until recently when a process based on "Solvent Extraction" was evolved (16,17).

(4.2.) Deposits in the U.S.S.R.

The largest deposits in the Inder lake regions of Kazakhstan contain ascharite, hydroboracite, colemanite and ulexite, whilst the smaller deposits in the Caucasus contain datolite (5).

Both types of ores are decomposed using hot sulphuric acid, the boric acid extracted is then fractionally

TABLE 1

Some Boron Minerals (5,6).

Name of Mineral	Chemical Formula	Occurrence
	(1) Fluoroborates	
Ferrucite	$NaBF_4$	Mt. Vesuvius
	(2) Boric acid	
Sassolite	H_3BO_3	Tuscany, California
	(3) Salts of Boric Acid and Isopolyboric acids	
Kotoite	$Ng_3(BO_3)_2$	Korea, Hungary
Ludwigite	$(MgFe^{2+})Fe^{3+}(BO_3)_2$	Hungary
Kernite	$Na_2B_40_74H_20$	California
Borax	$Na_2B_40_710OH_20$	Tibet, S. America
Ulexite	$NaCaB_5O_9.8H_2O$	California, S. America
Colemanite	$Ca_2B_6O_{11}.5H_2O$	Asia Minor, California
	(4) Double Salts of Boric & Polyboric acids	
Boracite	$Mg_5B_{14}O_{26}.MgCl_2$	Germany
Sulphoborite	$Mg_6H_4(BO_3)_4(SO_4)_2.7H_2O$	Germany
	(5) Salts of Complex Heteropolyboric acids	
Datolite	$2CaO.B_2O_3.2SiO_2.H_2O$	U.S.S.R.
Axinite	$HCa_2(Fe.Mn)A1_2BSi_4O_{16}$	U.S.S.R.
Tourmaline	$Na(Fe.Mn.Mg)_3A1_6B_3Si_6O_{27}(OH)_4$	Widespread
	(6) Borates with Complex Compositions	
Bulsite	$(Fe.Mg)_{12}FeSnB_6O_{27}(OH)_4$	
Melanocerite	$Na_4Ca_{16}(U.La)_3Zr_6B_3Si_2O_{57}F_{12}$	

crystallised after removing the insoluble material (19).

(4.3) Extraction of boron from Ludwigite and Tourmaline.

(4.3.1.) Ludwigite.

This mineral is an iron magnesium borate $(MgFe^{2+})_2Fe^{3+}BO_5$ and is found in Hungary and Rumania amongst many other localities.

Attempts have been made by Banateanu et. al. (20) to extract the boron content from this mineral. Because of the high magnesium content acid leaching was not attempted. The most successful technique discovered was the calcination of the mineral at 800^0C in the presence of sodium carbonate, followed by hot water leaching of the sodium borate formed during the calcination process. Under optimum conditions 99% was extractable when the calcination was carried out in a reducing atmosphere, whilst 95% was extracted when reacted in an oxidising atmosphere and only 88-90% when in a static nitrogen atmosphere.

(4.3.2) Tourmaline.

Apparently the main attempts to extract boron from tourmaline were made by the Japanese during the nineteen forties (21,22,23,24).

For example,Kamiko (22) calcined a mixture of tourmaline and sodium carbonate at $780\text{-}850^0$ C for 30 minutes. The sodium borate formed was extracted using hot water. The borate solution formed was then neutralised by bubbling in carbon dioxide. The first crop of borax was obtained on cooling this solution and the remainder by fractional crystallisation. Under optimum conditions Kamiko (22) found that 95 per cent of the total boron could be extracted. Similar techniques have been used by other Japanese workers, some however, using an acid as the leaching agent (23, 24).

Recently Matsaberidze et. al. (25) have investigated the feasibility of extracting the boron present in tourmaline by acid leaching of the mineral that has been calcined, without the addition of a flux, at temperatures close to 1000^0C. Under optimum conditions it was found that 100% of the boron was extractable, if the mineral had been previously heated at 950^0C for 1 hour.

CHAPTER 2

Tourmaline.

(1) General Introduction.

Tourmaline is characteristically a mineral of granites, granite pegmatites, and pneumatolytic veins. It also occurs in some metasomatic and metamorphic rocks and as a detrital mineral in sediments. The name appears to be Cingalese in origin. The main compositional varieties of this mineral are the magnesium tourmalines or dravites, the iron tourmalines often known as schorls, and the alkali tourmalines or elbaites which are usually rich in lithium.

(2) Composition of various Tourmalines.

The basic formula of tourmaline has until recently been uncertain. Penfield and Foote (26) proposed the formula $H_9Al_3(B(OH))_2Si_4O_{19}$ with the hydrogen replaceable by metal ions, whilst other formulae have been proposed by Kunitz (27) and by Machatschki (28). A summary of the early views has been given by Ward (29).

Recently structural determinations by Donnay et. al. (30). and by Ito (31) make it reasonably certain that the formula is $NaR_3Al_6B_3Si_6O_{27}(OH)_4$. The sodium may be partially replaced by potassium, lithium or calcium. The unknown "R" can be iron, manganese, magnesium or aluminium plus lithium depending on the series. A summary of some analyses of various tourmalines is given in Table 2 (32).

TABLE 2

Composition of Some Tourmalines (32).

Oxide	Compositions of Some Tourmalines					
	Schorls		Dravites		Elbaites	
	% oxide	% oxide	% oxide	% oxide	% oxide	% oxide
	No.7	No. 3	No. 2	No.5	No. 1	No. 6
SiO_2	35.20	33.50	36.52	36.70	37.89	36.36
TiO_2	0.51	0.25	0.17	1.38	0.04	tr.
B_2O_3	8.82	8.31	10.32	9.50	10.28	10.30
Al_2O_3	28.49	31.80	33.41	30.97	43.85	40.48
Cr_2O_3	–	–	–	0.03	–	–
Fe_2O_3	0.79		–	1.73	–	–
FeO	11.55	13.80	0.30	2.94	0.11	3.64
MnO	0.07	3.75	0.57	–	0.11	1.05
MgO	5.63	2.00	11.25	8.83	–	0.09
CaO	2.75	0.45	0.42	1.63	0.07	0.67
Na_2O	2.12	2.65	2.34	2.49	2.43	2.20
K_2O	0.13	0.15	0.57	0.21	–	0.44
Li_2O	0.08	–	–	–	1.66	1.27
F^-	0.08	–	0.12	–	0.10	0.10
H_2O^+	3.52	3.30	3.76	3.49	3.47	3.64

Recently tourmalines have been found naturally that have unusual compositions. Mason et. al. (33) found a sample having a composition close to $NaFe_3^{3+}Al_6B_3Si_6O_{27}(OH,F)_4$ with the iron present in the ferric state instead of the usual ferrous. The cell dimensions were found to be unusual and observed to lie outside the usual solid solution series, see Figure 1. Several other properties, including the density and refractive index, were also found to be different from that usually obtained. Another unusual tourmaline has been described by Frondel. et. al. (34) having a formula intermediate between $NaMg_3Fe_6^{3+}B_3Si_6O_{27}(OH,F)_4$ and dravite $NaMg_3Al_6B_3Si_6O_{27}(OH.F)_4$. Tourmalines from several localities in the South West of England have been analysed by Power (35) with a view to elucidating the geochemical history of the mineral. It was found for example that "hydrothermal" tourmaline contains a higher Mg,Ca,Sr,Ni,Cr,V,Sc, and Sn content than tourmaline formed during the earlier cooling of the magma.

(3) Crystallography and Structure.

The unit cell dimensions were first determined by Kulaszewski (36) and Machatschki (28) and later confirmed by Buerger (37) who also established the space group as rhombohedral R3m.

The unit cell dimensions of the various forms of tourmaline have been determined by a number of investigators, a summary of their results is given in Table 3.

Epprecht (38) has determined the accurate cell dimensions of tourmalines of known composition and found that two series could be distinguished, one between elbaite and schorl and the other between schorl and dravite, see Figure 1.

TABLE 3

Cell Dimensions of Various Tourmalines.

	Variety of Tourmaline				
Cell Dimensions Å.	Dravites	Schorls	Elbaites	Uvite	Ref.
	$Na(MgFe)_3Al_6B_3Si_6O_{27}(OH,F)_4$	$Na(FeMn)_3Al_6B_3Si_6O_{27}(OH,F)_4$	$Na(LiAl)_3Al_6B_3Si_6O_{27}(OH,F)_4$	$CaMg_4Al_5B_3Si_6O_{27}(OH)_4$	
a	15.94-15.98	15.93-16.03	15.84-15.93	–	32
c	7.19-7.23	7.12-7.19	7.10-7.13	–	32
	Cell dimensions of tourmaline with "end member" composition				
	$NaMg_3Al_6B_3Si_6O_{27}(OH;F)_4$	$NaFe_3Al_6B_3Si_6O_{27}(OH,F)_4$	$NaLi_3Al_6B_3Si_6O_{27}(OH,F)_4$	$CaMg_4Al_5B_3Si_6O_{27}OH_4$	
a	15.942	16.032	15.842	15.83	38,43
c	7.223	7.142	7.009	7.19	38,43

FIGURE 1.

Tourmaline axial ratios and cell dimensions (after Epprecht (38)).

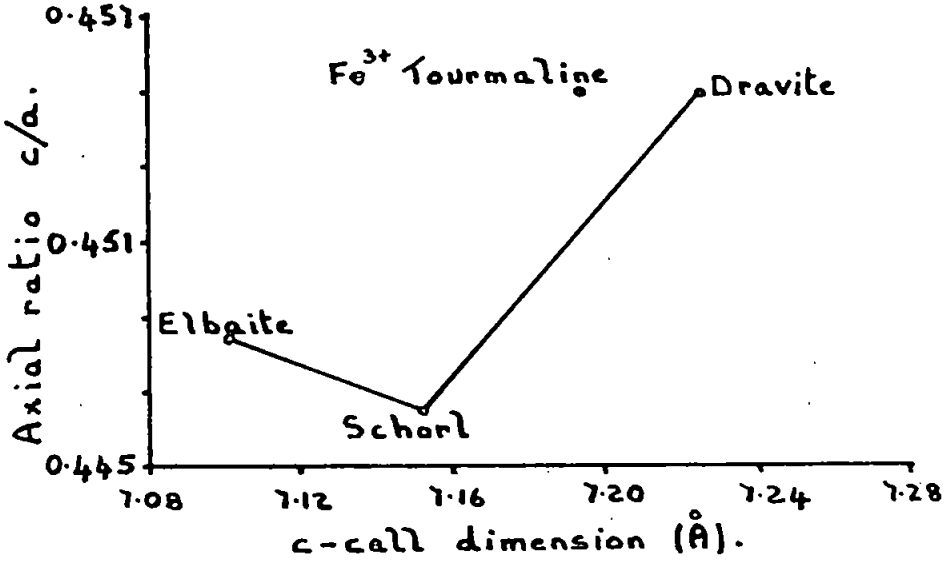

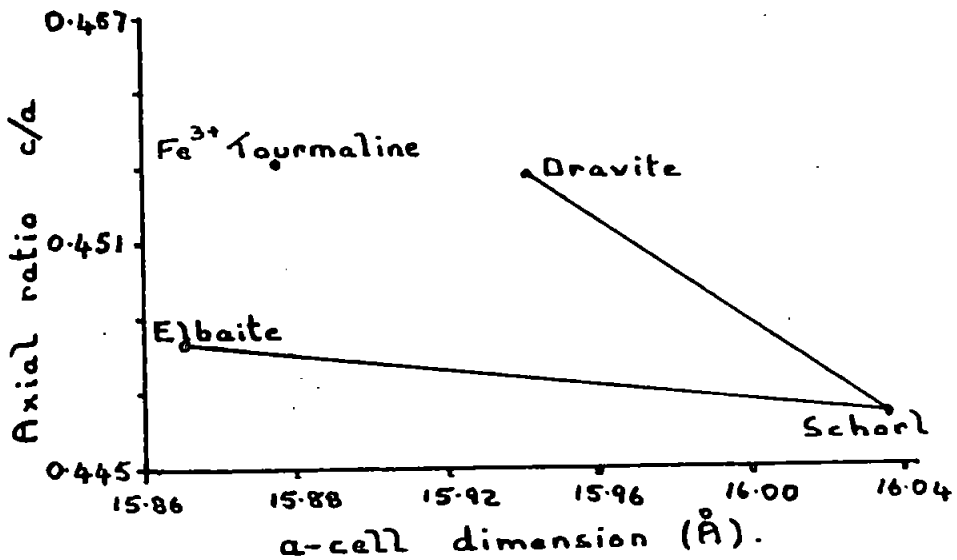

The crystal structure has been determined by three groups of workers.

Hamburger and Buerger (39) used an almost colourless magnesium tourmaline and an iron tourmaline, their proposed structure was latter refined by Donnay and Buerger (30) assuming the formula to be $NaR_3Al_6B_3Si_6O_{27}(OH)_4$. Belov and Belova (40,41) determined the structure of a dravite assuming the formula unit $NaR_9B_3Si_6(O.OH)_{30}$, whilst Ito and Satanaga (42,31) determined the structure of elbaite assuming the formula $(Na.Ca)(LiAl)_3Al_6(OH)_4(BO_3)_3Si_6O_{18}$.

Donnay and Buerger (30) found that the magnesium ions are surrounded octahedrally by oxygen and hydroxyl ions; the three octahedra surround the three fold axis at the origin and each shares an edge with each of its two equivalent neighbours. The magnesium ions and the surrounding ions thus constitute a small trigonal fragment of a brucite $Mg(OH)_2$ type layer.

The six silicon atoms are each surrounded tetrahedrally by four oxygen atoms, each of the six tetrahedra sharing two of its oxygens with the neighbouring tetrahedra to form a six membered ring of composition Si_6O_{18}, with the oxygen tetrahedra all pointing in the same direction.

The aluminium, boron and sodium atoms remaining serve in different ways to bond together the central core. The boron atoms were considered to be surrounded by three oxygen atoms in a threefold co-ordination, see however Lowenstein (44).

Ito and Sadanaya (31,42) considered the Si_6O_{18} ring to have hexagonal symmetry rather than ditrigonal as proposed by Donnay and Buerger (30). This mode of packing around the ring was found to be similar to that realised in amphiboles and micas (42).

The structure determined by Belov and Belova (40,41) is similar to that obtained by Donnay (30), but with some differences in the exact atomic positions.

Kurylenko (45) using crystallographic data obtained during the previously discussed crystal structure determinations, has arranged the cations and anions according to the homologous points of the space group R3m, see Table 4.

This table shows that the various varieties of tourmaline are formed by substitutional changes occurring in the sodium tetrahedrons and magnesium octahedra whilst the boroaluminosilicate rings remain the same.

More recently Buerger et. al. (46) re-determined the structure using very accurate data. The structure obtained basically confirmed that obtained by Donnay et. al. (30) and Ito (31,42) except that the SiO_4 tetrahedra pointed in the opposite direction. Attempts to refine the structure proposed by Belov and Belova (40,41) were unsuccessful and it was concluded that their structure was incorrect.

The absolute orientation of the structure has been determined by Donnay and Barton (47) and recently confirmed by Barton (48). In these two separate investigations the orientation of the SiO_4 tetrahedra was found to be the same as that orginally proposed by Donnay et. al. (30), but reversed in a latter investigation by Buerger et. al. (46). Barton (48) has also determined the structure of the ferric iron tourmaline, named Buergerite. Although the structure was very similar to that found for dravite (30) some of the ferric ions were found to replace the octahedral aluminium in the 18(c) homologous position, see Table 4.

TABLE 4

Distribution of Ions in particular Lattice positions in Crystal Structure of Tourmaline (45).

Variety of Tourmaline	Homologous Points			Reference
	3(a)	9(b)	18(c)	
Dravite	$2Na^{+}$ $\frac{1}{2}(OH)^{-}$ $\frac{3}{2}F^{-}$	$9(OH)^{-}$ $9Mg^{+2}$	$9BO_3^{3-}$ $18Al^{3+}$ $18SiO_3^{-2}$	30
Dravite	$\frac{3}{2}Na^{+}$ $3(OH)^{-}$ $\frac{1}{2}K^{+}$	$9(OH)^{-}$ $9Mg^{+2}$	$9BO_3^{3-}$ $18Al^{3+}$ $18SiO_3^{-2}$	40
Rubelite (Lithium tourmaline)	$2Li^{+}$ $3(OH)^{-}$ $1Na^{+}$	$9(OH)^{-}$ $6Al^{3+}$	$9BO_3^{3-}$ $18Al^{3+}$ $18SiO_3^{-2}$	31
Schorl	$2Na^{+}$ $2F^{-}$	$9(OH)^{-}$ $7Fe^{2+}$ $1Mg^{2+}$ $1Ca^{2+}$	$9BO_3^{3-}$ $18Al^{3+}$ $18SiO_3^{-2}$	30
	Composition characteristic of Tourmaline deposit		Basic Tourmaline Skeleton	

(4) Synthesis.

Frondel et. al. (49) were able to recrystallise tiny prisms of tourmaline by hydrothermal treatment at 400^0-500^0C of a glass formed by melting natural tourmaline. Michel-Levy (50) was able to grow a rare type of tourmaline when a shale was heated with potassium borate solution at 400^0C and 450 bars pressure. Michel-Levy (51) subsequently investigated the growth of tourmaline crystals when mixtures of silica, alumina, borax, iron, magnesia, etc. are heated with water in an autoclave at varying temperatures and pressures.

Smith (52) synthesised tourmaline from its component oxides in water at 400^0-500^0C and found that its stability field in concentrated solutions is wholly in the weakly alkaline range. Frondel et. al. (53) have synthesised iron tourmaline, by the reaction of a solution of NaCl and H_3BO_3 on coarse fragments of minerals, the latter contributing the Si, Al and Fe required. Most of the common rock forming minerals were investigated, using temperatures and pressures ranging from 350^0C and 2000 bars to 550^0C and 700 bars.

In general Frondel et. al. (53) found that tourmaline was not formed if the added minerals contributed alkalies to the solution.

Taylor et. al. (54) have synthesised not only the usual varieties of tourmaline but new phases in which the X and Y positions of tourmaline $X_1Y_3Al_6B_3Si_6O_{27}(OH)_4$ are partly occupied by Na, K, Ca and Mg and V, Cr, Ni, Cu and Zn respectively.

(5) Optical and Physical Properties.

Kunitz (27) has demonstrated the direct relationship between the chemical composition and certain physical properties of tourmaline.

Quensel (55) and Slivko (56) have plotted the refractive indices and specific gravity against the weight percentage of ferrous oxide and of (Fe^{2+}+Fe^{3+} +Mn^{2+}) respectively and showed that there is a direct relationship between the iron content and the refactive index and specific gravity, see Figure 2.

The colour of tourmaline is extremely variable but in general terms it can be related to the composition in so far as the iron tourmalines are black, while the elbaites tend to be light shades of blue, green or pink and the dravites vary from brown to yellow and almost colourless (32).

Bradley et. al. (57) compared the absorption curves of pink and green tourmaline with those obtained for metal ions in solution and found that the pink colouration was probably due to manganese ions whilst the green was due to ferrous ions.

Wilkins et. al.(58) have studied the origin of the colour in tourmaline and the colour changes which occur when the mineral is heated. In this work the absorption spectra were obtained in the range 3000 to 20000$\overset{0}{A}$ using polarised radiation parallel and perpendicular to the $c-$ axis in the crystal. The data combined to show that the colour is generally due to the amount of Fe^{2+} , Fe^{3+} and Mn^{2+} ions present and to electronic transitions within each ion. With small to moderate concentrations of transition metal ions the colours are clear pink, green and blues according to the $Fe^{2+}/(Fe^{2+}+Fe^{3+}+Mn^{2+})$ ratio in the specimen. When the crystals were heated at about 800^{o}C for at least 15 hours, the intensity of the absorption peaks and the position of the absorption edges both altered. These changes were correlated with the evolution of hydrogen when the ferrous ions are oxidised by hydroxyl ions; this type of oxidation has also been observed when amphiboles (59) are heated.

The optical absorption spectra of schorl, buergerite and a chromium bearing tourmaline have recently been studied by Manning (60). The spectrum of the chromium bearing tourmaline indicated that the Cr^{3+} ions are located in "loose sites", possibly octahedral ones in the spiral chain. The buergerite spectrum showed bands due to Fe^{2+} ions in the near infra-red and red, but most features were swamped by charge-transfer bands. When this spectrum was compared to that for schorl, it was concluded that the Fe^{3+} ions were located in the Al^{3+} sites in the spiral chain in schorl, but mainly in the "brucite type unit" in buergerite.

(6) Decomposition.

The decomposition has been studied by a number of workers using various techniques.

One of the first being Machatschki (61) who used X-ray powder techniques combined with weight loss measurements. The major proportion of the weight loss occurred between 810^{0}C and 900^{o}C, this was associated with the dehydration of the mineral and when combined with X-ray experiments the decomposition temperature was found to be 850 $\pm$ 10^{o}C. The X-ray powder photographs obtained of the decomposed mineral were found to be too complex to be analysed.

The decomposition has been studied using several techniques by Kurylenko (62, 63, 64). One of the most useful techniques was Differential Thermal Analysis. Kurylenko (62) has examined most varieties of tourmaline using this technique and observed the presence of several characteristic endothermic processes. The first ones were associated with the loss of water.

FIGURE 2.

Optical properties (55) and Densities (56) of tourmalines in relation to the number of ($Fe^{2+} + Fe^{3+} + Mn^{2+}$) ions present.

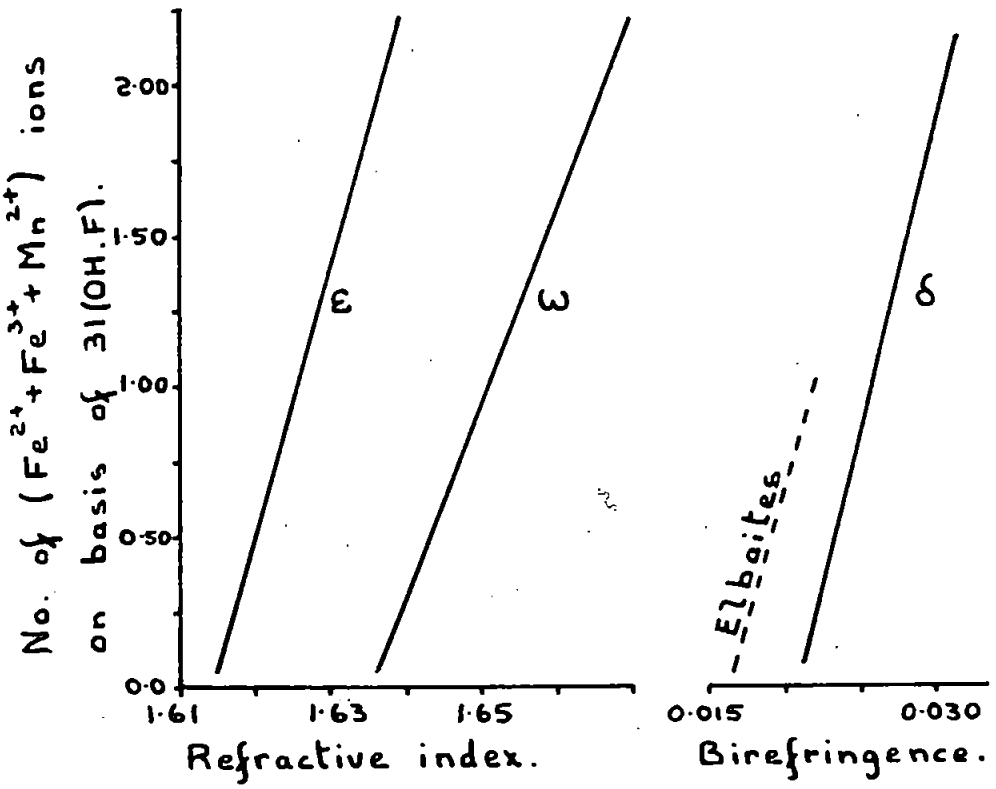

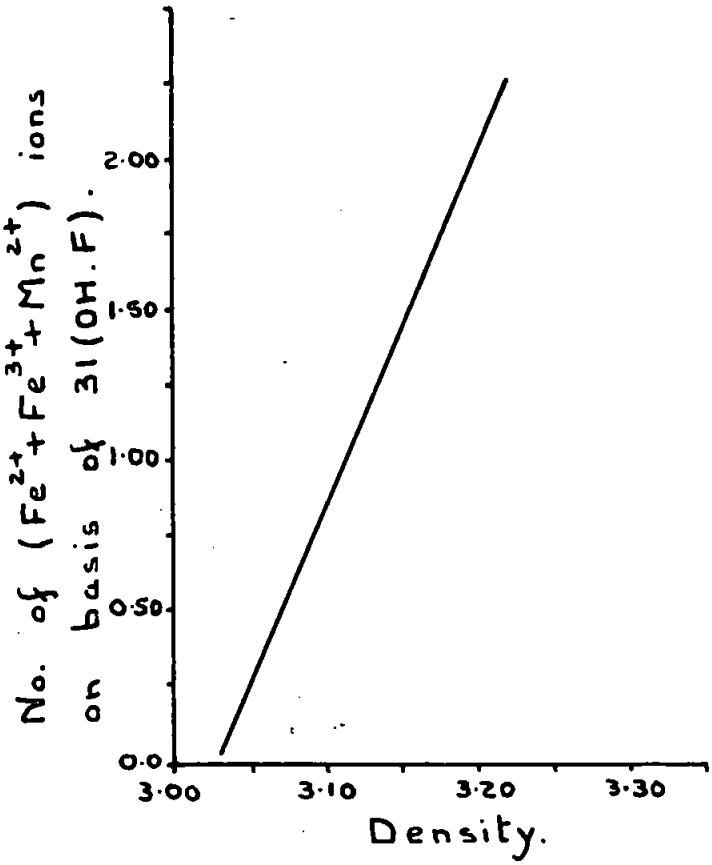

and the final one with the departure of boric oxide, see Table 5. Kurylenko (62) has also determined the approximate fusion temperature of various types of tourmaline by microscopic examination of the heated crystals, see Table 6.

TABLE 5

Differential Thermal Analysis of Various Tourmalines (62).

Variety of Tourmaline and locality.	Endothermic Peak observed at temperature given °C.			
	Dehydration of Tourmaline			Departure of B_2O_3
Schorl (Switzerland)	144	430	770	965
Schorl (Brazil)	145	480	770	960
Schorl (Madagascar)	144	460	770	950
Altered Schorl (Madagascar)	230	450	–	965
Elbaite (Elba)	145	–	–	970
Dravite (Bohemia)	240	–	–	975
Rubellite (U.S.A.)	315	–	–	945

TABLE 6

Fusion Temperature of Various Tourmalines (62).

Variety of Tourmaline	Colour Changes		Fusion Temp. °C.
	Original	Final	
Schorl (Brazil)	Black	Brown-Black	1150
Schorl (Switzerland)	Black	Brown-Black	1150
Elbaite (Messa Grande)	Colourless	Opaque White	1350
Elbaite (U.S.A.)	Pale Pink	Opaque White	1350
Dravite (Bohemia)			1400

Kurylenko (64) has examined in detail the differential thermal analysis curve obtained for dravite. The first derivative of this curve was drawn and a small maximum at 470°C and a minimum at 680°C were observed. The first inflexion was associated with the loss of 16% "lattice water" and the second with the loss of 33%. Between 680°C and 960°C the remaining 67% was lost.

Between 660-680°C Kurylenko (63,64) found that one third of the "lattice water" (or $4(OH)^-$) was lost and that some amorphous silica was formed. The silicate rings are therefore partially destroyed during

this dehydration process. It was found previously that the decomposition temperature of tourmaline was above 850°C (61,62), therefore the low temperature dehydration does not affect the overall crystal lattice. Kurylenko (45) has discussed this partial breakdown of the lattice in relation to the structure determined by Belov and Belova (40,41). The crystal lattice was found to basically consist of two stage six membered rings of tetrahedrons with silicon atoms in the upper stage and aluminium and boron atoms in the lower. Kurylenko (45) suggested that only the upper ring is affected during the low temperature dehydration process, see Table 7. This was supported by the examination of a long exposure X-ray oscillation photograph of a partially dehydrated tourmaline crystal. This photograph consisted of two sets of layer lines; with one of low intensity interposed between the usual layer lines due to tourmaline. The cell dimension calculated for the "crystal" producing the layer lines of low intensity was 14.2 Å ; almost double the c—cell dimension of unheated tourmaline. This result is consistent with the theory expressed by Kurylenko (45) that only one half of the two stage rings is affected by the low temperature dehydration process.

TABLE 7

Unstable lattice formed by the low temperature partial dehydration of Dravite (45).

Temperature °C.	Homologous Points		
	3(a)	9(b)	18(c)
20	$3Na^{+}3(OH)^{-}$	$9(OH)^{-}\ 9\ Mg^{2+}$	$9BO_3^{3-}18Al^{3+}\ 18SiO_3^{-2}$
680	$3(OH)^{-}$ ↑	OH^{-} ↑	
Residue	$3Na^{+}$	$8(OH)^{-}\ 9Mg^{2+}$	$9BO_3^{3-}18Al^{3+}\ 18SiO_3^{-2}$

By the use of X-ray powder photography Kurylenko (63) found that the following products were formed when dravite is completely decomposed:-

(1) SiO_2

(2) Al_2O_3

(3) Enstatite ($MgSiO_3$)

(4) Jeremeyevite ($AlBO_3$)

Korzhinskii (65) found that there was a sharp increase in refractive index and birefringence when various tourmalines were heated in the temperature range 600-800°C, Korzhinskii (65) also found that the main products formed on complete decomposition of schorl were mullite ($3Al_2O_3.2SiO_2$) and maghemite (γ-Fe_2O_3).

One interesting method of decomposing tourmaline has been used by Tsu-Min-Fuh (66) and consists of heating the mineral in the presence of water in an autoclave. This technique known as "Hydrothermal Breakdown" has been used to decompose a number of minerals. It was found that at temperatures between 800°C and 900°C a spinel and cordierite were formed. Assuming that dravite was decomposed the following scheme can be drawn to illustrate the breakdown:-

$$2\ Na\ Mg_3\ Al_6\ B_3\ Si_6\ O_{31}\ H_4$$

$$\downarrow$$

$$2\ Mg\ O.\ Al_2O_3 + 2Mg_2\ Al_4\ Si_5O_{18} + Na_2O + 3B_2O_3 + 4H_2O + 2SiO_2$$

spinel cordierite

CHAPTER 3

Boron – Oxygen Chemistry.

The chemistry of boron-oxygen compounds has been extensively reviewed in a number of books (5, 6, 67). Only certain aspects of the chemistry of boric oxide and boric acid will therefore be covered.

(1) Boric Oxide (B_2O_3).

Several forms of this oxide are known, these being the ordinary hexagonal form which is crystallised at atmospheric pressure in the temperature range 200^o - 250^oC, a dense high temperature and pressure orthorhombic form crystallised at 600^oC and 40,000 atmos, and finally the vitreous form having a range of densities depending upon the thermal history of the sample (6). Some of the basic physico-chemical properties of the oxide are presented in Table 8.

The structure of the hexagonal modification has been determined by Strong (68), who found that this form consists of a truly three dimensional network of planar BO_3 triangles. The structure of the orthorhombic modification was determined by Previtt and Shannon (69). The structure of vitreous and liquid boric oxide has not however been completely settled. There are two main types of models proposed, namely the random network model and the molecular model. The structure models for both the glass and liquid have been recently reviewed by Krogh-Moe (70), with special reference to spectroscopic and diffraction data. Krogh-Moe (70) thought that a structure consisting of a random three-dimensional network of BO_3 triangles with a comparatively large fraction of six-membered boroxol rings was the one most consistent with the experimental data.

The geometrical structure of boric oxide has been the subject of a number of investigations. The technique used most frequently has been infra-red spectroscopy, either of the high temperature vapour (71,72) or of species trapped in an inert gas matrix (73).

Most of the recent investigations (71,73,74) have concluded that the structure is V-shaped (1) with the apex angle uncertain, varying between 95^o and 150^o depending on the investigation, see below. This structure is the presently accepted one. However, more recently Hanst and Early (72) measured the infra-red absorption spectrum of boric oxide vapour and concluded that some of the absorption bands previously allocated to boric oxide are actually due to the presence of metaboric acid (HBO_2).

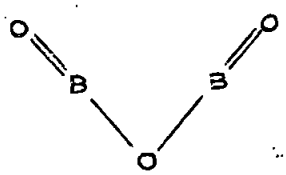

(I)

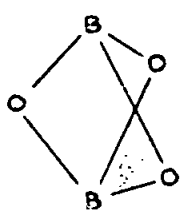

(II)

If this is true then the original C_{2v} symmetry allocated to the oxide and leading to the structure (1) is incorrect. The infra-red spectrum obtained, when combined with electric deflection experiments of molecular beams of boric oxide, leads to a trigonal bipyramidal structure (11) having D_{3h} symmetry. The geometrical structure of boric oxide is therefore uncertain at present.

TABLE 8

Some Physical Constants of Boric Oxide.

Property	Vitreous Form			Crystalline Forms:- Hexagonal (H) Orthorhombic (O)		
	Temp. °C.	Most Reliable Data	Ref.	Temp. °C.	Most Reliable Data	Ref.
Density of Liquid	900	1.520	82,83			
Density of Solid		1,801 to 1.844	79		2.56(H) 3.11(O)	68 69
Temperature of softening	325 to 450		76			
Melting Point				450±2		80,81
Boiling Point	2250		78			
Heat of fusion (kcal/mole).					5.27	6
					6.72	6
Heat of vapourisation (kcal/mole).				25(a)	104.2	78
				25(b)	84.0	78
				25(a)	103.1	77
				1230	93.3	77

Suffix:- a Calculated assuming C_{2v} symmetry.

b Calculated assuming D_{3h} symmetry.

(2) Boric Acids.

Orthoboric acid is obtained from the fumaroles of Tuscany as the mineral sassolite (H_3BO_3) and can easily be prepared from borates by reaction with mineral acids. Some of the more important physical constants of orthoboric acid are listed in Table 9.

When orthoboric acid (H_3BO_3) is heated above 100°C it loses a water molecule and changes to metaboric acid (HBO_2). The existence of three polymorphic forms of metaboric acid was demonstrated by Kracek et. al. (75) in an investigation of the water-boric acid system.

The structure of orthoboric acid has been determined by Zachariasen (84, 88) who found that the unit cell was triclinic and contained four $B(OH)_3$ molecules. The crystal structure consists of layers of coplanar BO_3 groups, which is consistent with the ready cleavage of the crystal into flakes. The atomic arrangement within

each individual layer is the same, but the layers are randomly displaced with respect to each other, indicating that only Vander Waals forces bind the layers together. The borate groups are linked together through the oxygen atoms by hydrogen bonding. It was found that the hydrogen atoms involved did not lie on a straight line between the oxygen atoms, but are slightly displaced towards the hydrogen atom of the parallel hydrogen bond.

TABLE 9

Some Physical Constants of Boric acid.

Property	Most Reliable Data	Literature Reference
Density of orthoboric Acid($g/cm.^3$).	1.48	84
General Thermodynamic functions of boric acids		85
Solubility of boric acid in water ($g.H_3BO_3/100g.H_2O$).		86
0^oC	2.77	
10	3.65	
20	4.88	
30	6.77	
50	11.41	
100	37.99	
Dissociation constant in dilute aqueous solution. 25^0C	5.80×10^{-10}	87

The structure of each of the three polymorphs of metaboric acid have been determined:-

(1) HBO_2(III)

The structure of this polymorph was determined by Tazaki (230) and found to have a sheet like structure containing B_3O_3 rings, with the sheets being bonded together by Van der Waals forces.

(2) HBO_2(II)

Zachariasen (89, 90) found that the structure of this monoclinic form consisted of endless zigzag chains, of composition $B_3O_4(OH)(OH_2)$, directed along the b axis; with hydrogen bonds forming links between the chains of different layers as well as between chains of the same layer. Two thirds of the boron atoms are trigonally bonded to oxygen and one third are tetrahedrally bonded. The "water" oxygen of the asymmetric unit occupies an unshared corner of the tetrahedron, whereas the hydroxyl oxygen occupies an unshared corner of a BO_3 triangle.

(3) HBO_2(I)

Because of the similarity of HBO_2(I) to crystalline boric oxide Hendricks (91) suggested that the structure consisted of eight $(HBO_2)_3$ groups bonded together in space through hydrogen bonds to give cubic symmetry. This

was confirmed using X-ray methods by Parsons et. al.(92) who proposed that all the boron atoms were tetrahedrally co-ordinated. The detailed structure has been determined by Zachariasen (90) who found that each boron atom was bonded tetrahedrally to four oxygen atoms and each oxygen to two boron atoms; with strong hydrogen bonding between the tetrahedra in the three dimensional network.

CHAPTER 4

Review of some Oxide Phase Systems.

Some oxide phase systems that were thought to be relevant to the mechanism of decomposition of tourmaline will be reviewed.

(1) The B_2O_3 - SiO_2 System:-

This system has been investigated by several workers, but wide discrepancies have been obtained. Bleininger and Teeter (93) have presented cone fusion data but their results are only a crude approach to the phase diagram. Morey et. al. (94), Morey (95) and Englert et. al. (96) found that the quenching method was incapable of yielding direct results owing to the failure of the borosilicate glasses to crystallise. Inconsistencies have been observed in relation to both the shape and position of the liquidus curves obtained indirectly in the above investigations.

Dimbleby et. al. (98) have claimed to have observed two immiscible liquids, embracing the range from 30 to 80 per cent boric oxide. However, most investigators are of the opinion that the system is completely miscible over the entire composition range (94, 99, 100). Zhdanov (101) has, however, reported microheterogeneity in the borosilicate glasses containing 60,70 and 75% silica. Differences of opinion have also arisen as to the existence of intermediate compounds. For example, Jenckel (97) attributed breaks in the curves plotted for volume expansion and freezing-in temperatures against composition to a compound of approximate composition $3B_2O_3.2SiO_2$. However, in the most recent study by Rockett and Foster (100) no evidence for the formation of a definite binary compound was obtained even after the most careful X-ray investigation. At the present time it appears that most of the direct evidence would favour the view that no distinct crystalline phase with unique optical properties or X-ray pattern is formed.

(2) The Na_2O–B_2O_3–SiO_2 System:-

This ternary system has been investigated in detail by Morey (95) who found that several binary compounds were formed and also one ternary compound of formula $Na_2O.B_2O_3.2SiO_2$. However, all of the binary compounds were limited to the Na_2O-B_2O_3 and Na_2O-SiO_2 systems.

(3) The Al_2O_3 - SiO_2 System:-

The phase equilibrium relations and fields of compound formation for this system has been determined by Aramaki and Roy (102). The only binary compound obtained was mullite ($3Al_2O_3.2SiO_2$).

(4) The B_2O_3 - Al_2O_3 - SiO_2 System:-

A partial investigation of this system has been carried out by Dietzel and Scholze (103). Strong evidence was obtained for substantial solid solution between the compounds $3Al_2O_3.2SiO_2$ and $9Al_2O_3.2B_2O_3$. Such solid solution effects were substantiated by the work of Gelsdorf et. al. (104), Gielisse et. al. (106) and by the synthesis of a boron containing alumino-silicate by Letort (105).

The X-ray results obtained by Dietzel and Scholze (103) of this solid solution are of special interest. The X-ray patterns obtained were found to be close to that of pure mullite ($3Al_2O_3.2SiO_2$). The most important difference observed was the systematic shortening of the c- cell dimension which appeared to be dependent on the proportion of boric oxide present in the crystals. The other two cell dimensions of the boron containing alumino-

silicate were found to be the same as those for mullite itself.

(5) $B_2O_3 - Al_2O_3$ System:-

This system has been investigated by a number of workers. Two binary compounds have been found to be formed. The compound $9Al_2O_3.2B_2O_3$ was identified by Bauman and Moore (107) and by Scholze (108) who also reported the presence of the second compound $2Al_2O_3.B_2O_3$. Similar results have been obtained by Gielisse and Foster (109), who also found that the 1:1 aluminium borate ($Al_2O_3.B_2O_3$), found as the mineral jeremejevite, could not be synthesised at normal pressures.

TABLE 10

Other Phase Systems of Interest.

System	Compounds formed and other Information.	Reference
$FeO-Al_2O_3-SiO_2$	Complex; mullite crystalline phase close to tourmaline composition.	110
$FeO-Al_2O_3$	Complex; spinel ($FeO.Al_2O_3$) phase present close to tourmaline composition.	111
$FeO-B_2O_3$	Two binary compounds have been synthesised; $FeO.B_2O_3$ and $2FeO.B_2O_3$.	112, 113
$FeO-SiO_2$	No binary compound formation close to tourmaline composition.	114
$MgO-SiO_2$	Complex; $MgSiO_3$ phase present close to tourmaline composition.	148
$MgO-Al_2O_3$	Complex; Spinel phase present close to tourmaline composition.	149

CHAPTER 5

Pyrohydrolysis.

Is the reaction of a substance with steam at elevated temperatures.

(1) Pyrohydrolysis of Fluorides.

This method has been applied to the quantitative determination of the fluoride ion (116,117, 118).

Pyrohydrolysis is capable of liberating hydrogen fluoride by passage of steam over a variety of substances, including the fluorides of Al, Zr, V and Na by utilising the favourable equilibrium constants and high reaction rates at elevated temperatures (115). The general reaction is:-

$$MF_x + xH_2O \longrightarrow M(OH)_x + xHF$$

One of the earliest reported uses of this technique was by Warf et. al. (116) who found that the fluorides could be separated into two fairly distinct groups:-

(1) The rapidly hydrolysable:-

This group included the fluorides of Al, Th, U, Zr and rare earths.

(2) The slowly hydrolysable:-

This group includes the fluoridesof beryllium, the alkali metals and alkaline earth metals.

Warf et. al. (116) also found that the addition of uranium oxide (U_3O_8) considerably accelerated the hydrolysis, even of the more stable alkali fluorides.

This pyrohydrolysis technique has been used in a number of fluoride determinations, the main variations being the accelerator and the material used for the tube furnace (117, 118).

Recently two separate investigations into the kinetics of the pyrohydrolysis have been reported. Myasnikov et. al.(119) have determined the rate of pyrohydrolysis of aluminium fluoride (AlF_3). The rate equation obtained was of the form:-

$$W = KSp^N_{H_2O} \quad \exp(-E/RT)$$

Where:- (1) W = Rate of Pyrohydrolysis.

(2) K = A constant.

(3) S = Cross-sectional area of boat containing AlF_3.

(4) p = Partial pressure of water in steam-air mixture being passed.

(5) N = 2/3.

(6) E = Activation energy of process; equals 89 kcal/mole.

The rate of pyrohydrolysis of lithium and sodium hexafluorotitanates (M_2TiF_6) have been determined by Mikhailov et. al. (120). Using X-ray diffraction techniques Mikhailov et. al. (120) found that the reactions proceded as follows:-

(1) $M_2TiF_6 + H_2O = M_2TiOF_4 + 2HF$

(2) $M_2TiOF_4 + H_2O = 2MF + TiO_2 + 2HF$

The rate of pyrohydrolysis was found to follow the two rate equations given below:-

(a) Obeyed by Li_2TiF_6.

$1 - \sqrt[3]{1-\alpha} = kt$. Activation energy equals 13.7 kcal/mole

(b) Obeyed by Na_2TiF_6.

$\alpha^2 = kt$. Activation energy equals 6.1 kcal/mole.

Where α represents the percentage of the fluorotitanate decomposed.

(2) Pyrohydrolysis Applied to Boron Chemistry.

(2.1) Analytical.

Williams et. al. (121) have suggested that because of the volatility of boric oxide at glass melting temperatures, coupled with the fact that boric acid is readily steam distilled, pyrohydrolysis might be useful in separating boric oxide from borosilicate glasses. Using a temperature of about 1350°C quantitative removal of the boric oxide from several types of glasses was achieved, although difficulties were experienced when lead glasses were investigated. The addition of various compounds to the powdered glass was found to accelerate the pyrohydrolysis. The most effective accelerator was found to be a mixture of uranium oxide and sodium metasilicate; the mechanism by which these compounds work is as yet unknown. Pyrohydrolysis has also been used by Wiederkedr and Goward (122) to determine the amount of boron in certain alloys.

(2.2) Industrial.

The industrial recovery of boric acid from certain borate ores using the pyrohydrolysis technique has been investigated (123, 124, 125).

Harman (123) found that boric acid could be recovered from borate ores when pyrolysed at 150 -1000°C. Powdered colemanite containing 25% by weight of water was found, after charging into a furnace at 550°C, to evolve white fumes which when condensed were found to contain a mixture of boric acid and boric oxide. Similar results have been obtained by Mikhailov (124) and Mikhailov and Vedernikova (125) when the datolite ores present in the Soviet Union were investigated.

(2.3) Thermodynamics.

The vapour equilibrium of the boric oxide – water system has been the subject of a number of investigations (126, 127, 128, 129).

The existence of gaseous hydroxides of boron has been known for many years. For example, Stackelberg et. al. (126) observed the sublimation of H_3BO_3 and determined the heat of formation of the gas. Margrave and Damron (127) postulated that HBO_2 gas was a significant species in water vapour over boric oxide, in the temperature range 500 -900°C, from studies of log $P(H_2O)$ versus log P(boron species) curves.

In a more recent investigation Randell and Margrave (128) assumed that $H_3BO_3(g)$, $HBO_2(g)$ and $(HBO_2)_3(g)$ were the important species from the reaction between water vapour and liquid boric oxide in the temperature range 700-1100°C. The following three equations can then be written:-

$$B_2O_3(l) + H_2O(g) = 2HBO_2(g)$$

B_2O_3 (l) + H_2O (g) = H_3BO_3 (g)

$3B_2O_3$ (l) + $3H_2O$ (g) = $2(HBO_2)_3$ (g)

At temperatures below 1000°C Randell and Margrave (128) found that the slopes of log (total pressure) versus log P (H_2O) curves were consistent with the assumption that H_3BO_3 gas is the predominant species present. At temperatures above about 1000°C a different slope was obtained which was consistent with the assumption that the vapour contained a mixture of HBO_2 and $(HBO_2)_3$. The heat of formation (ΔH_f) of these two species was found to be equal to:-

$\Delta H_{fo°K}$ (HBO_2) = 134.9 ± 1 kcal/mole

$\Delta H_{fo°K}$ $(HBO_2)_3$ = 537.5 ± 3 kcal/mole

Meschi et. al. (130) have studied this reaction using a Knudsen effusion cell combined with a mass spectrometer. Water vapour was introduced into the Knudsen cell containing boric oxide and the vapour effusing from the cell was analysed by the spectrometer. The following species were found to be present in the effusing vapour H_2O, B_2O_3, HBO_2, H_3BO_3 and $(HBO_2)_3$, the one present in the largest amount being HBO_2. The data pertaining to the trimer $(HBO_2)_3$ was extremely difficult to obtain accurately in the temperature range covered of 1060 to 1450°K. The concentration of this trimer was found to be less than 1% of that of the monomer HBO_2. A summary of the results obtained is given in Table 11.

The most significant difference between the results obtained by Randell et. al. (128) compared to those of Meschi et. al. (130) is the proportion of the trimer present in the temperature range 1000 to 1273°K. By the more indirect method Randell et. al. (128) stated that 50% of the total pressure was due to the trimer, whilst Meschi et. al. (130) found that only 1% was due to the trimer. The results obtained in the latter investigation are probably the most accurate.

TABLE II

Thermodynamic constants for the Heterogeneous reaction between Boric Oxide and Water Vapour (130).

Temp.	H_2O^+	HBO_2^+	$B_2O_3^+$	Log K_1 eqn. 1	Log K_2 eqn.2	$(HBO_2)_3^+$	$H_3BO_3^+$
1273	9.9×10^4	5.52×10^6		-2.731	----	2.27×10^4	
1357	4.51×10^4	1.08×10^7	3.69×10^6	-2.277	0.714	5.06×10^4	
1451	2.2×10^4	2.34×10^7	2.75×10^7	-1.803	0.812	1.77×10^5	1.15×10^5

$$B_2O_3\,(l) + H_2O\,(g) = 2\,HBO_2\,(g) \quad \text{--- (1)}$$

$$K_1 = \frac{P^2\,(HBO_2)}{P\,(H_2O)}$$

$$\Delta H_o(1) = 47.6 \pm 2 \text{ kcal/mole}$$

$$B_2O_3\,(g) + H_2O\,(g) = 2HBO_2\,(g) \quad \text{--- (2)}$$

$$K_2 = \frac{P^2(HBO_2)}{P\,(B_2O_3)\,P(H_2O)}$$

$$\Delta H_o\,(2) = -2.1 \pm 2 \text{ kcal/mole}$$

CHAPTER 6

The Structure of Glass.

The structure of glass has been considered from two different concepts. The earliest being the "crystallite" theory by Lebedev (131) and the other the "random network" theory by Zachariasen (132).

Lebedev's concept was that the structure can be considered as an accumulation of submicroscopic formations of various silicates, the chemical nature of which is determined by the composition. These micro-structural regions are separated by layers in which the degree of disorder increases with increasing distance from the microcrystalline region. These regions may be definite chemical compounds or solid solutions however, either would probably have a considerably deformed crystal lattice.

According to the theory developed by Zachariasen (132) silicate glasses consist of a continuous network with ions, atoms etc. at its junctions. However, in contrast to a regular crystalline network this network in glasses is irregular. For example, the structure of quartz glass like the structure of crystalline quartz is built up of SiO_4 tetrahedrons. Whereas in a crystalline network every tetra-hedron is regularly orientated with respect to any other tetrahedron, in the network of quartz glass some degree of regularity in the mutual orientation extends only to the nearest tetrahedra. As the distance from a given tetrahedron increases the mutual regularity of orientation diminishes, until complete randomisation occurs between distant tetrahedra.

The problems involved in determining experimentally the structure of glass has been discussed at length in two conferences held in the Soviet Union (133). Both the crystallite theory and the random network theory were stated to explain the experimental results obtained. However, in the more recent of the two conferences the crystallite theory was thought to explain most satisfactorily the recent experimental results, especially when the more complex glasses were considered.

Of special interest from the structural view point are the sodium borosilicate glasses. These glasses after annealing at 500 -550^{o}C were found to form a porous glass when leached with acids. This leaching process was found to extract the sodium and boric oxides preferentially leaving a porous silica glass. During the annealing treatment two processes were thought to occur ((133):-

(a) The first more rapid one which leads to a decrease in the size of the pores. This process is probably due to a re-orientation of the chemical bonds.

(b) The second slow process is probably the growth of the sodium borate regions, by the diffusional growth of large regions at the expense of the smaller ones.

These results together with many other physical chemical properties of sodium borosilicate glasses lead to the view that they consist of submicroscopic heterogeneities within a silica framework (133). The microscopic separation of the various phases of certain glasses has been observed experimentally using electron microscopy. Skatulla et. al. (134) found that phase separation occurs even in an optically clear glass and that droplet separation is enhanced by heat treatment. Recently the Scanning Electron Microscope has been used in

conjunction with the usual Electron Microscope to investigate the formation and growth of these microheterogeneous regions in borosilicate glasses (135, 136, 137). Makishima et. al. (135) have found that phase separation increased with increase in the time and temperature of the heat treatment and that these phase separated regions also became more interconnected. These results have been confirmed in similar investigations by Haller et. al. (136) and by Cordelier (137).

Kiyohisa et. al. (138) have determined the minimum time (t) required for complete phase separation for various borosilicate glasses at a number of temperatures ($T^{o}K$). A linear relationship was found to be obeyed between the minimum phase separation time (t) and the reciprocal of the temperature ($T^{o}K$); although t values changed by up to 10 times with glass composition. A linear relationship was also found to be obeyed between log t and the Na_2O/B_2O_3 ratio in the glass. This observation means that the rate of phase separation increases as the proportion of Na_2O in the glass increases. The apparent activation energy of this phase separation process was found to be equal to 62 kcal/mole.

CHAPTER 7

Heterogeneous Reactions.

The first two sections of this chapter will be concerned with general heterogeneous reactions, whilst the third will deal specifically with the attack by liquids and gases on glass.

(1) Liquid-Solid Reactions.

When a solid is attacked by a liquid the product may be either soluble or insoluble in the liquid.

If the product is insoluble the reaction will depend on the rate at which the reagent can pass through the product layer. Systematic studies of this type of reaction do not appear to have been undertaken (139).

If the product is soluble then the rate of dissolution is found to be usually diffusion controlled with an activation energy of about 5 kcal/mole. The rate of dissolution (R) would then obey Ficks diffusion law (140):-

$$R = \frac{D.s.(c_s - c)}{t}$$

Where s and $(c_s - c)$ are the surface area and concentration terms respectively, with t being the reaction time and D the diffusion constant.

This equation has been found to be obeyed in the cases of the dissolution of sodium chloride (141) in water and of metals in acids (142).

Certain solid-liquid reactions have been found where the chemical reaction is the rate determining step. The dissolution of calcium carbonate in dilute hydrochloric acid is an example of such a reaction (143). Palmer et. al. (144) have found that the rate of dissolution of silica in hydrofluoric acid is also chemically controlled.

(2) Solid-Gas Reactions.

In general an heterogeneous surface reaction can usually be broken into the following elementary steps (145):-

(1) Diffusion of reactants to surface.

(2) Adsorption of reactants on surface.

(3) Chemical reaction on the surface.

(4) Desorption of products from surface.

(5) Diffusion of products from surface.

It is usually found that the rate controlling step is the chemical reaction at the surface, however, in certain very rapid reactions diffusion has been found to be the rate controlling process. In this instance the temperature (T) dependence of the reaction is proportional to $T^{1/2}$ (145).

If however, the reaction produces a solid on the surface the rate may be determined by transport processes across the product layer (146). The rate laws governing such reactions may be classified into four main types (147):-

(a) Linear Rate.

Here the product does not provide an effective barrier to further chemical change and the rate will

therefore be independent of the product layer thickness (150). The weight of product (W) formed is thus directly proportional to the reaction time (t), see equation (1):-

$$W = kt \quad \text{---------- (1)}$$

(b) Protective Film Formation.

Here the product forms a coherent, strongly adherent layer which prevents the reaction proceeding; at higher temperatures some mobility of one of the reactants may be possible and further reaction will then occur.

(c) Parabolic rate law.

This rate equation can be represented in the form (2). This type of rate law has been found to be obeyed in several gas-solid reactions (151).

$$W^2 = kt \quad \text{--------- (2)}$$

(d) Other rate laws.

Not all solid gas reactions obey one of the three types discussed previously (164). The oxidation of zirconium follows a cubic law (3), whilst the later stages of the oxidation of aluminium follows an inverse logarithmic law (4).

$$W^3 = kt \quad \text{---------- (3)}$$

$$1/W = k_1 - k_2 \log (k_3 + t) \quad \text{----------(4)}$$

(3) Corrosion of Glass.

(3.1) Introduction.

Much of the work on the chemical attack of glass has had the practical purpose of determining the durability of glass. This aspect has been reviewed by Beattie (152), Morey (153) and by Shand (154). Corrosion may occur in one or a combination of several ways, thus the glass may (155):-

(a) React with the corrosive agents to form new compounds on the surface.

(b) Be preferentially dissolved leaving a leached surface layer.

(c) Be totally dissolved by continuously exposing fresh glass.

(3.2) Attack by water and steam.

Silica is almost insoluble in water except at temperatures above 250°C and thus the attack of glass by water only occurs due to the existence of soluble components such as alkalis.

Charles (156) has studied the effect of saturated and 90% saturated water vapour at temperatures between 150 and 250°C on soda-lime glass. It was found that a sharply defined layer of decomposed material was formed on the glass; the depth of which was measured as a function of time at various temperatures. Charles (156) suggested that the glass is corroded when terminal sodium ions were present at the surface. The disruption of the silica network can then be represented by the following equations:-

$$-\overset{|}{\underset{|}{Si}}-O^- \cdots\cdots Na^+ + H_2O \longrightarrow -\overset{|}{\underset{|}{Si}}-OH + Na^+ + OH^-$$

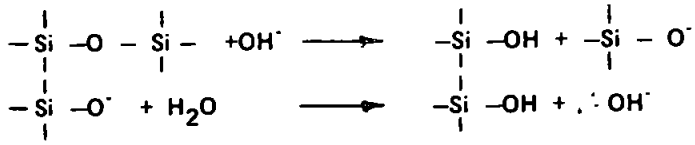

The rate of attack was thought to be controlled by the diffusion of sodium ions through the corroded layer. This was supported by the concordance in the activation energy of sodium ion diffusion of 19.4 kcal/mole and the value of 20± 4 kcal/mole for the activation energy of corrosion. Similar results have been obtained by Lyle (157) and by Douglas et. al. (158), see Table 12.

(3.3) Acid Attack.

Kuehne (159) found that the rate of leaching using M.H_2SO_4 of sodium borosilicate glasses approximately followed the parabolic rate law.

Jones and Homer (160) have studied the rate of dissolution of a number of glasses in acid and found that the parabolic law was followed. Jones and Homer (160) found that the activation energy for the dissolution of most glasses was close to 17 kcal/mole, see Table 12.

Kiyohisa et. al. (138) have investigated the acid leaching of boric oxide and sodium oxide from phase separated borosilicate glasses. The rate of 0.5M. H_2SO_4 leaching of the B_2O_3/Na_2O phase was measured at various temperatures. The rate of leaching was found to obeyed the usual parobolic rate equation (1):-

(Thickness of leached layer) = $kt^{0.5}$ ..... (1)

The activation energy of the leaching process was found to be equal to 6.8 kcal/mole. The rate controlling process was thought to arise from the slow diffusion of B_2O_3/Na_2O through the porous SiO_2 membrane filled with the acid.

The activation energy found by Kiyohisa et. al. (138) for the leaching process from a segregated glass is less than half that found previously for leaching of normal glasses, see Table 12.

(3.4) Alkali Attack.

Berger (161) found that the attack of powdered glass by alkali was linear provided the products of the corrosion were not allowed to accumulate in solution, however, the rate of attack was found to be approximately parabolic if the products were not removed.

The activation energy for alkali attack on most glasses has been found to be close to 18 kcal/mole, see Table 12.

Geffcken and Berger (162) have studied the attack on glass by sodium carbonate solutions of different concentrations at 100°C. They found that if the function (1) was plotted a straight line could be obtained for concentrations from 0.1M. to 2.0M. Na_2CO_3.

$C/R = a + bc$ ..... (1)

Where C is the concentration of sodium carbonate, R is the rate of dissolution of glass and a and b are constants.

This type of equation resembles the hyperbolic equation developed by Langmuir for the fraction of

TABLE 12

Activation Energy of dissolution of Various glasses.

Glass; with approximate composition.	Activation Energy of Dissolution of Glass (kcal/mole).					
	Attack by Water Vapour.		Attack by Acid.		Attack by Alkali.	
	Value	Ref.	Value	Ref.	Value	Reference
Soda-Lime Silica 75% SiO_2: 15% Na_2O: 10% CaO + MgO.	18.3	158			16.6	158
Borosilicate crown 66% SiO_2: 12% B_2O_3: 20% Na_2O + K_2O.	20±4	156	17.0	160	17.0	163
Chemical "Pyrex" 80% SiO_2: 12% B_2O_3 5% Na_2O: 3% Al_2O_3.					18.5 18.5	162 163
Glasses including:- Barium crown:- 50% SiO_2: 4% B_2O_3: 8% K_2O: 7% ZnO: 31% BaO.			17.0	160.	15.3	163
Flints:- 46% SiO_2; 9% Na_2O + K_2O; 45% PbO.			17.0	160	17.8	163
Phase separated borosilicate glass.			6.8			138

the surface covered by adsorbed gas in equilibrium with the gas at a given pressure.

EXPERIMENTAL

CHAPTER 8

Materials used and their Processing.

(1) Materials.

The various tourmalines used in this study were obtained from:-

(1.1) Roche Rock, Nr. St. Austell, Cornwall (8/1).

The specimens removed consisted of large lumps of iron tourmaline containing about 5% impurities.

(1.2) Unknown locality; probably Dartmoor (8/2).

This specimen of iron tourmaline in the form of a large lump contained about 5 per cent silica and was supplied by Dr. A. B. Meggy.

(1.3) Lee Moor, E.C.L.P. China Clay Works, Nr. Plymouth (8/3).

This density separated iron tourmaline in the form of crystals about 1 to 3 mm. in size was kindly supplied by Mr. P. Roberts of the Geology Department.

(1.4) Minas Gerais, Brazil (8/4).

This sample of magnesium tourmaline was bought from Parkinson and Co. Ltd. Doulting, Shepton Mallet, Somerset.

Standard carbonate free 0.1M.NaOH was obtained from British Drug Houses Ltd. (B.D.H.), Poole, Dorset. This was diluted to 0.05M.NaOH using freshly distilled water and kept in a plastic 5 litre tank with a soda-lime trap. All the other chemicals used were obtained from B.D.H. Ltd. Poole, or from May and Baker Ltd., Dagenham.

(2) Processing.

The large lumps of iron tourmaline were roughly crushed in a "Denver" jaw crusher and then ground in a mechanical mill to the required size prior to sieving. A list of mesh numbers with the corresponding hole size for each of the sieves used is given in Table 13.

In some pyrohydrolysis experiments 1 $cm.^3$ cubes were required. These cubes were cut from a large lump of iron tourmaline (8/1) using a "Mottacutta" rock cutting machine manufactured by Cutrock Engineering Ltd.

TABLE 13

Standard Sieve Sizes.

Mesh Number	Hole Size (m.m.)	Mesh Number	Hole Size (m.m.)	Mesh Number	Hole Size (m.m.)
3/16	4.76	14	1.20	52	0.300
5	3.35	16	1.00	100	0.150
8	2.06	18	0.850	200	0.075
12	1.40	22	0.710	300	0.053

CHAPTER 9

Survey of Instruments Used.

(1) Description of furnaces used.

(1.1) Oven furnace:-

The oven type furnace used was manufactured by Griffen and George Ltd. The heating chamber of dimensions 10 x 8 x 28 cm. was made of a high grade brick with silicon carbide heating elements mounted transversely in the roof. The temperature is controlled by an automatic electronic proportional control which maintains the set temperature to within ± 5°C up to a maximum of 1350°C.

(1.2) Tube furnace:-

This was also manufactured by Griffen and George Ltd. The heating chamber of length 200 mm. was heated with silicon carbide rods. The working temperature was measured by a platinum alloy thermocouple and is controlled by a variable transformer up to a maximum of 1450°C. The tubes used were made of recrystallised alumina (Al_2O_3) of 25 mm. internal diameter, with a wall thickness of 3 mm. and 760 mm. in length.

(2) Cambridge pH meter.

A Cambridge Pye Master pH meter and millivoltmeter was used in the quantitative potentiometric determination of boron. This meter consists of the usual lithium glass and calomel/saturated KC1 reference electrodes connected to an electronic amplifier.

To obtain a better stabilisation of the zero the instrument was left switched on, with the electrodes immersed in distilled water, even when not being used. At the beginning of each boron determination the meter was standardised using a pH 7.00 buffer solution.

(3) X-ray Equipment.

The X-ray generator used was a Solus-Schall Ltd. high voltage generator fitted with a sealed Phillips-Mullard X-ray tube. This tube was of the sealed type and contained a copper target. The output was always maintained at 40 Kv, 15mA. when being used. The copper radiation was monochromatised using a nickel filter to remove the K_β component.

(3.1) Flat-plate transmission camera.

This Unicam camera was designed to take 82.5 x 108 mm. plate or film which was set perpendicular to the incident axis of the X-rays at a distance of 30mm. from the specimen. The crystal being examined is first carefully attached to a fine glass filament using Durofix glue. The filament is then stuck vertically into the small piece of plastercine which is attached to the top of the camera's goniometer arcs. The specimen can then be accurately aligned using the attached telescope, before being exposed to the X-rays.

This camera was used to study the changes in orientation that may occur during the decomposition of single crystals of tourmaline. If these single crystals decompose to completely randomly orientated microcrystals then the photographs obtained will consist of concentric uniform circular haloes of the usual "powder photograph" type (202). However, if the microcrystals have what is termed a "preferred orientation" with a definite crystal axis

or crystal plane of each particle approximately parallel to a certain direction or plane, then the photograph will not consist of uniform circular haloes (202).

(3.2) X-ray Diffractometer INT/B (Solus-Schall).

The diffractometer used is based on a design by Berthold (166), with a focusing arrangement similar to that described by Bragg and Brentano (167). This system enables large flat powder specimens to be used, thus enabling easy specimen mounting with high sensitivity and good resolving power. The diameter of the measuring circle is 500 mm. from front slit to counter slit.

The counting equipment consists of a proportional counter operating at 1950 volts, working in conjunction with a chart recorder which can travel at 120, 300 or 600 mm. per hour. A channel analyser selects pulses having an intensity between a certain lower and upper value depending on the channel position, this analyser was found to be useful in reducing the fluorescence caused by the iron present in the schorl samples. A rate-meter registers counts from 1 x 10 to 3 x 10^5 per sec. with a linear response. The rotation of the specimen and the counter tube can be in a clockwise or anti-clockwise direction by hand or by motor. When the motor is used the three speeds available to accomplish the circular movement are 1/3, 1 or 2 degrees per minute.

The samples analysed are powdered and then mixed with acetone and "Durofix" into a thin paste which could be poured onto a small glass microscope slide (2 x 2 cms.). When dry the slide was mounted vertically and aligned with the axis of rotation of the counter on the central specimen holder by means of a jig.

The recordings of the diffracted radiation were used for:-

(a) Qualitatively analysing the specimens by use of Bragg's equation (168):-

$$2d = \lambda / \sin\theta$$

Where d is the interplanar spacing

θ is the diffracted angle.

(b) Measurement of cell dimensions of crystalline species present in sample.

(c) Measurement of the width of the lines obtained. These measurements could be used to determine the crystallite size of the species present in a particular sample.

(3.2.1) X-ray Line Broadening.

The X-ray trace always consists of peaks which are broadened due to instrumental causes. In certain instances the peaks may be further broadened due to:-

(3.2.1.1) Small crystallite size:-

If the crystallites in a specimen are less than about 1000Å (0.1μ) appreciable intrinsic line broadening will result. The mean crystallite size (d) is related to the intrinsic broadening (β) by the Scherrer equation (169):-

$$\frac{D = \beta K}{\lambda \cos\theta}$$

Where K is a constant

λ is the X-ray wavelength

θ is diffracted angle of line being measured.

(3.2.1.2) Broadening due to lattice distortion.

The mean strain (N) is related to the intrinsic broadening (β) by the equation (207):-

$$N = \beta \cot \theta$$

This type of broadening is due to variations in the dimensions of the unit cell (207).

Methods of separating the contributions due to each type of intrinsic broadening has been described by Klug and Alexander (170) and by Warren and Averback (171).

(4) Polarising Microscope.

A Vickers Polarising microscope was used to examine the effect of heat on crystals of tourmaline. This microscope was also used to determine the size of the crystallites formed when tourmaline decomposes. This was achieved by comparing the size of the crystallites with a standard graticule mounted in the eyepiece of the microscope (172). The optical technique used is capable of determining particle size in the range 500μ to 0.35μ.

(5) Differential Thermal Analysis.

This technique was first devised by Roberts-Austen (173) and considerably simplified soon after by Burgess (174). The method uses two thermo-couple junctions embedded in the test sample and the inert material. These thermocouples are connected in opposition so that any small differences in the temperatures of the two junctions, when they are heated together, can be measured using a sensitive recording voltmeter. These temperature differences can be attributed to exothermic and endothermic processes occurring in the test sample. The equipment used in this work is based on a design by Grimshaw et. al. (175). About 0.5 g. of the sample was packed alongside the reference material, alumina, in a ceramic block. The block was heated in an electric furnace (Griffin and George Ltd). The temperature of the block and the temperature differential were recorded automatically over the temperature range of 100^{o}C to 1100^{o}C.

This technique was used to determine the decomposition temperature of tourmaline and also to investigate the nature of the material formed when tourmaline decomposes.

CHAPTER 10

Analysis.

(1) Determination of Boron.

(1.1) Review.

The methods of analysis for boron have been reviewed in a number of books (176, 177, 178, 179). Colorimetric, gravimetric and titrimetric methods have been proposed, but their application to many materials requires a difficult and frequently lengthy separating procedure.

(1.1.1) The Separation of Interfering Ions.

The most general method involves the removal of boron by distillation as its methyl ester (178). However, incomplete volatilisation can occur in the presence of aluminium, iron and silicon (175). The precipitation of such elements as their hydrous oxides can result in part of the boron being absorbed by the precipitate (175). Probably the most useful and certainly one of the most convenient methods of removing interfering ions is by the use of Ion Exchange resins. This technique was first used by Martin and Hayes (180), who found that the cation exchange resin used was capable of quantitatively removing interfering metal ions without loss of boron. Wolszon et. al. (182) and Schutz (183) have used a mixed bed technique consisting of a strong cation exchange resin mixed with a weak anion exchange resin. This system was found to be capable of removing all the cations and anions apart from boric, silicic and carbonic acids (184).

(1.1.2) Quantitative Methods.

(1.1.2.1.) Gravimetric determinations.

These methods are tending to become obsolete because titrimetric and other methods are so much more rapid and invariably more precise (178).

(1.1.2.2) Titrimetric determinations.

The basis of most titrimetric methods is that boric acid, a very weak acid in itself, becomes a relatively strong acid when complexed with certain polyhydroxy-compounds, such as invert sugar (180), glycerol (176) or mannitol (181). The main variations of the titrimetric method are:-

(a) Normal titration.

Using indicators such as p-nitrophenol and phenolphthalein for detecting the end point (185).

(b) Iodine-Thiosulphate titration (186).

The strong acidic properties of mannitol-boric acid are used to liberate iodine from an iodine-iodate solution the boric acid can then be determined indirectly via the iodine assay (178).

(c) Potentiometric titration.

This is probably the most convenient method of determining boron titrimetrically and after removing interfering ions the only further inconvenience is dissolved carbon dioxide which is easily removed by gently boiling the solution in a covered beaker. The main variation in experimental procedure cited in the literature is the variation in the value of the pH taken as the equivalence point, see Table 14.

TABLE 14

Potentiometric determination of boron.

Literature Reference	Value of pH after Addition of First Alkali	Value of pH Taken as equivalence Point after Addition of Mannitol
Hollander M and Rieman W. (187)	6.30	6.30
Martin J. R. and Hayes J. R. (180)	6.90	6.90
Kramer H. (181)	7.00	7.00

(1.1.2.3) Colorimetric determinations.

These methods are both inaccurate and extremely difficult to perform satisfactorily they are however capable of determining minute traces (< 10μg.) of boron. A number of dyes have been found that give characteristic colorations with boric acid in the presence of concentrated sulphuric acid. One of the best is probably 1,1 -dianthrimide (176,188), but curcumin (189), carminic acid (190)and chromotrope 2B (191) have also been used successfully.

(1.1.2.4) Miscellaneous methods.

One interesting method of determining boron has been described recently by Carlson and Paul (192). This technique utilises a liquid ion exchange membrane electrode, containing the boron specific resin Amberlite XE-243. The active group present is N-methylglucamine which complexes the boron when present as the tetrafluoroborate ion. By the use of this potentiometric method which is sensitive only to the tetrafluoroborate ion the need to separate interfering ions is alleviated.

Several instrumental techniques have been used to determine boron including Polarography (193,194) and Atomic Absorption Spectrometry (195).

(1.2) Experimental Procedure.

The procedure used in the determination of boron closely followed that described by Kramer (181). The exact method used, however, depended on the experiment being considered.

(1.2.1) Preparation of Ion Exchange column.

A glass chromatograph tube 20mm. by 300mm. with a sealed in coarse porosity fritted disk was used to contain the resin. To regulate the flow of liquid through the resin the tube was fitted with a rubber tube extension and screw clip. The tube was filled with a slurry of the cation exchange resin "Zeo-Karb 225" until a resin column about 200 mm. in length was formed. Before being used the resin was regenerated in the hydrogen form with 100 ml. of 4M.HCl and then washed with 50 ml. aliquots of water until the effluent gave a negative test for chloride ions.

(1.2.2) Use of Ion Exchange column.

If the solution obtained contained interfering cations the boron containing solution was always passed through the ion exchange column before beginning the potentiometric titration.

To ensure that the solution was not too acidic for passing through the resin 4 M. NaOH was added until a precipitate just formed, 4M.HCl was then added dropwise until the precipitate just redissolved. This slightly acid solution was then passed through the ion exchange column followed by four 50 ml. portions of water. The wash water being added when about 0.1cm. of supernatant solution is above the resin. The rate of flow was adjusted until about 15 ml. of solution was passing per minute. The solution collected was covered with a watch glass and then gently boiled for 5 minutes to remove carbon dioxide. The solution was then left to cool to room temperature before beginning the titration.

(1.2.3) Potentiometric titration.

The pH meter's electrodes and stirrer are introduced into the solution and if the solution is strongly acidic M.NaOH was slowly run in until the pH is approximately six. 0.05 M.NaOH was slowly run in until the pH 7.00 was obtained. About 10 g. of mannitol was then added and 0.05M.NaOH added until pH 7.00 was obtained. about 5 g. of mannitol was then added, if the pH fell more 0.05M.NaOH was added, this procedure was repeated until the further addition of mannitol did not affect the pH. The total volume of 0.05M.NaOH required to raise the pH to 7.00 after the addition of mannitol was recorded.

1 ml. of 0.05M.NaOH $\equiv$ 1.741 mg. of B_2O_3.

(2) Quantitative Determination of Iron.

(2.1) Review.

The methods of analysis for iron have been reviewed in a number of books (176, 177, 178, 179, 196).

(2.1.1) Gravimetric methods.

The classical method involves precipitation using NH_4OH followed by ignition and weighing as Fe_2O_3 (177). The precipitation with organic reagents has been used; oxine and its derivatives being widely used (197). All such methods are non specific for iron so lengthy separations are often required (177).

(2.1.2). Titrimetric methods.

Iron has been determined titrimetrically by a large number of methods based on redox (177), precipitation (177) and chelation (177) reactions. Probably the most convenient involves the oxidation of ferrous iron using $K_2Cr_2O_7$, $KMnO_4$ or $Ce(SO_4)_2$, or the EDTA titration(177).

(2.1.3) Colorimetric methods.

Numerous reagents have been proposed including O-phenanthroline (198),5-phenylsalicylic acid (199), potassium thiocyanate (200) and cupferron (177).

(2.2) Experimental Procedure.

The volumetric method used closely follows that described by Vogel (201).

(2.2.1) Reduction of ferric ion.

A drop of the solution to be analysed was tested for the presence of ferric ions using acidified potassium thiocyanate solution, if positive the ferric ions were reduced by the following method. To the solution in a conical flask was added 10 g. of granulated "analar" zinc and then 10 ml. of concentrated sulphuric acid. The reaction was accelerated by the addition of a few drops of copper sulphate solution. The flask was then stoppered with a rubber bung carrying a bunsen valve (201). This mixture was then left for at least 4 hours before testing a drop of the solution for the presence of ferric ions. It was found in all the experiments undertaken that the ferric ions were always completely reduced after this period of time. The solution was then filtered quantitatively into another conical flask.

(2.2.2) Titrimetric Analysis.

The solution obtained after the reduction was acidified by adding about 5 ml. of concentrated sulphuric acid. About 5 ml. of syrupy phosphoric acid was then added, followed by two drops of the indicator barium diphenylamine sulphate. This solution was then titrated against standard M/120.$K_2Cr_2O_7$, until the first permanent blue-violet coloration was obtained.

1 ml. of M/120.$K_2Cr_2O_7$ $\equiv$ 2.792 mg. of Fe.

(3) Determination of boron and iron in Tourmaline.

About 1.0 g. of <300 mesh tourmaline was weighed out into a nickel crucible and then intimately mixed with about 6 g. of sodium carbonate (176). The crucible was then covered and heated gently for 5 minutes to remove moisture. The crucible was then strongly heated over a Meker burner for 30 minutes. When cool the crucible was placed in a 150 ml. beaker containing 50 ml. of water. To complete the dissolution 10 ml. of concentrated hydrochloric acid was slowly poured down the side of the covered beaker. After dissolution the solution was quantitatively filtered and then transferred to a 250 ml. standard flask. 50 ml. of this solution was used each time for the boron and iron determinations.

CHAPTER 11

Decomposition Experiments.

These experiments can be conveniently divided into four sections:-

(1) The first series of experiments were designed to determine the decomposition temperature of iron tourmaline. The method used involved heating crystals of the density separated tourmaline (8/3) on a platinum lid for 1 hour at 10°C intervals between 800°C and 900°C.

The crystals were examined after the heat treatment by X-ray diffraction techniques and by the polarising microscope.

(2) About 500 g. each time of the (8–100) mesh iron tourmaline (8/1) was heated in the oven furnace for 1 hour at 100°C intervals between 900 and 1300°C and for 6 hours and 14 hours at 900°C. The material was then crushed in the mechanical mill, two fractions being collected after sieving, one between (100–300) mesh and the other smaller than 300 mesh.

The (100–300)mesh fraction was used in the extraction experiments to be described later, whilst the fine material was mainly used in an X-ray diffractometric investigation of the decomposed material.

(3.1) Small quantities of the (100–300) mesh iron tourmaline (8/1) was placed in an alumina boat and heated in the tube furnace at a number of temperatures between 800 and 1200°C in a steam of nitrogen, methane or ammonia. In another series of experiments (100-300) mesh tourmaline (8/1) was mixed with activated charcoal in the weight ratio of four to one. A small portion of this mixture was poured each time into an alumina boat. This boat was then introduced into the tube furnace in a stream of nitrogen and then left for specific periods of time at various temperatures between 800 and 1200°C.

The decomposed material was then examined by X-ray techniques to investigate the variation in the nature of the decomposition products with changing conditions.

(3.2) A large quantity of the (8-100) mesh iron tourmaline (8/2) was mixed with activated charcoal in the weight ratio of four to one. About 150 g. was poured each time into a graphite crucible which after replacing the graphite lid, was placed in the oven furnace for 1 hour at temperatures between 800 and 1300°C in intervals of 100°C.

The material was then roughly crushed using the "jaw" crusher and the remaining activated charcoal was removed through a 300 mesh sieve. The material was then milled and two fractions were collected one between (100-300) mesh and the other smaller than 300 mesh.

The (100-300) mesh fraction was used in some liquid extraction studies, whilst the fine material was examined by X-ray diffractometry.

(4) The powdered magnesium tourmaline (8/4) was decomposed in the oven furnace at 100°C temperature intervals between 900 and 1300°C. The decomposed material was then finely crushed before being examined by X-ray diffractometry.

CHAPTER 12

Liquid-Extraction Experiments.

(1) Apparatus.

In all the liquid extraction experiments the (100-300) mesh decomposed tourmaline was used. The boiling acid experiments were carried out in pyrex round bottomed flasks fitted with a condenser. In the acid extraction studies carried out at lower temperatures 150 ml. conical flasks, with stirrers, were used. The flasks containing the appropriate volume of acid were left immersed in the constant temperature bath for at least two hours prior to adding the decomposed tourmaline.

In the boiling alkali and water experiments a 250 ml. silica round bottomed flask, fitted with a silica condenser, was used.

(2) Analysis.

(2.1) Acid Extraction:-

At the end of the requisite extraction time the suspension was quickly filtered to stop further reaction. After washing the filter paper etc. and cooling to room temperature the solution was made up to the mark in a 100 ml. standard flask.

The solution was then divided into two for the determination of the amount of boric oxide and iron extracted, see Chapter 10.

(2.2.) Alkali and Water Extraction:-

At the end of the requisite extraction time the suspension was quickly filtered and after washing the filter paper etc. the solution was made just acid to methyl orange. The solution was then boiled gently for 5 minutes to remove carbon dioxide. Since the iron is not extracted by these reagents and only a relatively small quantity of silica is present in the solution the whole of the solution was used for the boron determination, see Chapter 10. 1. 2.

(3) X-ray Diffraction.

In certain instances the powder remaining after the extraction process was examined by X-ray diffractometry, see Chapter 9. 3.

CHAPTER 13

Pyrohydrolysis Experiments.

(1) Apparatus.

The tube furnace described in Chapter 9.1 was used for the pyrohydrolysis experiments.

In the final form this apparatus was fitted with a pre-heater. This was made by wrapping the alumina tube for a length of 300 mm. with double stranded 36 gauge nichrome wire. The wire was then covered with a layer about 20 mm. thick of wet alumina cement. After leaving the cement to dry another length of double stranded wire was wrapped round the cement. This wrapping was then covered with a layer of alumina cement about 40 mm. thick. After leaving the cement to dry for a couple of days the two wrappings were connected in series and then connected to a variac. Using this assembly the inside of the alumina tube could be maintained at 1050°C, see Figure 3.

The source of steam was a small boiler designed to produce a constant given quantity of vapour flowing through the furnace. To achieve this constant given flow of vapour the water was maintained at a given level using a variable drip feed system, see Figure 4.

The vapour emerging from the furnace was condensed, after being cooled by flowing through a short length of copper tubing, by a small condenser and then collected in weighed beakers.

(2) Procedure.

The temperature of the inside of the alumina tube was measured with the water vapour flowing using a platinum alloy thermocouple. It was found that when using temperatures above 1250°C that the surface was cooled by between 5 and 10°C. This was taken into account by plotting the heating and cooling profiles of the furnace when the steam is disconnected and then re-connected. In this way the optimum time could be assessed between the introduction of the sample and re-connecting the steam supply. Using this method the error in the actual temperature of the sample just after being introduced in relation to the equilibrium temperature with the steam passing could be minimised.

The solution collected in the weighed beakers was analysed for boron after requisite time intervals, see Chapter 10. Since the solutions did not contain any interfering ions they were titrated directly without prior use of the ion exchange column.

FIGURE 3.

High temperature pyrohydrolysis apparatus.

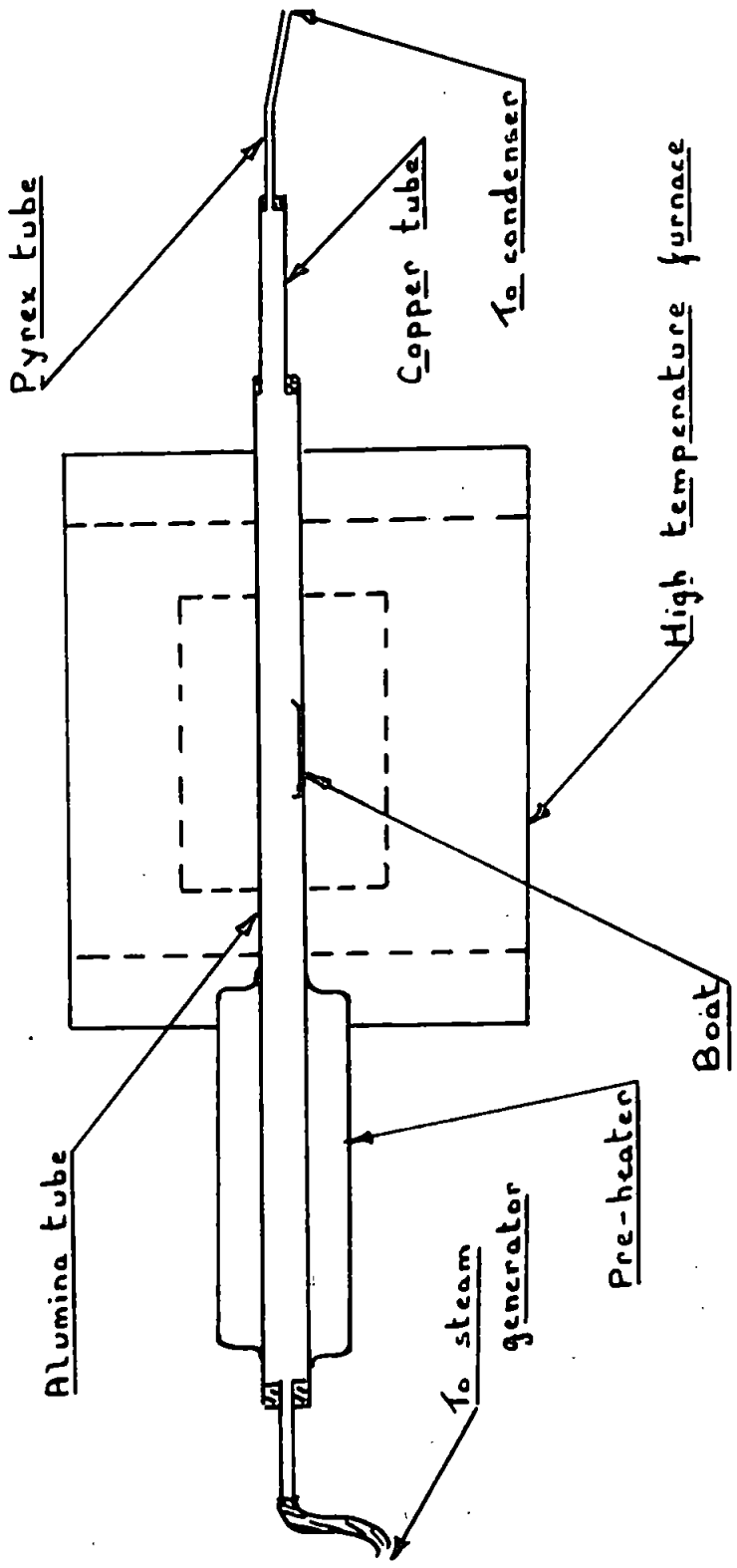

RESULTS AND DISCUSSION

CHAPTER 14

Analysis of Tourmaline.

(1) Qualitative Analysis.

Qualitative spectrographic analysis of the powdered schorl samples (8/1, 8/2, 8/3) was carried out using a Hilgar Large Quartz Spectrometer in the wavelength range 2760 to 4720 Å. The photographic plates obtained were compared with a set of reference plates to ascertain the elements present in the schorl samples, a summary of the results obtained is given in Table 15.

TABLE 15

Qualitative Analysis of Iron Tourmalines used.

Approximate order of abundance	Sample (8/1) Roche Rock	Sample (8/2) Dartmoor	Sample (8/3) Lee Moor
Major	Na, Si, Al, Fe	Na, Si, Al, Fe	Na, Si, Al, Fe
Minor		Ca, K, Mg, Sn	Ca, K, Mg, Sn
Trace	Ti, K	Li, Ti	Li, Ti.

(2) Quantitative Analysis.

The tourmalines (8/1) and (8/2) were quantitatively analysed by the methods described in Chapter 10. Only boron and iron were determined as these were the only elements present that were studied in detail. The results of these analyses are compared with quantitative spectrographic analysis of tourmalines in the S. W. of England by Power (35) in Table 16.

The "Roche Rock" tourmaline (8/1) was therefore found to have a composition close to that for the "end member" of the schorl series. The composition of this iron tourmaline is therefore close to $NaFe_3Al_6B_3Si_6O_{31}H_4$.

The two "Dartmoor" tourmalines (8/2 and (8/3) were found to contain a small amount of magnesium, see Table 15, A comparison with the results obtained by Power (35) indicated that these tourmalines lie on the dravite-schorl solid solution series with compositions close to $NaFe_2MgAl_6B_3Si_6O_{31}H_4$.

TABLE 16

Quantitative Analysis of Iron Tourmalines used.

Element and Oxide	Analysis of Roche Rock schorl		Analysis of Dartmoor Tourmalines		
	Sample (8/1)	Analysis Power (35) No. 54/1P	Sample (8/2)	Analysis by Power (35) No. 26/P	No. T2
B_2O_3	8.98		8.70		
Fe	10.90	11.2	8.87	9.5	7.6
Mg		0.10		2.65	2.95
Mn		0.26		0.33	0.12
Na		1.35		1.39	1.14
Ca		0.12		0.48	0.49
Li		—		3.8×10^{-2}	3.0×10^{-2}
Ti		0.12		0.40	0.16
Sn		2.2×10^{-3}		3.0×10^{-2}	4.7×10^{-2}

CHAPTER 15

Decomposition of Tourmaline.

(1) Decomposition in Air.

(1.1) Decomposition Temperature.

(1.1.1) Using Polarising Microscope.

The effect of heat on the density separated tourmaline (8/3) was investigated using a polarising microscope.

The original crystals were observed to be a brown-green colour in ordinary transmitted light. When heated for 1 hour at temperatures between 750 and 840°C the crystals were observed to be deep red in transmitted light; this colour change is probably due to the formation of a surface layer of Fe_2O_3. When these heated crystals were examined under plane polarised light they were all found to be strongly pleochroic and uniaxially negative (204), as are all naturally occurring tourmalines (32).

After heating the crystals for 1 hour at 870 ± 10°C it was found that most of the crystals were opaque and the few that were thin enough to be examined in transmitted light appeared to be optically isotropic. One interesting observation was that the more "perfect" crystals appeared to have a slightly higher decomposition temperature.

(1.1.2) Using X-ray Diffractometry.

In this investigation the (100-300) mesh schorl (8/2) was heated for 1 hour in steps of 10°C from 840 to 900°C. On examining the X-ray diffractometer traces of this thermally treated material it was found that reflections due to schorl were no longer present in the powder that had been heated for 1 hour at 890 ± 10°C.

(1.1.3) Using Differential Thermal Analysis.

A Differential Thermal Analysis trace of the (100-300) mesh tourmaline (8/1) was obtained using alumina as the reference material and a heating rate of about 10°C/minute.

The curve obtained showed a steady drift of the base line starting at 220°C indicating the presence of some slow exothermic process. This could be the oxidation of the ferrous ions present in the structure by OH^- ions during the low temperature dehydration process (58), which was shown by Kurylenko (63) to begin at temperatures close to 200°C.

A small endothermic peak was obtained at 910°C and a much larger one with the peak at 970°C was also observed. These peaks are very close to the main endothermic process peak observed at 960°C by Kurylenko (63) and thought to be associated with the volatilisation of boric oxide. However, these peaks are almost certainly associated with the heat changes occurring during the breakdown of the crystal lattice of tourmaline.

(1.1.4) Conclusions.

The probable decomposition temperature of schorl as determined by optical and X-ray techniques is 880 ± 10°C. This value is in reasonable agreement with a decomposition temperature of 850 ± 10°C obtained by Machatschki (61).

Kurylenko (63) found that the decomposition temperature was 970°C, using Differential Thermal Analysis, which does not appear to be consistent with the lower value of 880 ± 10°C found in this investigation. This may be due to the rate of decomposition being extremely slow at 880°C and any heat changes involved in the decomposition process may therefore be recorded only at higher temperatures, when the dynamic Differential Thermal Analysis technique is used.

(1.2) Size of Crystals present in decomposed tourmaline.

(1.2.1) Using Polarising Microscope.

The only sample of decomposed schorl (8/3) that was transparent enough to be examined by transmitted light was one that had been heated for 1 hour at 1350°C and then quenched in water.

When a thin sliver of this decomposed schorl was examined under the polarising microscope the bulk of the material was found to be isotropic and pale green in colour. Embedded in this amorphous iron glass were needle shaped anisotropic crystals.

The size of about fifty such microcrystals were determined by comparison with the standard graticules mounted in the microscope's eyepiece, see Chapter 9. The mean size of these microcrystals, together with the standard deviation, was found to be equal to : 25 ± 10μ by 3 ± 2μ by 3 ± 2μ.

(1.2.2) Using X-ray Diffractometry.

Because all the decomposed tourmaline samples were opaque, apart from the one described above, an attempt was made to determine the mean crystallite size using X-ray diffractometry, see Chapter 9.3.

X-ray traces were obtained for the tourmaline samples decomposed at 100°C. intervals between 900 and 1300°C; when compared with a reference trace obtained of (100-300) mesh powdered mullite no measurable broadening could be observed for any of the decomposed samples.

These results suggest that the mean crystallite size of the microcrystals are larger than about 1μ (168). The X-ray diffraction photograph obtained of a stationary "crystal" of decomposed schorl (8/3), using the flat-plate camera, consisted of a concentric series of continuous diffracted rings with no trace of spotiness, see Figure 5, This observation indicates that the mean size of the microcrystals is less than about 10μ (203).

(1.2.3) Conclusions.

The combination of the X-ray results with those obtained using optical microscopy lead to the conclusion that the size of the microcrystals formed when tourmaline is decomposed, in the temperature range 900 to 1350°C, is always approximately the same and equal to 25 ± 10μ by 3 ± 2μ by 3 ± 2μ .

(1.3) Orientation of Crystals present in Decomposed Tourmaline.

Many layer type silicates such as magnesium chlorites (206) have been found to produce orientated decomposition products (205). It was therefore thought possible that tourmaline may similarly produce orientated decomposition products because of its polar and highly orientated structure.

X-ray photographs of several of the single crystals of schorl (8/3) that had been previously heated

in the temperature range of 800 to 900^{o}C were obtained using the flat plate camera, see Chapter 9.3.

The photographs obtained were either due to a slightly altered single crystal of tourmaline or of a completely decomposed "crystal" which showed the typical circular diffracted rings of a polycrystalline material, see Figure 5. No intermediate state was observed in this investigation between tourmaline itself and the completely decomposed polycrystalline material; although Kurylenko (45) has found some evidence for the existence of a partially decomposed tourmaline lattice, see Chapter 2.6.

The flat plate transmission photographs of the decomposed tourmaline "crystals" consisted of a concentric set of circular rings of unequal thickness throughout their circumference. It was observed that the diffracted rings were always sharpest in the direction of the original a-axis in the crystal and became more diffused as the angle from this axis increased. Similar photographs have been obtained by Hull (199) for slightly orientated polycrystalline aluminium wire. It would therefore appear that the needle shaped microcrystals are partially orientated, with the needles pointing on average in a certain specific direction, relative to the original crystal axes in tourmaline.

It was found in the last section (1.2) that the thickness of these microcrystals is approximately $3 \pm 2\mu$, which is only slightly above the upper limit of significant X-ray line broadening. The diffuse nature of the diffracted rings in the direction of the original c - axis could therefore be due to the needle shaped microcrystals pointing on average away from this axis, see Figure 5. If this assumption is true then there is probably some relationship between the original crystal structure of tourmaline and the orientation of the microcrystals formed during the decomposition process.

(1.4) Nature of Decomposed tourmaline.

(1.4.1) Crystalline products formed.

The finely crushed schorl (8/1) and dravite (8/4) that had been decomposed for 1 hour in 100^{o}C intervals between 900 and 1300^{o}C, see Chapter 11, was carefully examined by X-ray diffractometry using Cu (K_{α}) radiation. The calculated interplanar spacings for each of the samples is presented in tabulated form in Tables 17 and 18.

In view of the complex composition of tourmaline it was thought desirable to study some simpler oxide systems in order to elucidate the exact nature of the decomposition products. Therefore the effect of heat on certain oxides and relevant oxide mixtures was investigated. In these control experiments a temperature of 1100^{o}C and a reaction time of 4 hours were used, as it was thought that these conditions would be representative of the thermal conditions used to investigate the decomposition of tourmaline.

Kaolinite ($Al_2O_3.2SiO_2.2H_2O$) was one of the binary systems studied, because this mineral contains the same molar ratio of Al_2O_3 to SiO_2 as tourmaline. A mixture of boric oxide and kaolinite was made up, in the same molar ratio as these oxides exist in tourmaline, to investigate the effects of boric oxide on the decomposition of kaolinite. Alumina and alumina mixed with the requisite proportion of boric oxide were also investigated. After the heat treatment each of these reference samples was crushed and then examined using the X-ray

FIGURE 5.

Flat plate transmission X-ray photograph of a decomposed tourmaline crystal and a schematic representation of the probable overall orientation of the micro-crystals within this decomposed "crystal".

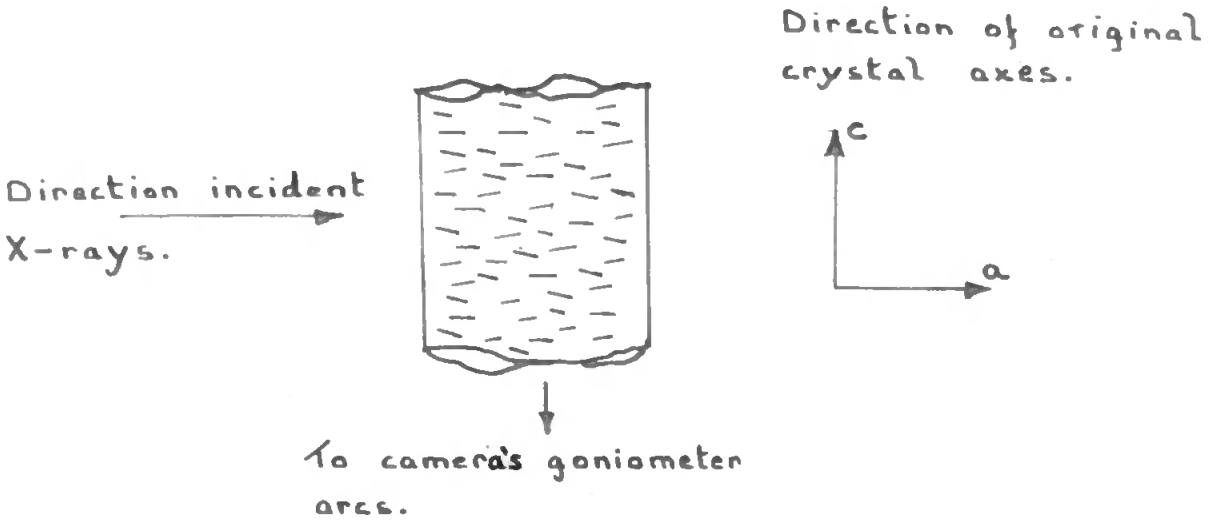

diffractometer described in Chapter 9.3.2. The calculated interplanar spacings for each of the samples are presented in tabulated form in Table 19.

The system $B_2O_3 - SiO_2$ was not investigated as earlier work found that binary compound formation did not occur (100). For a similar reason the system $Na_2O - B_2O_3 - SiO_2$ was not investigated as Morey (95) found no evidence for compound formation in the composition range close to that in tourmaline. In the ternary system $FeO - SiO_2 - Al_2O_3$ investigated in slightly reducing conditions by Schairer and Yaji (110), mullite was the only compound that crystallised in the composition range close to that in tourmaline.

The interplanar spacings obtained in this investigation for the thermally treated $Al_2O_3 - B_2O_3$ mixture are consistent with those obtained by Scholze (108) for the compound $9Al_2O_3.2B_2O_3$. The X-ray spacings due to $9Al_2O_3.2B_2O_3$ are compared with those from mullite ($3Al_2O_3.2SiO_2$) in Figure 6. The overall pattern for each is very similar indicating that the complete substitution of the silicon atoms in the mullite lattice by boron atoms only slightly affects the overall crystal structure (103). However, there are a few significant differences between the two patterns that can be used for identification purposes.

The interplanar spacings obtained of decomposed kaolinite, the thermally treated kaolinite – boric oxide mixture and decomposed schorl (8/1) are compared with those given the literature for mullite in Figure 6. The overall pattern obtained from decomposed schorl (8/1) indicates that the main decomposition product is a mullite like crystalline phase. The presence of any free Al_2O_3 or $9Al_2O_3.2B_2O_3$ would be easily identified using the spacings of 2.084 Å and 1.603 Å for Al_2O_3 or the 4.38 Å spacing for $9Al_2O_3.2B_2O_3$. The absence of such reflections indicates that all the Al_2O_3 present in schorl is used during the decomposition process in the formation of the mullite like phase.

Only the low intensity spacing of 2.92 Å is then unaccounted for in the decomposed schorl (8/1), although the spacing at 3.64 Å is also in doubt, see Table 20. The 2.92 Å spacing was compared with that listed in the ASTM index (212) and of the compounds scanned the only probable one with the same spacing was $\gamma - Fe_2O_3$; the other two main reflections listed for $\gamma - Fe_2O_3$ are also found to be present in decomposed schorl:-

$\gamma - Fe_2O_3$ (212) (d Å).	2.94 (90)	2.51 (100)	2.08 (90)
Decomposed Schorl (d Å).	2.92 (20)	2.50 (50)	2.08 (20)

The X-ray diffraction results indicate that decomposed schorl contains a mullite like phase and a small quantity of $\gamma - Fe_2O_3$ as the only crystalline phases. This confirms the results obtained by Korzhinkii (65) in a similar investigation.

The spacings obtained for decomposed dravite (8/4) are compared with those for mullite and decomposed schorl (8/1) in Figure 6. The overall pattern due to decomposed dravite (8/4) indicates that the only crystalline product is a mullite like phase. However, when tourmaline decomposes with complete removal of the free alumina to the mullite like phase a considerable proportion of "free" silica remains:-

$$Na_2O.(XO)_6\ 6Al_2O_3.3B_2O_3.12SiO_2.4H_2O \longrightarrow 2(3Al_2O_3.2SiO_2) + 4H_2O + Na_2O.3B_2O_3.8SiO_2.$$

FIGURE 6.

Comparison of X-ray reflections of mullite with those obtained from decomposed tourmaline, decomposed kaolinite, etc.

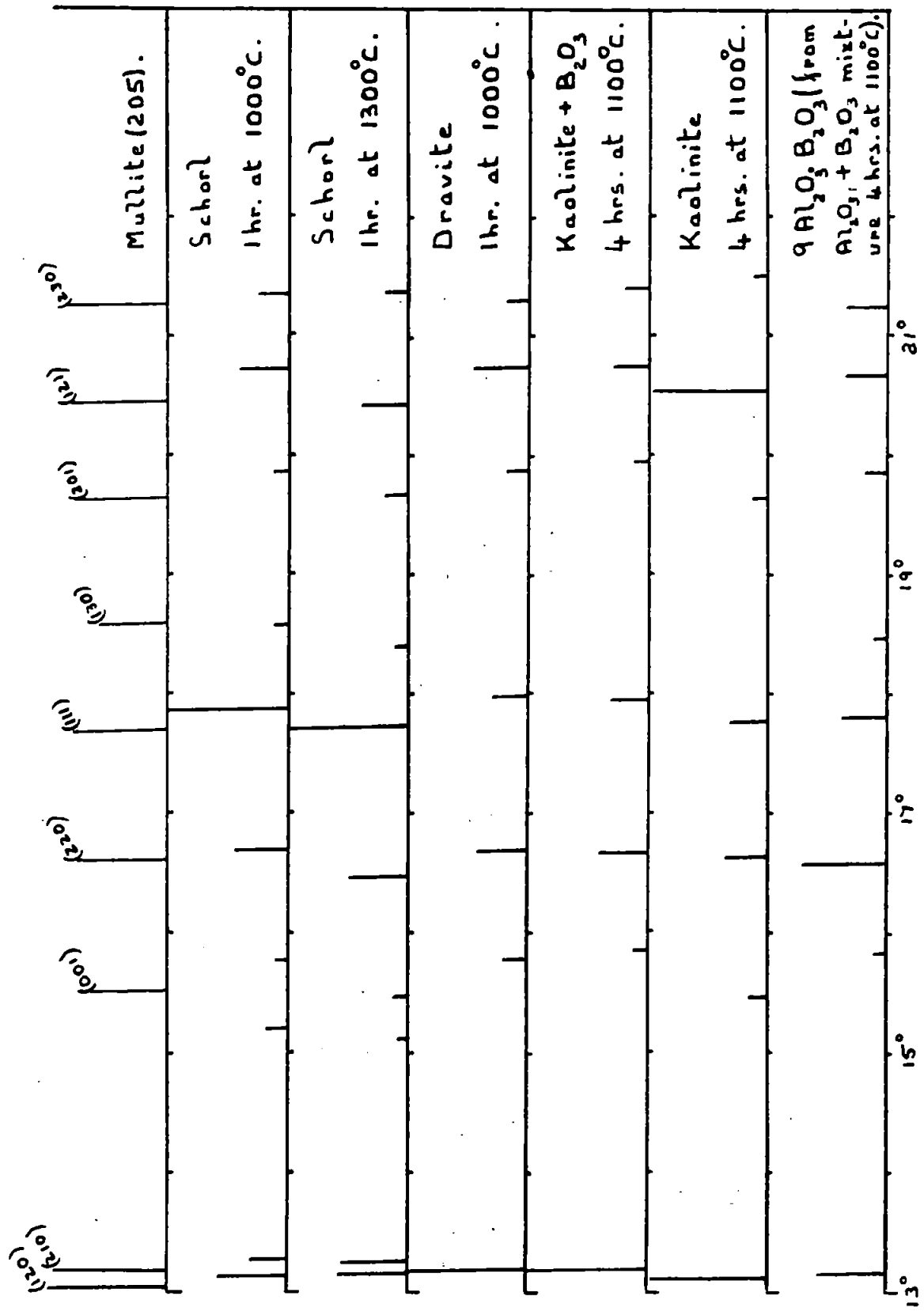

TABLE 17

X-ray Diffractometry of material formed when

when Schorl Decomposed in Air.

Decomposition of Tourmaline from Roche Rock (8/1).									
900°C for 1 hour.		1000°C for 1 hour.		1100°C for 1 hour.		1200°C for 1 hour.		1300°C for 1 hour.	
I	d Spacing	I	d Spacing	I	d Spacing	I	d Spacing	I	d Spacing
2	5.32	2	5.32	3	5.32	5	5.34	3	5.36
		1	3.64	1	3.64	1	3.64		
6	3.38	6	3.38	6	3.38	6	3.36	6	3.37
6	3.34	4	3.34	5	3.35	6	3.33	6	3.34
		2	2.992	1	2.932			3	2.941
1	2.823	1	2.823	1	2.832	1	2.841	1	2.850
3	2.667	5	2.675	7	2.683	10	2.675	6	2.699
7	2.494	10	2.501	10	2.501	8	2.495	10	2.521
		1	2.410	1	2.416	1	2.442	1	2.429
1	2.253	1	2.258	2	2.258	2	2.269	3	2.275
3	2.170	4	2.170	5	2.180	6	2.190	5	2.195
2	2.107	3	2.107	3	2.107	2	2.107	2	2.106
		2	2.079	2	2.079	1	2.079	1	2.079
		1	1.819	3	1.822	4	1.819	2	1.836
1	1.675	2	1.679	4	1.682		1.682	2	1.693
		1	1.601	1	1.598			3	1.603
		1	1.581	2	1.583	1	1.586		
1	1.508	3	1.508	3	1.506	2	1.515	3	1.521
2	1.464	3	1.467	2	1.469	1	1.471	3	1.471
		1	1.442	2	1.445	1	1.445	1	1.431
		1	1.413	2	1.417	1	1.423		
		1.	1.371	3	1.369	1	1.395		
		1	1.322	1.	1.322				
		1	1.300						
		1.	1.266						
		2	1.247	2	1.251				

(Cont. of Table No. 17).

Key:- I is the relative intensity of reflections.

d (Å) is calculated using the Bragg Equation (168).

TABLE 18

X-ray Diffractometry of material

formed when Dravite Decomposed.

Decomposition of Tourmaline from Brazil (8/4)									
900°C for 1 hour		1000° C for 1 hour		1100°C for 1 hour		1200°C for 1 hour		1300°C for 1 hour	
I	d spacing Å	I	d spacing Å	I	d spacing Å	I	d spacing Å	I	d spacing Å
9	5.32	10	5.32	9	5.36	8	5.38	9	5.38
10	3.37	9	3.37	10	3.38	10	3.39	10	3.39
2	2.816	1	2.823	1	2.823	1	2.832	3	2.841
7	2.675	5	2.675	5	2.667	5	2.683	7	2.691
5	2.488	3	2.488	4	2.501	4	2.501	4	2.518
2	2.252	2	2.258	1	2.258	1	2.264	1	2.269
5	2.165	5	2.170	4	2.175	4	2.170	5	2.185
4	2.097	2	2.116	3	2.111	2	2.111	2	2.116
		1	1.717						
1	1.682	1	1.682	1	1.678	1	1.682	1	1.687
		1	1.576	1	1.576	1	1.581	1	1.586
4	1.503	4	1.506	4	1.506	3	1.508	4	1.510
		1	1.447						
		1.	1.411	1	1.415	1	1.417	1	1.419
				1	1.254	1	1.254		

Key:- I .is the relative intensity of reflections

d calculated using Bragg equation (168).

TABLE 19

X-ray Diffractometry of Some Thermally

Treated Model Phase Systems.

Oxides heated for 4 hours at 1100°C.							
Kaolinite		Kaolinite $+B_2O_3$		Alumina (Al_2O_3)		Al_2O_3 $+ B_2O_3$	
I	d (Å) spacing	I	d (Å) spacing	I	d (Å) spacing	I	d (Å) spacing
1	5.32	10	5.32			10	5.40
						8	4.38
						2	3.77
				4	3.50		
10	3.37	10	3.35	7.	3.38		
1	2.876	1	2.806				
				4	2.723		
3	2.675	4	2.675			7	2.691
				9	2.556		
3	2.515	3	2.488			4	2.508
				3	2.379	1	2.432
1	2.280	1	2.248	1	2.258	2	2.258
10	2.185	3	2.165			4	2.175
1	2,092	2	2.102				
				10	2.084		
				6	1.901		
				10	1.603		
2	1.581	1	1.583			1	1.588
5	1.515	2	1.510			3	1.510
3	1.433	1	1.447			1	1.447
				6	1.402		
				7	1.385		
				7	1.371		

TABLE 20

Comparison of Interplanar Spacings of Mullite with those obtained from Decomposed Schorl.

Tourmaline (8/1) 1 hour at 1000°C		Mullite ($3Al_2O_3.2SiO_2$) reference (205)			Tourmaline (8/1) 1 hour at 1000°C		Mullite ($3Al_2O_3.2SiO_2$) reference (205)		
I	d Å	I	d Å	hkl	I	d Å	I	d Å	hkl
2	5.32	7	5.37	110			7	1.698	321
1	3.64	2	3.76	200			7	1.693	420
6	3.30	9	3.418	120			8	1.596	041
4	3.34	10	3.383	210			6	1.573	401
2	2.922						9	1.522	331
1	2.823	7	2.878	001			6	1.459	421
5	2.675	8	2.686	220			8	1.439	002
10	2.501	9	2.538	111				Etc.	
1	2.410	6	2.414	130					
1	2.258	8	2.289	201	Note: The reflections present ~~undecomposed~~ in decomposed tourmaline after d_{hkl} = 1.819 Å were not included as they could not be matched exactly with particular Mullite reflections.				
4	2.170	9	2.201	121					
2	2.079	8	2.115	230					
		4	2.103	320					
		5	1.886	400					
1	1.819	7	1.839	311					
	Etc.	3	1.791	330					
		6	1.709	240					

If X = Mg then

$$3MgO + 8SiO_2 \longrightarrow 3(MgO.SiO_2) + 5SiO_2$$

This free silica could react with the magnesia producing, for example enstatite ($MgO.SiO_2$) (149), as the decomposition scheme written above would indicate. Kurylenko (63) has in fact observed the presence of enstatite in decomposed dravite. The difference between the results obtained in these experiments as compared to those obtained by Kurylenko (63), may be due to a difference in the rate of cooling the decomposed dravite or to a difference in the sensitivity of the X-ray equipment.

(1.4.2.) Cell Dimensions of "Mullite" Phase in Decomposed Tourmaline.

The interplanar spacings of decomposed kaolinite were found to be similar to those for mullite, whilst the spacings for the thermally treated kaolinite-boric oxide mixture, although similar in overall pattern, were closer to those for decomposed tourmaline, see Figure 6. It was therefore thought probable that these differences could be due to the substitution of boric oxide for silica or alumina in the mullite like phase in decomposed tourmaline and in the thermally treated kaolinite-boric oxide mixture.

The cell dimensions of all the mullite like phases formed were calculated to establish whether or not the incorporation of boric oxide affected a particular cell parameter, or all, and if the decomposition temperature changed the precise composition of this phase.

Before the cell dimensions can be calculated each reflection must be indexed. An attempt was made to determine the indices for the various reflections produced by the mullite like phase in decomposed schorl, by constructing a $\sin^2\Theta_{hkl}$ difference table as described by Henry et. al. (207). This technique involves the construction of a $\sin^2\Theta$ difference table and can be used with increasing difficulty for the cubic, tetragonal, hexagonal and orthorhombic systems respectively. For the most general of the systems the $\sin^2\theta$ equation (3) required, is obtained by combining the Bragg equation (1) with the expression (2) relating the interplanar spacings (d_{hkl}) to the cell dimensions for the orthorhombic system (207):-

$$2d \sin\Theta_{hkl} = \lambda \quad \text{.....(1)}$$

$$\frac{1}{d^2_{hkl}} = \frac{h^2}{a^2} + \frac{k^2}{b^2} + \frac{l^2}{c^2} \quad \text{.....(2)}$$

(2)

$$\sin^2\Theta_{hkl} = \frac{\lambda^2}{4a^2}h^2 + \frac{\lambda^2}{4b^2}k^2 + \frac{\lambda^2 l^2}{4c^2}$$

$$\sin^2\Theta_{hkl} = Ah^2 + Bk^2 + Cl^2 \quad \text{.....(3)}$$

The three constants in equation (3) have to be evaluated before the reflections can be indexed and the cell dimensions calculated. The technique described by Henry et. al. (207) for solving this equation involves plotting the differences in the $\sin^2\Theta_{hkl}$ values of the low angle reflections and then trying to discern if any value or multiple of that value occurs particularly frequently.

The results obtained using this technique are shown in tabulated form in Table 21. However, no

particularly frequent values could be discerned which were of use, the technique was therefore abandoned. The low angle reflections in the decomposed materials were therefore assumed to have the same index as that of the corresponding reflection in mullite, see Table 20.

TABLE 21

Difference in $Sin^2 \theta_{hkl}$ values for Reflections from Schorl Decomposed for 1 hour at 1000°C.

Sin^2	Differences												
0208													
0518	310												
0529	321	11											
0745	527	217	207										
0826	618	308	297	90									
1017	809	499	488	191	101								
1176	968	658	647	440	350	249							
1255	1047	737	726	519	429	328	79						
1331	1123	813	802	595	505	404	155	76					
1367	1159	849	838	631	541	440	191	112	36				
1786					960	859	610	531	455	419			
2083							910	831	755	719	300		
2306									975	939	520	220	
2370											614	314	96
											810	510	296

The (001), (201) and (121) reflections were used for calculating the three cell dimensions. The first two reflections were chosen because they had the simplest indices required for the calculation of the a and c cell dimensions and were therefore not subject to the same cumulative errors that would occur if more complex reflections were chosen: The strong (121) reflection was chosen because it was easily measured and also because this measurement was subject to a slightly smaller error than the lower angle reflections (207).

The cell dimensions were calculated using equation (1) which relates the interplanar spacings (d_{hkl}) to the cell dimensions for the orthorhombic system (207):—

$$\frac{1}{d^2_{hkl}} = \frac{h^2}{a^2} + \frac{k^2}{b^2} + \frac{l^2}{c^2} \quad ----(1)$$

This equation (1) reduces to the three following when the (001), (201) and (121) reflections are used for calculating the cell dimensions:-

$$\frac{1}{d^2_{001}} = \frac{1}{c^2}; \quad \frac{1}{d^2_{201}} = \frac{4}{a^2} + \frac{1}{c^2};$$

$$\frac{1}{d^2_{121}} = \frac{1}{a^2} + \frac{4}{b^2} + \frac{1}{c^2}$$

Using these three equations the cell dimensions of the mullite like phase in schorl (8/1) that had been heated for 1 hour at 1200°C were calculated as follows:-

$$\frac{1}{d^2_{001}} = \frac{1}{c^2}$$

$$\frac{1}{2.841^2} = \frac{1}{c^2}$$

$\therefore$ c = 2.841 Å.

Substituting for c in (201) reflection:-

$$\frac{1}{d^2_{201}} = \frac{4}{a^2} + \frac{1}{2.841^2}$$

$$\frac{4}{a^2} = \frac{1}{2.269^2} - \frac{1}{2.841^2}$$

$\therefore$ a = 7.538 Å.

Substituting for a and c in (121) reflection:-

$$\frac{1}{d^2_{121}} = \frac{1}{7.538^2} + \frac{4}{b^2} + \frac{1}{2.841^2}$$

$$\frac{4}{b^2} = \frac{1}{2.185^2} - \frac{1}{7.538^2} - \frac{1}{2.841^2}$$

$\therefore$ b = 7.670 Å.

The cell dimensions of the mullite like phases in the thermally treated kaolinite-boric oxide mixture, decomposed kaolinite and decomposed tourmaline are compared with those given in the literature for mullite ($3Al_2O_3.2SiO_2$) (205) in Table 22.

Each reflection on the diffractometer traces could be measured to within about 0.05°, which corresponds to an error in the interplanar spacing for the (001) reflection of approximately 0.01 Å. The c-cell dimension can therefore be determined to within 0.01 Å, however, the other cell dimensions could not be determined with this degree of accuracy due to cumulative errors. The calculation of these errors was not undertaken because the simple technique used to calculate the cell dimensions did not warrant the effort that would have to be spent on devising a useful statistical treatment of the results.

TABLE 22

Comparison of Cell Dimensions of Mullite like Phase

in Thermal Treated Tourmaline and certain Model Phase

Systems with those of Mullite ($3Al_2O_3.2SiO_2$).

	Roche Rock Schorl (8/1)		
	Cell Dimensions		
Temperature	a (Å)	b (Å)	c (Å)
1 hr. at 900°C	7.48	7.64	2.82 ± 0.01
1 hr. at 1000°C	7.53	7.60	2.82 ± 0.01
1 hr. at 1100°C	7.53	7.64	2.83 ± 0.01
1 hr. at 1200°C	7.54	7.67	2.84 ± 0.01
1 hr. at 1300°C	7.56	7.77	2.85 ± 0.01
Mullite (205)	7.537	7.671	2.878
Dravite from Brazil (8/4)			
1 hr. at 900°C	7.53	7.59	2.81 ± 0.01
1 hr. at 1000°C	7.53	7.60	2.82 ± 0.01
1 hr. at 1100°C	7.53	7.65	2.82 ± 0.01
1 hr. at 1200°C	7.52	7.63	2.83 ± 0.01
1 hr. at 1300°C	7.51	7.67	2.84 ± 0.01
Mullite (205)	7.537	7.671	2.878
Kaolinite 4 hrs. at 1100°C	7.54	7.64	2.86 ± 0.01
Kaolinite - Boric oxide mixture 4 hrs. at 1100°C	7.52	7.62	2.81 ± 0.01

$2(Al_2O_3.2SiO_2.2H_2O)$ ⟶ $2Al_2O_3.4SiO_2 + 4\,H_2O$

Kaolinite

metakaolin

↓

$2Al_2O_3.3SiO_2 + SiO_2$

spinel like phase

↓

$2Al_2O_3.2SiO_2 + SiO_2$

mullite like phase

↓

$2Al_2O_3.4/3SiO_2 + 2/3SiO_2$

mullite

The a and c cell dimensions of decomposed kaolinite are to within experimental error the same as those for mullite, however, the b- cell dimension appears to be slightly shorter. This result is in agreement with the mechanism proposed by Brindley and Nakakira (208) for the decomposition of kaolinite. Their proposed mechanism is shown schematically at the bottom of the previous page. Therefore the thermal treatment of kaolinite at 1100°C for 4 hours produces a slightly distorted mullite like crystalline phase.

When the cell dimensions of the thermally treated kaolinite-boric oxide mixture are considered, the major difference between these and those for decomposed kaolinite or mullite is the c-cell dimension. Since the only difference between the two kaolinite experiments was the addition of boric oxide to one, the difference in the c-cell dimension is probably due to the incorporation of boric oxide into the mullite phase. Similarly the c-cell dimension of the mullite like phase in decomposed tourmaline is shorter than the same parameter in either decomposed kaolinite or mullite ($3Al_2O_3.2SiO_2$), indicating that the mullite like phase contains boron. The degree of shortening, however, decreases as the decomposition temperature increases.

The ionic radius of B^{3+} is smaller than Si^{4+} or Al^{3+}, see Table 23. The subsitution for either ion by boron would probably lead to a contraction in one or more of the cell parameters. This theoretical argument lends further support to the previous X-ray evidence which indicated that the shortening of the c-cell parameter in the decomposed kaolinite-boric oxide mixture and in decomposed tourmaline is due to the incorporation of boron into the mullite like phase.

Table 23

Ionic Radii (ref. 209).

	Ionic Radii (Å)		
B^{3+}	0.23	Fe^{2+}	0.74
Si^{4+}	0.42	Fe^{3+}	0.64
Al^{3+}	0.51	Mg^{2+}	0.67

Dietzel and Scholze (103) have observed a similar contraction in the c-cell dimension of the mullite like microcrystals formed during the thermal treatment of ternary mixtures of Al_2O_3, B_2O_3 and SiO_2. The X-ray diffraction patterns of these crystals of known composition were presented in graphical form. The actual variation in the angle of the (001) reflection was therefore directly measured from their paper using a ruler. The interplanar spacings calculated from these measurements together with the composition of the mullite like crystals are given in Table 24.

The results obtained by Dietzel and Scholze (103) indicate that the main substitutional process is boron for silicon in the mullite lattice.

The a-cell dimension in decomposed schorl (8/1) and dravite (8/4) is always similar to that for the same parameter in mullite, see Table 22. However, the b-cell dimension is shorter in most of the decomposed

tourmaline samples; indicating that the same slightly distorted mullite lattice is formed as was observed in decomposed kaolinite. This shortening of the b - cell parameter was found to decrease as the decomposition temperature increased.

At the higher decomposition temperatures all the cell dimensions were closer to those of mullite, except for the b-cell dimension in the schorl (8/1) sample that had been heated for 1 hour at 1300°C. The longer b-cell dimension found for the mullite like phase in this sample may be due to the incorporation of the larger Fe^{2+} or Fe^{3+} ion into the lattice, see Table 23.

TABLE 24

X-ray diffraction and Analysis results obtained by Scholze and Dietzel (103) for the microcrystals formed in the Ternary $Al_2O_3 - B_2O_3 - SiO_2$ System.

Composition (Weight per cent).				(001) reflection	c Å
Sample	B_2O_3	Al_2O_3	SiO_2		
Mullite	-----	71.8	28.2	15.49	2.878
No.3	4.5	72.7	25.6	15.60	2.86
No.13	5.5	73.8	21.3	15.65	2.85
No. 23	8.0	76.5	16.3	15.70	2.84

(1.4.3) Composition of "Mullite" Phase.

The approximate composition of the boron containing mullite in decomposed tourmaline was calculated by comparing the c-cell dimensions found in these experiments with those obtained by Scholze and Dietzel (103) for crystals of known composition, see Table 24. Their results are presented in a useful graphical form in Figures 7 and 8. The two curves drawn show the variation in the c-cell dimension and the silica content with increasing boric oxide substitution.

The curve showing the variation of the c-cell dimension with increase in boric oxide substitution was extrapolated to cover the greater variation in the c-cell dimension that has been observed in the present investigation, see Figure 7.

An approximate estimate of the amount of boric oxide present in the mullite like phase in decomposed tourmaline can then be made. by assuming that Vegard's law (209) holds throughout the extrapolated portion of the curve. Where Vegard's law states that the lattice parameters vary linearly with the concentration of solute added to the solid solution (210), however, see Pines (211). This estimation also assumes that the slight difference in the b-cell dimension of the mullite like phase in decomposed tourmaline compared to that in mullite itself does not affect significantly the variation in the c-cell dimension with boron content.

The amount of silica present in the mullite like phase in decomposed tourmaline was found by extrapolating the curve drawn, from the results obtained by Sholze and Dietzel (103), of the variation in the proportion of silica present with boric oxide content, to cover the percentage of boric oxide found in the mullite

FIGURE 7.

Variation of the c-cell dimension(d_{001} Å) with proportion of B_2O_3 incorporated in the mullite-like phase (after Dietzel and Scholze (103)).

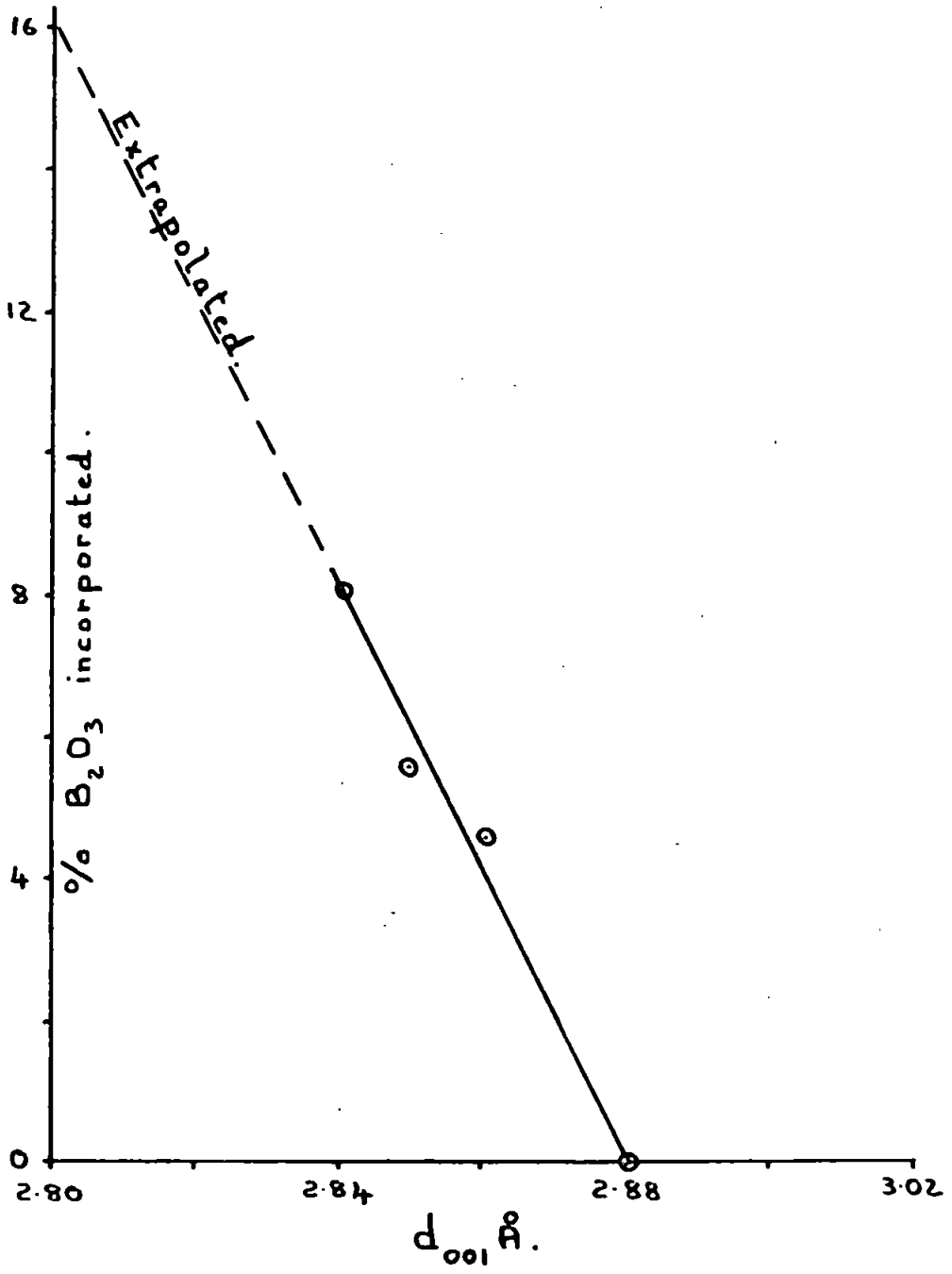

like phase in decomposed tourmaline, see Figure 8. The percentage of alumina present was obtained by difference from 100%.

The approximate compositions of the boron containing mullite like phases in decomposed tourmaline are given in Table 25.

TABLE 25

Approximate Composition of Mullite like Phase in Decomposed tourmaline as a Function of the Decomposition Temperature.

Sample	Approximate Composition (wt.%)		
	B_2O_3	Al_2O_3	SiO_2
(a) Schorl (8/1)			
1 hr. at 900°C	12	76	12
1 hr. at 1000°C	12	76	12
1 hr. at 1100°C	10	75	15
1 hr. at 1200°C	8	75	17
1 hr. at 1300°C	6	73	21
(b) Dravite (8/4)			
1 hr. at 900°C	14	78	8
1 hr. at 1000°C	12	76	12
1 hr. at 1100°C	12	76	12
1 hr. at 1200°C	10	75	15
1 hr. at 1300°C	8	75	17
(c) Kaolinite-Boric oxide 4 hrs. at 1100°C	14	78	8

The proportion of boron present in the mullite like phase in decomposed tourmaline decreases with increase in decomposition temperature. This is probably due to the faster rate at which tourmaline decomposes with increase in temperature. The interaction time between the boron and silicon atoms would then be considerably reduced, thereby leading to a decrease in the degree substitution. Because only one of the cell dimensions changes significantly the substitution probably only occurs for silicon atoms which are in specific lattice sites.

In general the composition of the mullite like phase in decomposed tourmaline therefore becomes closer to that of mullite ($3Al_2O_3.2SiO_2$) as the decomposition temperature increases. The exact composition is probably directly related to the rate of decomposition and also to the microscopic mechanism by which the crystal structure disintegrates.

(1.4.4) The Amorphous Phase.

The Differential Thermal Analysis (DTA) equipment described in Chapter 9.5 was used to investigate

FIGURE 8.

Proportion of SiO_2 present in mullite-like phase as a function of the amount of B_2O_3 incorporated into the crystalline lattice (after Dietzel and Scholze(103)).

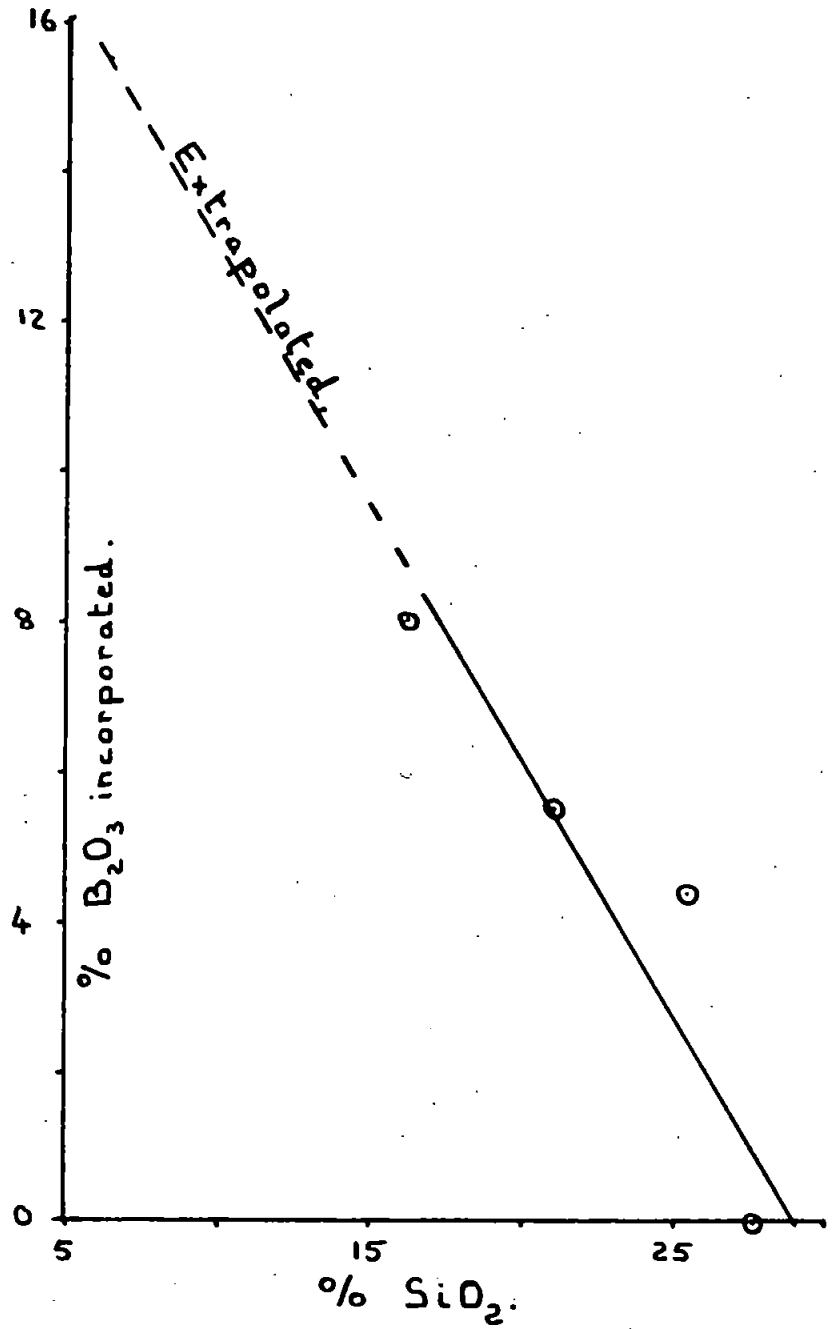

the nature of the amorphous phase present in decomposed schorl (8/1). It was thought that by the use of this technique, that it would be possible to detect the presence of such compounds as free boric oxide or one of the sodium borates, by the presence of endothermic peaks in the DTA curve at temperatures corresponding to their individual melting points.

No significant endothermic or exothermic peaks were observed in any of the DTA curves of decomposed schorl(8/1). These results indicate that no discrete phase exists on a macroscopic scale within the amorphous phase.

When the simpler thermally treated kaolinite-boric oxide mixture was similarly examined it was found impossible to obtain reproducible "DTA" curves with the equipment used. This technique will therefore not be discussed further; the nature of the amorphous phase in decomposed schorl (8/1) will, however, be discussed again in Chapters 16 and 17.

(2) Decomposition in Reducing Conditions.

Banateanu et.al. (20) found that when ludwigite ($(MgFe^{2+})_2Fe^{3+}BO_5$) was decomposed by sodium carbonate in a reducing atmosphere the boric oxide present in the product formed was more readily extractable than when decomposed in air, see Chapter 1.4.3. It was therefore thought probable that the product formed when tourmaline was thermally decomposed in reducing conditions would be similarly more extractable. The extraction experiments will be described in Chapter 16.2, whilst this section will be concerned with an X-ray diffractiometric investigation of the decomposed reduced material.

(2.1) Thermal Decomposition in atmosphere of Methane.

The apparatus used was similar to that drawn in Figure 3 except that the boiler etc. were removed and replaced by a methane cylinder and flowmeter. The excess methane was lead to an open window through a rubber tube connected to the exit of the tube furnace.

The methane supply was connected to the tube furnace and then adjusted until about 20cc./min. of gas was flowing through the furnace. After flushing for about 20 minutes a small alumina boat containing 2g. of the (100-300)mesh schorl (8/1) was pushed into the tube furnace. The sample was left for 1 hour in the furnace at $1000^{o}C$ and then pushed to a coolpart of the alumina tube and left to cool in the stream of methane. The sintered material was wiped free of surface charcoal and then crushed before an X-ray diffractometer trace was obtained, see Table 26.

(2.1.1) Crystalline species formed.

The interplanar spacings of the material formed when schorl (8/1) is heated for 1 hour at $1000^{o}C$ in a stream of methane are listed in Table 26, together with the probable crystalline species producing each reflection.

Most of the reflections are consistent with the assumption that a mullite like phase is one of the crystalline species formed. However, three new reflections are present which were not observed in air decomposed

schorl, see Table 17. These spacings were compared with those listed in the ASTM index (212) and of the compounds etc. scanned the only probable one with the same spacings was α–iron:-

α–iron (212)	2.03 (100)	1.17 (30)	1.14 (20)
d_{hkl} expt'al.	2.02 (100)	1.17 (30)	1.14 (20)

The X-ray diffractometer trace is consistent with the assumption that α–iron and a mullite like phase are the only crystalline species formed when schorl (8/1) is decomposed in a reducing atmosphere.

A similar experiment using ammonia as the reducing gas will not be discussed because the same interplanar spacings were obtained as those given in Table 26.

TABLE 26

Interplanar Spacings from material formed when Schorl

Decomposed at 1000°C for 1 hour in an atmosphere of Methane.

Relative Intensity	$d_{(hkl)}$ Å	Species	Relative Intensity	$d_{(hkl)}$ Å	Species
4	5.36	M	2	1.510	M
10	3.34	M	1	1.449	M
1	2.823	M	1	1.427	M
2	2.675	M	2	1.371	M
1	2.508	M	1	1.327	M
1	2.258	M	1	1.306	M
3	2.180	M	1	1.251	M
1	2.102	M	3	1.167	Fe
10	2.024	Fe	1	1.138	Fe
2	1.815	M			
1	1.679	M	Key:- M "Mullite"		
1	1.583	M	Fe α–iron.		

The cell dimensions of the mullite like phase were calculated using the method described in Chapter 15.1.4.2 and compared in Table 27 with those of the boron containing mullite formed when schorl is decomposed at 1000°C in air. The cell dimensions of the two mullite like phases are therefore the same to within the probable experimental error. The reduction of the iron oxide during the decomposition–reducing process does not therefore affect the formation of the boron containing mullite phase.

(2.2) Thermal Decomposition in the presence of activated charcoal.

(2.2.1) Using tube furnace.

In these experiments the (100-300) mesh schorl (8/2) was mixed with activated charcoal in the weight ratio of four to one. About 2g. of this mixture was poured each time into a small alumina boat. The apparatus

TABLE 27

Comparison of Cell Dimensions of Mullite like Phase formed

when Schorl is decomposed in different conditions.

Sample	Cell Dimensions (Å)		
	a	b	c
Schorl–Methane; 1 hr. at 1000°C	7.53	7.66	2.82
Schorl–Air; 1 hr. at 1000°C	7.53	7.64	2.82

used for these reducing experiments is basically the same as that drawn in Figure3 except that a nitrogen cylinder and flowmeter replaced the stream boiler. To flush out the furnace about 20 cc./min. of nitrogen was passed for about 20 minutes before introducing the sample. At the end of the desired reaction time the boat was pushed to a cool portion of the furnace and left to cool in the stream of nitrogen. The excess activated charcoal was then removed through a 300 mesh sieve before an X-ray diffractometer trace was obtained of the powder remaining. The interplanar spacings of the material formed by heating a mixture powdered schorl and activated charcoal for various periods of time at two different temperatures are given in Table 28.

Most of the intense reflections obtained from the material formed after heating the schorl-charcoal mixture for 1 hour at 810°C are consistent with those for the mineral itself, however, further reflections are present, most of which are the same as those obtained for the mullite like phase in air decomposed schorl, see Table 17. There are, however, two further reflections, one of which is more intense than any of the "mullite" reflections, which have not been observed in a previous X-ray diffractometer trace of decomposed tourmaline. The nature of the crystalline species producing these reflections will be elucidated in section 2.2.1.1.

This low temperature experiment is therefore extremely interesting, because the addition of activated charcoal appears to have considerably lowered the temperature at which the tourmaline lattice disintegrates. In Chapter 15.1.1 the decomposition temperature of schorl in air was found to be 880 ± 10°C, whilst in this reducing experiment new crystalline phases were formed after a reaction time of 1 hour at 810°C. The decomposition temperature of schorl has therefore been lowered by at least 70°C by the presence of activated charcoal.

(2.2.1.1.) Crystalline products.

The interplanar spacings of the material formed after heating the schorl-charcoal mixture for 1 hour at 810°C are consistent with the presence of mainly unreacted schorl, a very small amount of a mullite like phase plus a further unknown phase.

On heating the schorl-charcoal mixture for 4 hours at 810°C the reflections due to schorl disappear and all the reflections apart from three are consistent with a mullite like phase. The three remaining spacings were compared with those listed in the ASTM index (212) and of the compounds scanned the only probable one with the same spacings was heroynite ($FeO.Al_2O_3$):–

TABLE 28

X-ray Diffractometry of material formed when Schorl-Activated Charcoal mixtures are heated.

Schorl-Charcoal Mixtures								
1 hr. at 810°C			4 hrs. at 810°C			1 hr. at 1000°C		
I	d Å	species	I	d Å	species	I	d Å	species
2	5.33	M	2	5.37	M	4	5.36	M
7	4.20	T						
5	3.94	T						
10	3.33	M + T	8	3.34	M	10	3.35	M
1	2.877	?	2	2.877	?			
						1	2.841	M
1	2.860	M	2	2.662		4	2.683	M
6	2.578	T						
			2	2.542	M	3	2.508	M
5	2.460	H	10	2.446	H			
			1	2.275	M	3	2.275	M
2	2.180	M	2	2.160	M	4	2.180	M
1	2.114	M	1	2.115	M	3	2.107	M
5	2.030	T				8	2.023	Fe
1	1.805	M	1	1.815	M	5	1.812	M
3	1.656	T						
2	1.564	H	2	1.563	H			
			2	1.439	H			
						2	1.324	M
						2	1.165	Fe
						2	1.138	Fe

KEY:

M	Boron containing mullite.
T	Tourmaline (8/1).
H	Hercynite ($FeO.Al_2O_3$).
Fe	α – iron.

Hercynite (212)	2.45 (100)	1.56 (80)	1.45 (80)
Expt. 4 hrs. at 810°C	2.45 (100)	1.56 (20)	1.44 (20)

The probable presence of this compound in this complex system was supported by the work of Krause et. al. (213), who found that hercynite was formed when a $FeO - Al_2O_3$ mixture was heated for 4 hours at 1100°C in a reducing atmosphere.

The two reflections due to the unknown phase in the material formed after heating the schorl-charcoal mixture for 1 hour at 810°C are also consistent with the two most intense reflections from hercynite, see Table 28.

All the interplanar spacings from the material formed by heating a mixture of schorl and activated charcoal for 1 hour at 1000°C are consistent with the present of a mullite like phase and α –iron as the only crystalline phases.

(2.2.2) Using Oven Furnace.

In these experiments a large amount of the (8 – 100) mesh tourmaline (8/1) was mixed with activated charcoal in the weight ratio of four to one. About 100g. of this mixture was poured each time into a small graphite crucible which was introduced, after replacing the lid, into the oven furnace and then left for 1 hour at a number of temperatures between 1000 and 1300°C. The decomposed material was then roughly crushed in a jaw crusher and the excess activated charcoal was then removed through a 300 mesh sieve, see Chapter 11. The decomposed schorl (8/1) was then crushed and two fractions were collected, one between (100–300) mesh and the other smaller than 300 mesh. X-ray diffractometer traces were obtained using the finely ground material. The X-ray spacings obtained from the material formed at two reaction temperatures are given in Table 29.

At a reaction temperature of 1000°C the spacings obtained are consistent with the presence of a mullite like phase, α –iron and hercynite. However, at the higher reaction temperature of 1200°C the reflections due to hercynite disappeared, whilst those due to α –iron became of greater relative importance. The amount of α –iron formed therefore increases with reaction temperature. Since the amount of hercynite decreases with temperature the reaction producing α –iron probably proceeds by gradually eliminating the hercynite phase.

The material formed at the reaction temperature of 1000°C using (8-100) mesh schorl was found to contain hercynite, whilst the material formed at the same reaction temperature using (100–300) mesh schorl does not, see Tables 28 and 29. This apparent discrepancy is explained by the slower rate at which the larger granules are reduced by the activated charcoal.

(2.2.3) Mechanism of Decomposition in Reducing Conditions.

The decomposition of schorl under reducing conditions probably proceeds by the following series of reactions:-

(i). In the presence of activated charcoal the schorl lattice was found to breakdown at temperatures below the decomposition temperature of the mineral in air. The initial decomposition reaction (1) must therefore be between schorl and activated charcoal:-

$$Na_2O.6FeO.6Al_2O_3.3B_2O_3.12SiO_2.4H_2O + C \longrightarrow FeO.Al_2O_3 \quad \text{..... (1)}$$

(initial reaction)

TABLE 29

X-ray Diffractometry of material formed when Schorl-Activated Charcoal mixtures are heated.

(8-100) mesh Schorl (8/1) heated with Activated Charcoal					
1 hour at 1000°C			1 hour at 1200°C		
Intensity	d_{hkl} Å	Species	Intensity	d_{hkl} Å	Species
2	5.36	M	2	5.34	M
8	3.34	M	7	3.35	M
4	2.858	?			
4	2.675	M	5	2.683	M
2	2.501	M	2	2.501	M
10	2.448	H			
1	2.258	M	1	2.269	M
3	2.165	M	4	2.180	M
2	2.022	Fe	6	2.023	Fe
4	1.809	M	4	2.819	M
2	1.675	M	2	1.682	M
5	1.559	H			
2	1.503	M	3	1.509	M
2	1.433	H			
5	1.366	M?			
			1	1.165	Fe
			1	1.138	Fe

KEY:-

M. Boron containing mullite

H. Hercynite

Fe cc -- iron.

(ii) A subsequent slower low temperature process, which has been initiated by reaction (1), leads to the formation of a mullite like phase (2):-

Schorl partially decomposed

$$\downarrow$$

Mullite like phase $(3Al_2O_3 2SiO_2)$ + $FeO\ Al_2O_3$ ..... (2)

(iii) Higher temperature reactions (3,4) lead to the formation of α-iron and more of the "mullite" phase. The α-iron is probably formed by the reduction of the FeO in the hercynite ($FeO.Al_2O_3$) phase. This assumption was supported by the observation that the hercynite phase gradually disappeared as the amount of iron formed increased, see Table 28. Because free Al_2O_3 has not been observed in any sample of decomposed

Decomposed Schorl + C $\rightarrow \alpha$ – Fe ..... (3.1)

This reaction probably proceeds via the following elementary process:-

$FeO.Al_2O_3$ + C $\longrightarrow$ Fe + Al_2O_3 ..... (3.2)

schorl, the alumina produced in reaction (3.2) probably reacts with the amorphous silica, which has been produced during the decomposition process, forming more of the mullite like phase:-

Schorl $\longrightarrow$ Decomposition products + SiO_2

Al_2O_3 (from reaction 3.2) + SiO_2 $\longrightarrow$ Mullite like phase ..... (4).

CHAPTER 16

Liquid Extraction Studies.

(1) Extraction from Schorl (8/2) Decomposed in Air.

In all the liquid extraction experiments described in this chapter (100-300) mesh decomposed schorl (8/2) was used. This was obtained by crushing and sieving the (8-100) mesh air decomposed material, see Chapter 11.

(1.1) Effect of Decomposition Temperature.

In this series of experiments 5.00g. of (100-300) mesh decomposed schorl was boiled under reflux conditions with 100 ml. of 0.5M.H_2SO_4, see Chapter 12. This quantity of acid is considerably in excess of the amount that would be used in salt formation if the leaching process extracted all the sodium oxide and iron oxide from decomposed schorl. Therefore the acid concentration will remain almost constant throughout the leaching process. Because the acid strength and the granule size were the same in all the leaching experiments, any difference in the extractability with decomposition temperature, can probably be related to a change in some intrinsic property of the decomposed schorl.

(1.1.1) Extraction of Boric Oxide.

The amount of boric oxide extracted was determined using the technique described in Chapter 10. 1.2. The percentage of boric oxide extracted, as a function of the leaching time, was determined for each of the decomposed schorl samples and the results obtained are presented in graphical form on a log-log scale in Figure 9.

The rate of extraction was found to approximately follow the parabolic rate law (1) which has been shown to be obeyed for a number of heterogeneous reactions including the acid leaching of glass, see Chapter 7.

$$(B_2O_3) = kt^{0.50} \quad \text{.....(1)}$$

The value of the rate constant and the exponent were calculated from the log-log curves obtained for each of the decomposed schorl samples. The results obtained are presented in tabulated form in Table 30.

TABLE 30

Experimental Rate Constants for the Extraction of Boric Oxide using boiling 0.5M.H_2SO_4 as a function of the original Schorl Decomposition Temperature.

Extraction of B_2O_3 from 5.00g. of (100-300) mesh decomposed Schorl using 100ml. of boiling 0.5M.H_2SO_4. Rate law of form $(B_2O_3) = kt^n$ where (B_2O_3) is the percentage extracted after t hours.		
Decomposition temperature (^oC)	k	n
1 hr. at 900^{o}C	3.20	0.39
1 hr. at 1000^{o}C	6.51	0.41
1 hr. at 1100^{o}C	10.3	0.40
1 hr. at 1200^{o}C	18.3	0.41
1 hr. at 1300^{o}C	44.0	0.39.

FIGURE 9.

Rate of extraction of B_2O_3 as a function of the original schorl decomposition temperature.

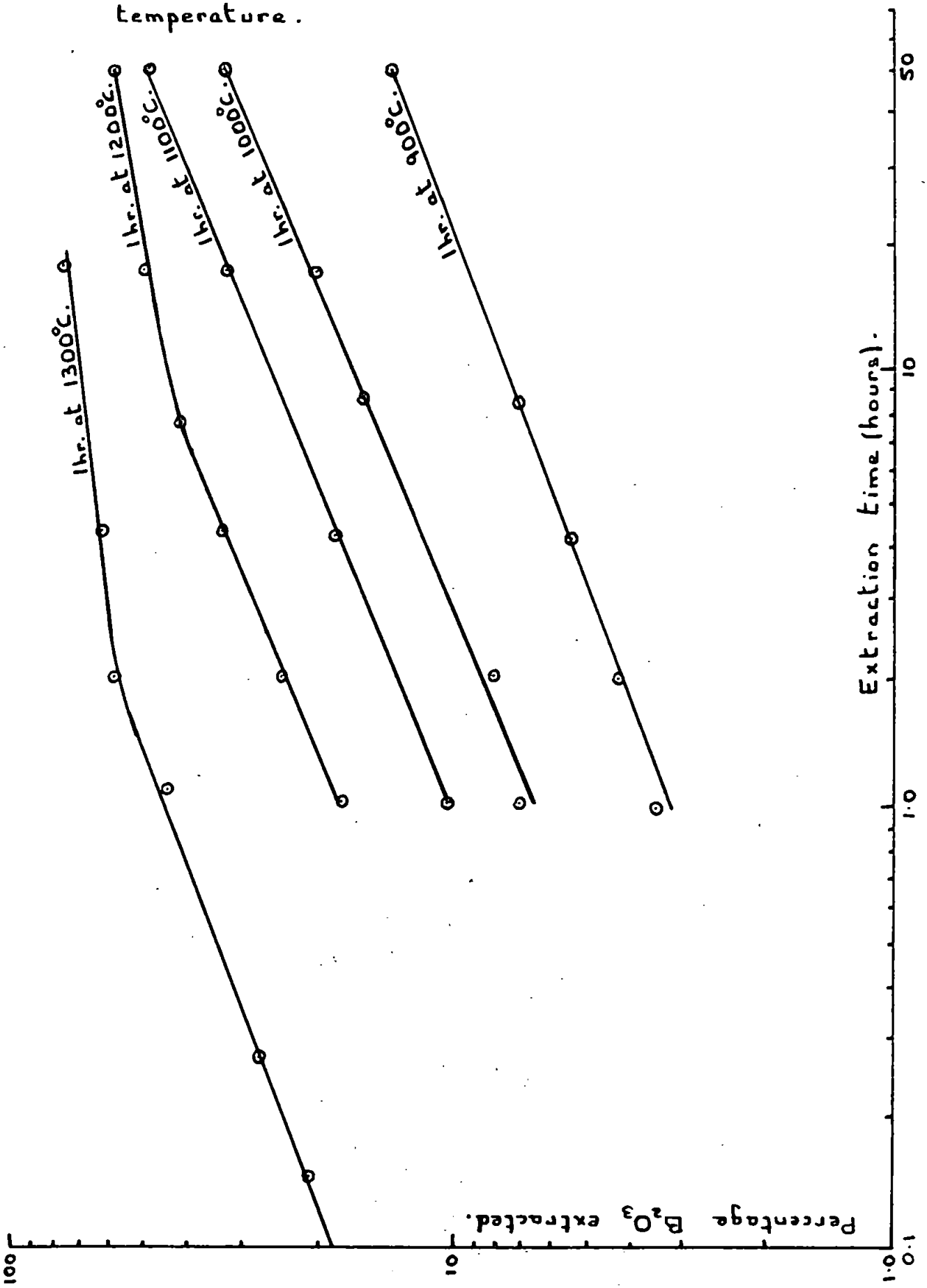

The parabolic type rate of extraction was found to be obeyed up to about 50% boric oxide extracted, the rate was then found to decrease rapidly. This decrease in the rate is almost certainly attributable to the complete depletion of the boric oxide present in a relatively extractable phase. The remaining boric oxide is therefore probably present in a different type of matrix. This is almost certainly the micro-crystalline phase which has been found to be a boron containing mullite, see Chapter 15.1.4.

The approximate parabolic rate of extraction of boric oxide was found to be obeyed to a slightly higher percentage extraction for schorl that had been decomposed at 1300°C compared to schorl decomposed at 1200°C, see Figure 9. This observation is in qualitative agreement with the X-ray diffraction results, which indicated that the amount of boric oxide present in the crystalline phase decreased with increase in the decomposition temperature, see Table 25.

The calculation of the approximate percentage of the total boric oxide which is present in the crystalline phase was undertaken using the composition data given in Table 25 and by assuming that the alumina is entirely bound up in the mullite like phase. This assumption is in agreement with the X-ray diffraction results described in Chapter 15.1.4.1.

The percentage of alumina in schorl is always close to 30% (32). The proportion of the total boric oxide which is present in the amorphous and crystalline phases can therefore be calculated using the results given in Table 25. The results obtained for schorl decomposed at 1200°C were calculated as follows:-

30% by wt. of Al_2O_3 in schorl $\equiv$ 75% by wt. of Al_2O_3 in "Mullite" like phase, see Table 25.

$\therefore$ 1% by wt. of "Mullite" phase $\equiv$ (30/75)% by wt. of schorl.

$\therefore$ 8% by wt.of B_2O_3 in "Mullite" phase (see Table 25) $\equiv$ (30/75) x 8% by wt.of schorl.

Therefore the 8% by wt. of boric oxide in the "mullite" like phase in decomposed schorl represents (30/75) x 8% (equals 3.2%) of the total boric oxide in tourmaline.

The total percentage of boric oxide in schorl (8/2) is equal to 8.70%, see Table 16.

Therefore percentage of total B_2O_3 in crystalline phase equals (3.2/8.7) x 100%.

Therefore percentage of total B_2O_3 in amorphous phase equals (100−(3.2/8.7) x 100)%.

The percentage of boric oxide present in the two phases was calculated for all the decomposed schorl (8/2) samples. The results obtained are presented in tabulated form in Table 31.

The maximum percentages of boric oxide easily extractable from schorl decomposed at 1200°C and 1300°C are compared in Table 31, with the derived X-ray results for the percentage of boric oxide present in the amorphous phase of schorl decomposed at 1200°C and 1300°C. The two results are in reasonable agreement in view of the many assumptions and errors involved in deriving the X-ray results.

The X-ray diffractometer trace of decomposed schorl is compared in Table 32, with an X-ray trace obtained of the material remaining after acid leaching. The similarity between the two traces indicates that the crystalline phase is not attacked to any significant degree by the boiling dilute acid.

The present investigation into the acid leaching of boric oxide from decomposed schorl does not appear

TABLE 31

Percentage of Boric Oxide present in the Amorphous and Crystalline Phases as a function of the Schorl Decompostion Temperature.

Tourmaline heated for 1 hour at:-	Approximate percentage of total B_2O_3.		Parabolic law valid up to (%).
	In crystalline phase.	In amorphous phase.	
900°C	54	46	
1000°C	54	46	
1100°C	46	54	
1200°C	37	63	50
1300°C	28	72	60

TABLE 32

Comparison of X-ray Diffractometer traces of Decomposed Schorl before and after Acid Leaching.

Schorl (8/2) heated for 1 hour at 1100°C.			
Before leaching.	After leaching 48 hrs. with 48% of B_2O_3 extracted.	Before leaching.	After leaching 48 hrs with 48% of B_2O_3 extracted.
d Å	d Å	d Å	d Å
5.32	5.36	1.822	
3.36	3.36	1.682	1.682
2.93		1.583	1.580
2.832	2.832	1.506	1.508
2.683	2.683	1.469	
2.501	2.508	1.445	1.446
2.416	2.404	1.417	1.415
2.258	2.258	1.369	1.371
2.180	2.178	1.251	1.251
2.107	2.107		
2.079	2.079		

to be consistent with a recent similar investigation by Matsaberidze et. al. (25). In the Soviet investigation it was found that 100% of the boric oxide was extractable, within a reasonable but unspecified time, by acid leaching of schorl decomposed at 950°C. However, in the present investigation, using 0.5M.H_2SO_4 and (100-300) mesh schorl, it would take over 1000 hours to extract all the boric oxide present in schorl decomposed at 950°C, if it is assumed that the approximate parabolic law of extraction is obeyed throughout, see Figure 9. The X-ray results presented in Table 31 indicate, however, that the rate of leaching would markedly decrease when about 54% of the boric oxide is extracted. The real time required to extract the whole of the boric oxide would therefore be considerably greater than 1000 hours.

The difference between the two investigations in the time required to extract the whole of the boric oxide present in almost certainly too large to be explained simply on the basis of a difference in particle size or acid strength. It could possibly be accounted for by some difference in the original thermal treatment of the mineral. For example, if the heated mineral was quickly cooled in water or a blast of air the formation and growth of the crystalline and amorphous phases may be incomplete, thereby producing a readily leachable material.

In view of the complexity of the system being investigated and incomplete information available on the study carried out by Matsaberidze et. al. (25), it would be inappropriate to discuss in any greater depth the apparent disagreement between the results obtained.

(1.1.1.1) Mechanism of Extraction and Nature of Amorphous Phase.

The logarithmof the experimental rate constants given by Table 30 were plotted against the reciprocal of the original schorl decomposition temperature in degrees absolute, see Figure 10. This plot is of the usual Arrhenius function (1), which relates the rate constant (k) to the temperature (°K) via the activation energy (E), for the process:-

$$k=A \exp(-E/RT) \quad \ldots\ldots\ldots\ldots(1)$$

A function of this type was found to be obeyed and a value for the activation energy of 19.2 ± 0.4 kcal/mole was obtained. The rate constant found for the extraction process from schorl decomposed at 1300°C was not included in the calculation of the activation energy, because this value did not lie on the same straight line as the other four points. Because of the relative complexity of the function the error included was simply obtained by drawing maximum and minimum slopes through the experimental points and then recalculating the activation energy. It must be remembered, however, that this activation energy is not exactly of the same type as those usually obtained in chemical kinetics, because all the leaching experiments were carried out at the same temperature.

An equation (2) has been derived by Halvesy (214) which relates the diffusion (D) of species in a solid at a temperature (T°K):-

$$D = D_o \exp(-E/RT) \quad \ldots\ldots\ldots\ldots(2)$$

This equation is of the same form as the Arrhenius equation (1) because diffusion can be regarded as a special case of the more general reaction rate theories (227). Therefore diffusion in the solid state takes place via an

FIGURE 10.

Arrhenius type plot of log(rate constant) for the extraction of B_2O_3 as a function of the original schorl decomposition temperature.

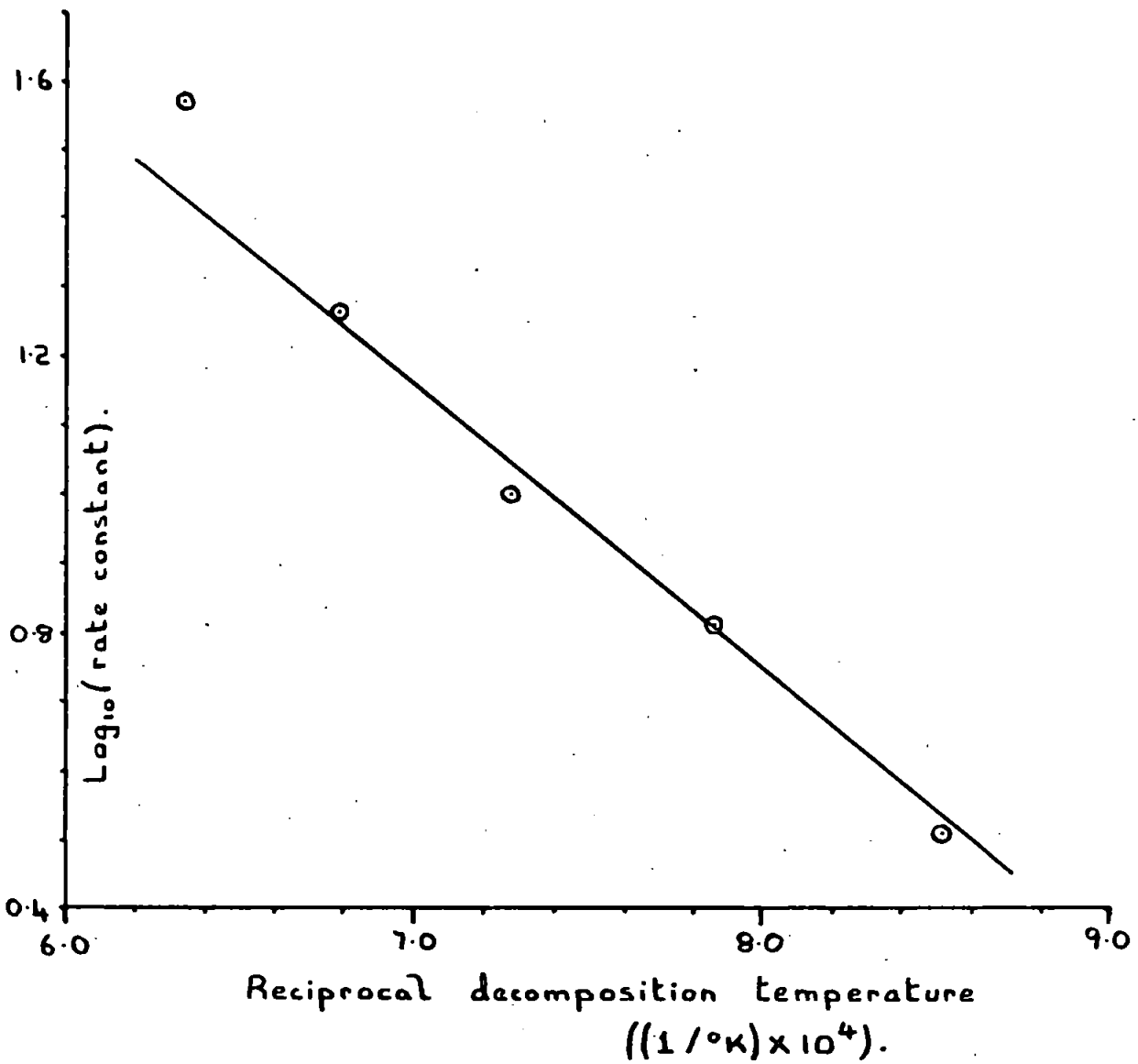

activated process with the activation energy (E) being the energy barrier between the initial and final states.

The activation energy obtained in these experiments can therefore be probably related to a temperature dependent diffusional process occurring in the amorphous phase of decomposed schorl.

This process is probably the diffusional growth of microheterogeneous regions within the amorphous phase in decomposed schorl. These regions could be formed by the diffusion of borates ions and sodium ions through the silica-iron oxide amorphous matrix; such microscopic areas would contain mainly borate and sodium ions.

Cordelier (137) and Makishima et. al. (135) have found that the size and the degree of interconnection of these "sodium borate" regions in borosilicate glasses, increased as the duration and temperature of the thermal treatment was increased. These two processes would probably form a material in which the boron and sodium oxides are more readily extractable as the temperature of thermal treatment is increased. The formation of the "sodium borate" regions would probably be governed by some diffusion controlled process. However, the activation energy found in the present investigation of 19.2 ± 0.4 kcal /mole for the diffusion process, cannot be directly related to the formation of these "sodium borate" microregions, because Kiyohisa et. al. (138) have found that the activation energy of phase separation in borosilicate glass is close to 62 kcal/mole.

The reason for the much lower value for the activation energy found in the present study could be due to:—

(1) The incomplete formation of the three dimensional lattice of the amorphous phase in decomposed schorl. This could lead to a lower value for the activation energy of the diffusion process.

(2) The fact that the activation energy found in the present investigation is not directly related to the formation of microheterogeneous regions within the amorphous phase. This is unlikely because one of the most important processes that occur, when complex glasses are heated, is the formation of microheterogeneous regions within the main silicate lattice, see Chapter 6.

(3) The presence of iron oxide in the amorphous matrix. This oxide may affect the energy barrier for the diffusion of borate and sodium ions through the silica-iron oxide amorphous matrix. If the Fe^{2+} ions are partially incorporated in the silica lattice this could lead to a certain amount of distortion and disruption in the structure. The overall effect of this would probably be a lowering of the energy barrier towards diffusion through the silica-iron oxide matrix.

The activation energy found in this investigation is, however, close to the activation energy of 19.4 kcal/mole for the diffusion of sodium ions through a silicate glass (156). No similar correlation with the activation energy of diffusion of borate ions through a silicate glass could be made as this data did not appear to be available.

The diffusional growth of these microheterogeneous regions within the amorphous phase of decomposed schorl is shown schematically below:-

$$Na_2O.6FeO.3B_2O_3.6Al_2O_3.12SiO_2 4H_2O \longrightarrow Na_2O.6FeO.3B_2O_3.6Al_2O_3.12SiO_2 + 4H_2O$$

Dehydrated schorl

1 hour at 1200°C

$Na_2O.6FeO2.5B_2O_3.7SiO_2$ + $2(3Al_2O_3.0.5B_2O_3\ 2.5SiO_2)$

Amorphous phase (Approximate composition obtained by difference).

Crystalline phase (Approximate molar composition calculated from data given in Table 25).

Growth of microheterogeneous regions.

$Na_2O.2.5B_2O_3$ + $6FeO.7\ SiO_2$

(Approximate composition of completely phase separated regions).

The rate equations obtained for the extraction of boric oxide from schorl (8/2) heated at 900°C for one, six and fourteen hours respectively are given below:-

1 hour at 900°C.

$(B_2O_3) = 3.20t^{0.38}$

6 hours at 900°C

$(B_2O_3) = 3.10t^{0.39}$

14 hours at 900°C

$(B_2O_3) = 2.70t^{0.40}$

The similarity in the three experimental rate constants indicates that the growth of the microheterogeneous regions within the amorphous phase is complete within one hour.

(1.1.2) Extraction of Iron.

The amount of iron extracted was determined using the method described in Chapter 10.2.2. The percentage of iron extracted as a function of the leaching time was determined for each of the decomposed schorl samples and the results obtained are presented in graphical form on a log-log scale in Figure 11.

The rate of extraction was calculated from the log-log curves obtained for each of the decomposed schorl samples. The rate equations obtained using boiling 0.5M.H_2SO_4 are given below:-

Schorl heated for:-

1 hour at 900°C.

$Fe = 2.13t^{0.49}$

1 hour at 1000°C.

FIGURE 11.

Rate of extraction of iron as a function of the original schorl decomposition temperature.

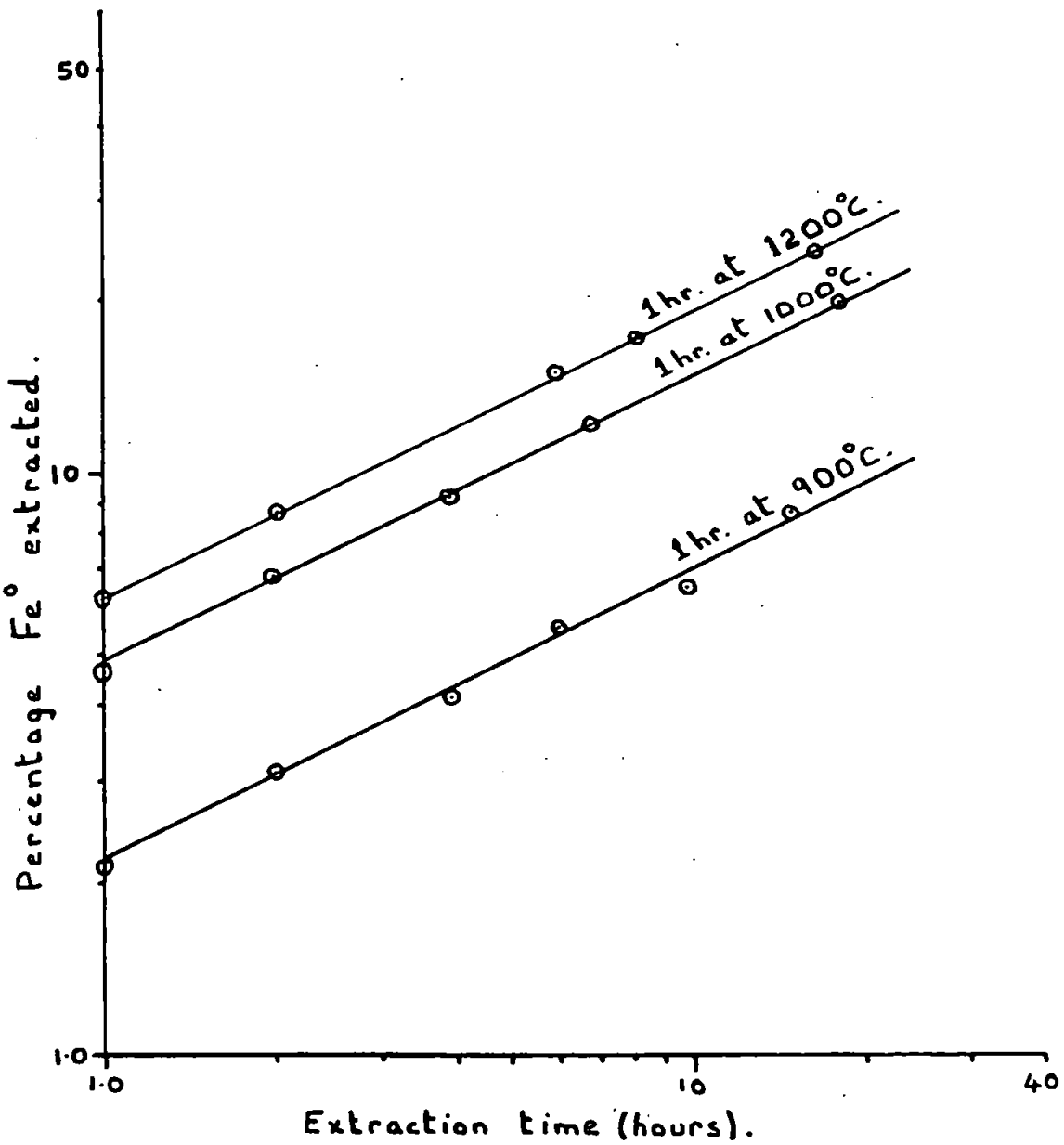

$$Fe = 4.81\ t^{0.48}$$

1 hr. at 1200°C

$$Fe = 6.20\ t^{0.51}$$

The results were treated in the same way as those obtained in the investigation of the effect of the decomposition temperature on the rate of extraction of boric oxide, see section 1.1.1.1. The activation energy of the diffusion process was determined by taking each time two of the rate constants from the three given above and then calculating the three possible values. The mean activation energy and the standard deviation were determined and found to be equal to 10.9 ± 2.0 kcal/mole.

The activation energy for the extraction of iron as a function of the schorl decomposition is about half that for the extraction of boric oxide. This indicates that the energy barrier towards the diffusion of Fe^{2+} ions is lower than that for the diffusion of borate or sodium ions.

The direct association of the activation energy found in these extraction experiments with the diffusion of Fe^{2+} ions through an amorphous matrix, does not appear to be consistent with the limited information available on the diffusion of ions through glass. For example, Borom (215) found that the activation energy for the diffusion of Fe^{2+} ions through a sodium disilicate glass was equal to 30 kcal/mole, whilst Charles (156) found that the activation energy for the diffusion of sodium ions through a silicate glass was equal to 19.4 kcal/mole. In view of the complexity of the system and lack of relevant information, the activation energy for the extraction of iron as a function of the schorl decomposition temperature, cannot be directly associated, with certainty, to the activation energy for the diffusion of Fe^{2+} ions through the amorphous matrix. However, the increased extraction of iron with decomposition temperature could be associated with diffusion in a more remote way. The increased rate of extraction may, for example, be related to the increased degree of distortion and disruption of the silica lattice as more Fe^{2+} ions are incorporated into the structure.

(1.2) Effect of Leaching Temperature.

In this set of experiments the (100-300) mesh decomposed schorl, which had been heated for 1 hour at 1200°C, was used. The experiments carried out in the constant temperature bath were continuously stirred to simulate the vigorous mixing which occurred when boiling acid was used, see Chapter 12.1.

The rate of extraction of boric oxide and iron from 5.00g of (100-300) mesh material using 100 ml. of 0.5M.H_2SO_4 was determined at three different temperatures. The percentages extracted as a function of the leaching time are presented in tabulated form in Table 33 and in graphical form on a log-log scale in Figure 12. The extraction process was found to closely follow the parabolic equation (1):-

$$(\%\ \text{extracted}) = kt^{0.5} \quad \ldots\ldots\ldots\ldots\ldots\ldots (1)$$

(1.2.1) Extraction of Boric Oxide.

The rate equations for the extraction of boric oxide at three different temperature were calculated from the log-log curves shown in Figure 12. The three parabolic equations calculated are:-

(1) At 100°C $(B_2O_3) = 17.4\ t^{0.50}$

(2) At 63.9°C $(B_2O_3) = 5.30t^{0.49}$

(3) At 34.0°C $(B_2O_3) = 1.74t^{0.49}$

The activation energy of the extraction process was determined by taking each time two of the rate constants from the three given above and then calculating the three possible values. The mean activation energy and the standard deviation were determined and found to be equal to 7.99 ± 0.19 kcal/mole.

TABLE 33

Extraction of Boric Oxide and Iron from Decomposed Schorl as a Function of the Extraction Temperature.

	(8-100) mesh Schorl (8/2) heated for 1 hr at 1200°C, crushed, 5.00 g. of (100-300) mesh material leached each time with 100 ml. of 0.5M.H_2SO_4.					
	Temperature at which extraction experiment was carried out					
	34.0°C		63.9°C		100°C	
	Percentage of species extracted.					
Extraction time (hours).	B_2O_3	Fe	B_2O_3	Fe	B_2O_3	Fe
1	1.73	0.80	5.18	2.72	17.8	6.10
2	2.20	1.07	7.30	3.81	22.5	8.60
4	3.44	1.71	10.3	5.21	36.5	12.3
5	3.82	1.70				
8	4.72	2.24	14.8	7.60	50.0	17.8
16	6.70	2.88	20.6	10.8		24.4

(1.2.2) Extraction of Iron.

The rate equation for the extraction of iron were calculated from the log-log curves shown in Figure 12. The three parabolic equations calculated were:-

(1) At 100°C $(\%Fe) = 6.14t^{0.52}$

(2) At 63.9°C $(\%Fe) = 2.72t^{0.50}$

(3) At 34.0°C $(\%Fe) = 0.78t^{0.51}$

The activation energy for the extraction process was determined by taking each time two of the rate constants from the three given above and then calculating the three possible values. The mean activation energy and the standard deviation were determined and found to be equal to 7.15 ± 1.04 kcal/mole.

(1.2.3) Conclusions.

The activation energy for the extractions of both boric oxide and iron were found to be the same to within the probable experimental error.

Because the activation energy for the extraction process is quite small it was thought that the reaction

may be controlled by the diffusion of dissolved species from the granule surface into the bulk solution. The dissolution of copper in an acidified potassium iodide – iodine solution is an example of such a reaction. Von–Name and Edgar (216) found that the activation energy for the dissolution of copper was equal to 6.5 kcal/mole. However, it is unlikely that the extraction of boric oxide and iron from decomposed schorl is controlled by this type of diffusion process, because the extraction process was found to follow a parabolic law instead of the linear rate equation found by Von-Name and Edgar (216).

The parabolic law has been found to be usually obeyed by reactions which are controlled by the diffusion of reactive species through a semi-porous solid to the continuously contracting reaction surface or by the diffusion of products away from the reaction surface. If the radius of the reactive surface decreases linearly with time then for a spherical surface the surface area will decrease as the inverse square. The quantity extracted will therefore correspondingly decrease as the inverse square of the reaction time leading to the parabolic time dependent law (1).

$$(\%\text{extracted}) = kt^{0.5} \quad \ldots\ldots\ldots\ldots\ldots\ldots(1)$$

The extraction of boric oxide and iron is therefore probably controlled by the rate of diffusion of active species to the reaction surface or of products away from this surface.

The activation energy for acid leaching of normal glasses has been found to be close to 20 kcal/mole, see Table 12. However, Kiyohisa et. al. (138) have found that the activation energy for the acid leaching of boric oxide and sodium oxide from phase separated glasses was equal to 6.8 kcal/mole. This value is extremely close to the activation energy for the extraction of both boric oxide and iron from decomposed schorl, which indicates that the amorphous phase in decomposed schorl may also contain phase separated regions.

Kiyohisa et. al.(138) thought that the rate controlling process may arise from the diffusion of B_2O_3/Na_2O through the porous silica membrane filled with acid. However, it is more likely that the extraction process is controlled by the diffusion of active species to the reaction surface or of products from this surface, or by the rate of reaction at the reaction surface. The mechanism controlling the overall rate of extraction will be discussed in greater detail in section 3 at the end of this chapter.

(1.3) Effect of Strength of Acid on the Rate of Extraction of Boric Oxide.

The extraction of boric oxide was investigated using sulphuric acid of various concentrations in order to elucidate in greater detail the mechanism by which the leaching process proceeds.

In this investigation 5.00g. of the (100-300) mesh decomposed schorl, which has been heated for 1 hour at 900°C, was used each time. The percentage of boric oxide extracted, using 100ml of boiling sulphuric acid of known strength, was determined after a leaching period of 4 hours. The results obtained are presented in graphical form in Figure 13.

The shape of this curve is reminiscent of the absorption curves of gases and liquids on solids (217). It was therefore thought likely that the shape of the curve could be related to the relative amount of absorption of the active species onto the reaction surface.

FIGURE 13.

Rate of extraction of B_2O_3 as a function of the sulphuric acid concentration.

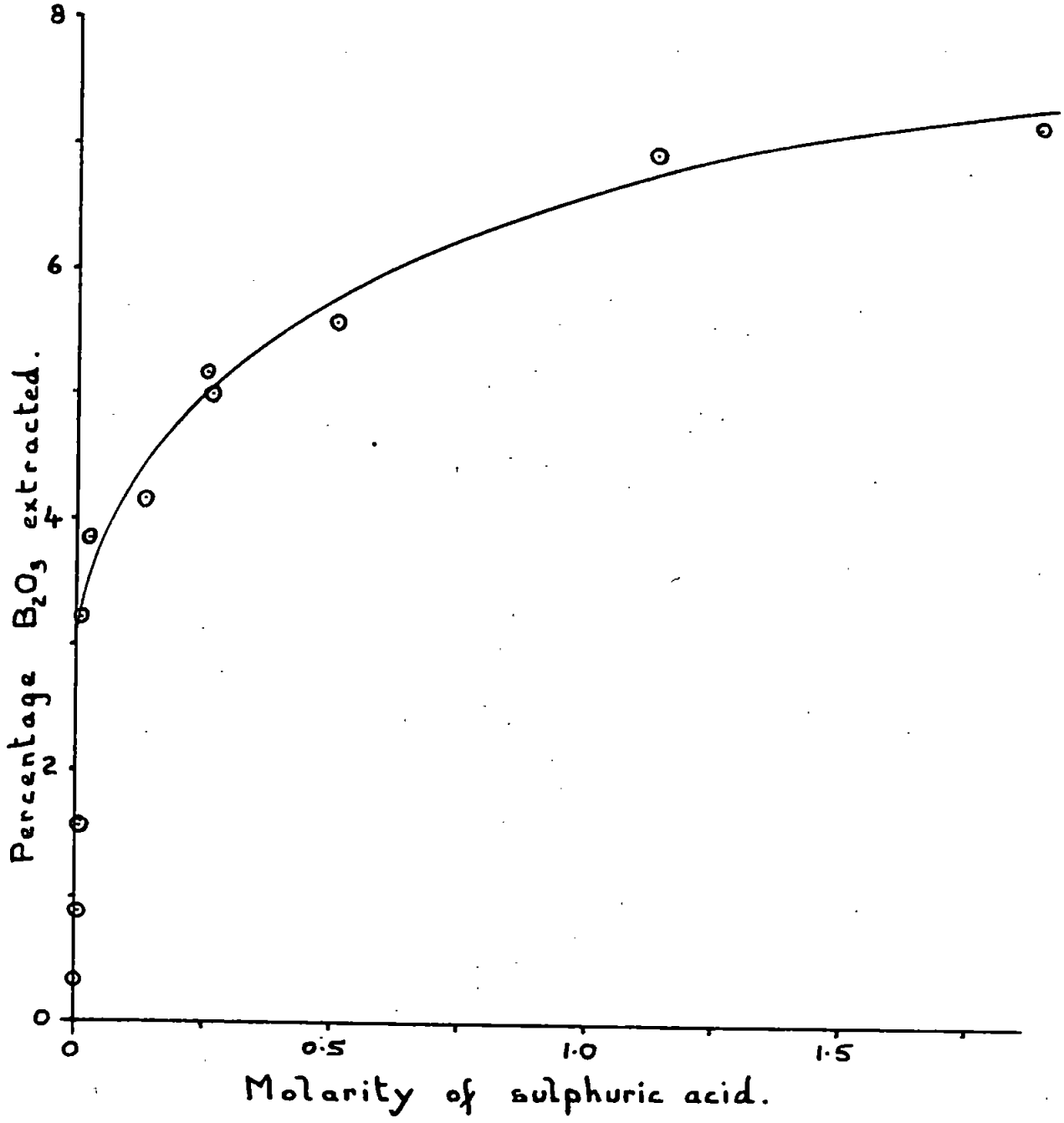

For the adsorption of gases on solids the Langmuir (217) adsorption equation (1) has been found to be widely obeyed:-

$$\Theta = \frac{Kp}{1+Kp} \quad \text{------(1)}$$

Where Θ is the fraction of the surface covered by adsorbed gas at a pressure (p) and K is the equilibrium constant of adsorption.

For the adsorption of solute molecules from a solution the pressure (p) can be replaced by the concentration of the solution (217). This substitution produces the following adsorption equation (2):-

$$\Theta = \frac{Kc}{1+Kc} \quad \text{-----(2)}$$

The amount of solute adsorbed (m) will be directly proportional to the fraction of the surface covered by solute molecules (Θ). The Langmuir equation can therefore bewritten in the form (3). given below:-

$$m = b\Theta = \frac{bKc}{1+Kc} \quad \text{-----(3)}$$

This equation was used in a slightly modified form (4) for plotting the percentage of boric oxide extracted as a function of the sulphuric acid concentration:-

$$\frac{c}{m} = \frac{1}{bK} + \frac{Kc}{bK} \quad \text{-----(4)}$$

The quantity of active species adsorbed (m) was taken, in the present investigation, to be directly proportional to the percentage of boric oxide extracted, in the adsorption function (5) given below:-

$$\frac{c}{a(\%B_2O_3)} = \frac{1}{bK} + \frac{Kc}{bK} \quad \text{---(5)}$$

Where a,b are the two proportionality constants and K the equilibrium constant of adsorption.

This derived adsorption equation was used to plot the experimental results. The adsorption curve obtained is shown in graphical form in Figure 14.

This equation was found to be obeyed up to a concentration of about 0.5M.H_2SO_4. At higher concentrations the amount extracted was found to become progressively larger than that predicted by the adsorption of a monolayer of active species on the reaction surface. At such concentrations multi-layer absorption may occur; this would lead to the extraction process proceeding at several reaction sites at the same time. The rate of extraction would then be greater than that predicted by the derived adsorption function (5).

The adsorption functions (4) has also been found by Geffcken and Berger (162) to be obeyed in the case of the alkali dissolution of a glass, see Chapter 7.3.4.

(1.4) General Rate Equation.

It was thought that the combination of the acid extraction studies into a single rate equation would be useful in deducing the percentage of boric oxide extractable from air decomposed schorl for a general set of

FIGURE 14.

Rate of extraction of B_2O_3 as a function of the acid concentration, plotted on two scales, using a derived Langmuir adsorption isotherm.

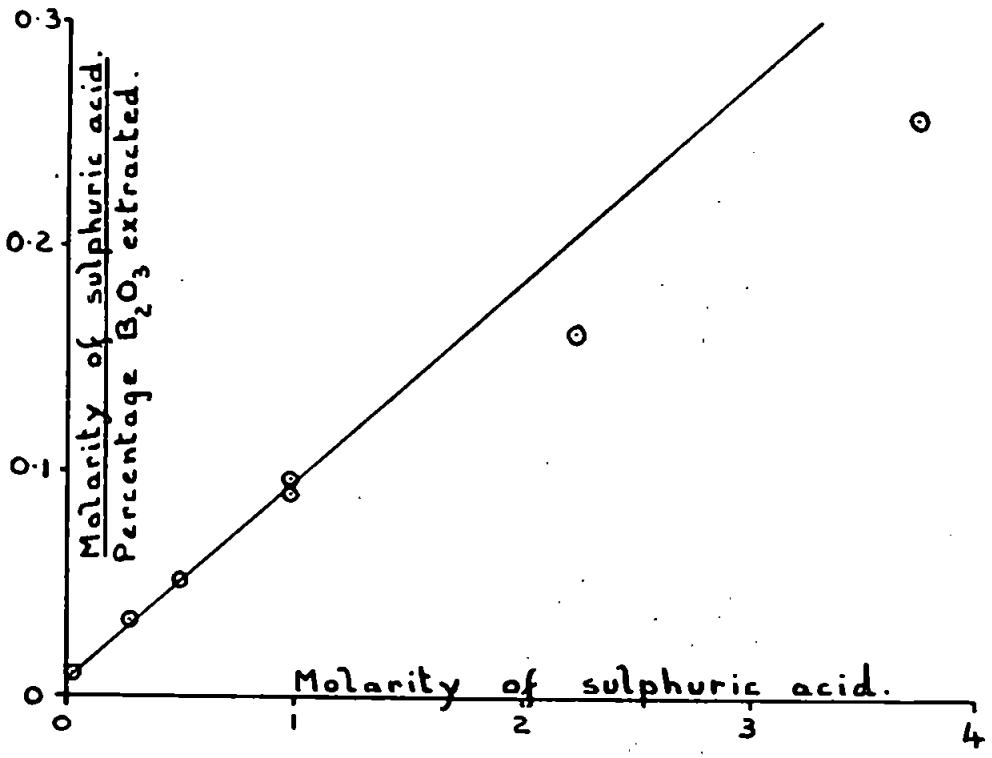

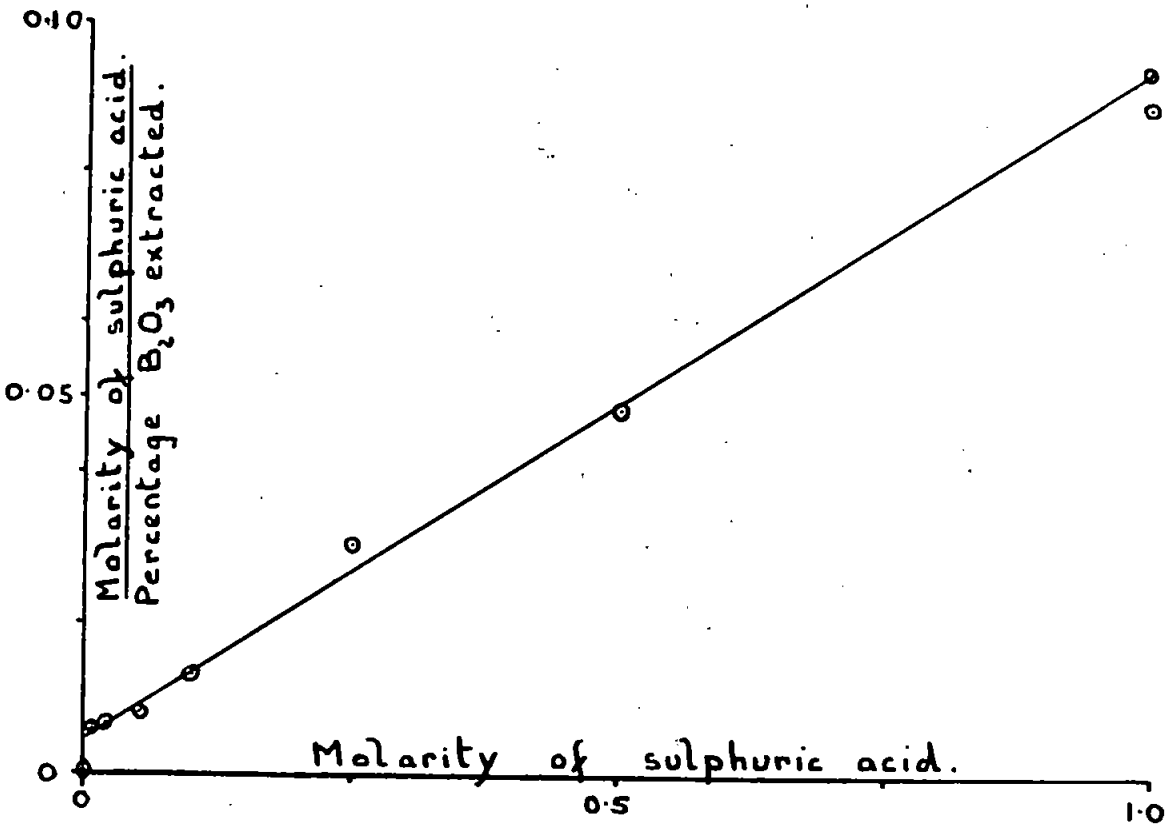

variables. The rate equation for the extraction of boric oxide from air decomposed schorl (8/2) was derived from the following experimental results:-

(i) The activation energy for the diffusion process was found to be equal to 19.2 ± 0.4 kcal/mole, see section 1.1.1.1.

(ii) The activation energy of the extraction process was found to be equal to 7.99 ± 0.4 kcal/mole, see section 1.2.1.

(iii) The rate equation found for the extraction of boric oxide from 5.00 g. of (100-300) mesh schorl, which had been heated for 1 hour at 1100°C, equals:-

$$(\%\ B_2O_3) = 10.3t^{0.41} \quad \text{------(1)}$$

The leaching agent required to derive this rate equation was 100ml. of 0.5M.H_2SO_4, see Table 30.

The total weight of n spherical granules of radius (r) and density (p) equals:-

$$M = 4/3\ \pi\ r^3\ np \quad \text{----(2)}$$

The total surface area (S_n) equals:-

$$S_n = 4\pi r^2 n \quad \text{------(3)}$$

By eliminating n from equations(2) and (3) the total surface area (S_n) becomes equal to:-

$$S_n = \frac{3M}{pr} \quad \text{----(4)}$$

The surface area per unit mass (S_o) therefore equals:-

$$S_o = \frac{3}{pr} \quad \text{--------(5)}$$

The (100-300) mesh granules of decomposed schorl, used in the extraction experiments, have a mean radius of about 0.005 cm. The rate equation (1) can therefore be reduced to an expression which relates the percentage of boric oxide extracted to a surface of unit area by dividing the rate constant by S_o:-

$$(\%\ B_2O_3) = \frac{10.3t^{0.41}}{S_o}$$

$$\therefore\ (\%\ B_2O_3) = 0.052t^{0.41}\ p/3 \quad \text{----(6)}$$

Because the extraction process proceeds via a surface reaction the rate of extraction is directly proportional to the surface area of the sample. Therefore the "specific" equation (6) can be generalised to relate the percentage of boric oxide extracted with the leaching time for granules of any size by multiplying equation (6) by the surface area per unit mass (S_o):-

$$\%B_2O_3 = 0.052\ \frac{p}{3}\ t^{0.41}\ S_0$$

$$\therefore\ \%\ B_2O_3 = \frac{0.052t^{0.41}}{r} \quad \text{--------(7)}$$

The rate constant in this equation (7) was obtained using a leaching temperature of 100°C and schorl which had been decomposed at 1100°C. This equation can be generalised to cover any leaching temperature

(Θ ^{o}K) and decomposition temperature ($T^{o}K$) using the experimental activation energies given above. The general rate equation for the extraction of boric oxide using 0.5M.H_2SO_4 then becomes equal to:-

$$\%B_2O_3 = 0.052\, t^{0.41} \exp\ [[(19200 \pm 400)/2)\ (1/1373 - 1/T)]$$
$$\times \exp\ [((7990 \pm 190)/2)\ (1/373 - 1/\Theta)]\ /r$$

This equation is valid only up to approximately 50 per cent boric oxide extracted because the remainder is incorporated in the relatively inextractable crystalline phase.

(2) Extraction from Schorl Decomposed in Reducing Conditions.

Banateanu et. al. (20) found that the boron present in the mineral ludwigite ($MgFe^{2+}$) $Fe^{3+}(BO_3)_2$ was more readily extractable, if the mineral was decomposed by sodium carbonate in reducing conditions, see Chapter 1.4.3.

In the experiments to be described in this section 1.00g. of (100-300) mesh decomposed - reduced schorl (8/1) was used. The particular sample of decomposed schorl (8/1) used was the one that had been heated for 1 hour at 1200°C in the presence of activated charcoal, see Chapter 11.3.2.

(2.1) Comparison of Extractability of Schorl decomposed in different conditions.

The rate of extraction of boric oxide and iron from decomposed-reduced schorl using 20ml. of boiling 0.5M.H_2SO_4 was determined using the technique described in Chapter 12. The results obtained are compared in Table 34 with those obtained using schorl decomposed at the same temperature in air.

The material formed when schorl is decomposed in reducing conditions is considerably more leachable than the material formed when schorl is decomposed in air. This difference is almost certainly attributable to the existence of elemental iron in the decomposed-reduced material, see Chapter 15.2.

(2.2) Effect of Extraction Temperature.

The effect of the leaching temperature on the rate of extraction of boric oxide and iron was investigated in an endeavour to elucidate in greater detail the nature of the amorphous phase in decomposed-reduced schorl.

The rate of extraction of boric oxide and iron from 1.00g. of (100-300) mesh decomposed-reduced schorl was determined at three different temperatures, using each time 20 ml. of 0.5M.H_2SO_4 as the leaching agent. The results obtained are presented in tabulated form in Table 35.

The rate of extraction of iron was found to be nearly independent of both the extraction time and temperature. This indicates that within the first hour all of the elemental iron present is extracted, whilst the iron oxide remaining is thereafter only slowly leached out by the dilute acid. Because approximately 50% of the iron is extracted within 1 hour at all the three leaching temperatures, the percentage of the original iron oxide present which has been reduced to elemental iron is about 50%.

In contrast the rate of extraction of boric oxide was found to be both strongly time and temperature dependent, see Figure 15. The rate equations for the extraction process carried out at 31.6°C and 61.3°C were found to be parabolic:-

FIGURE 15.

Rate of extraction of B_2O_3 as a function of the leaching temperature.

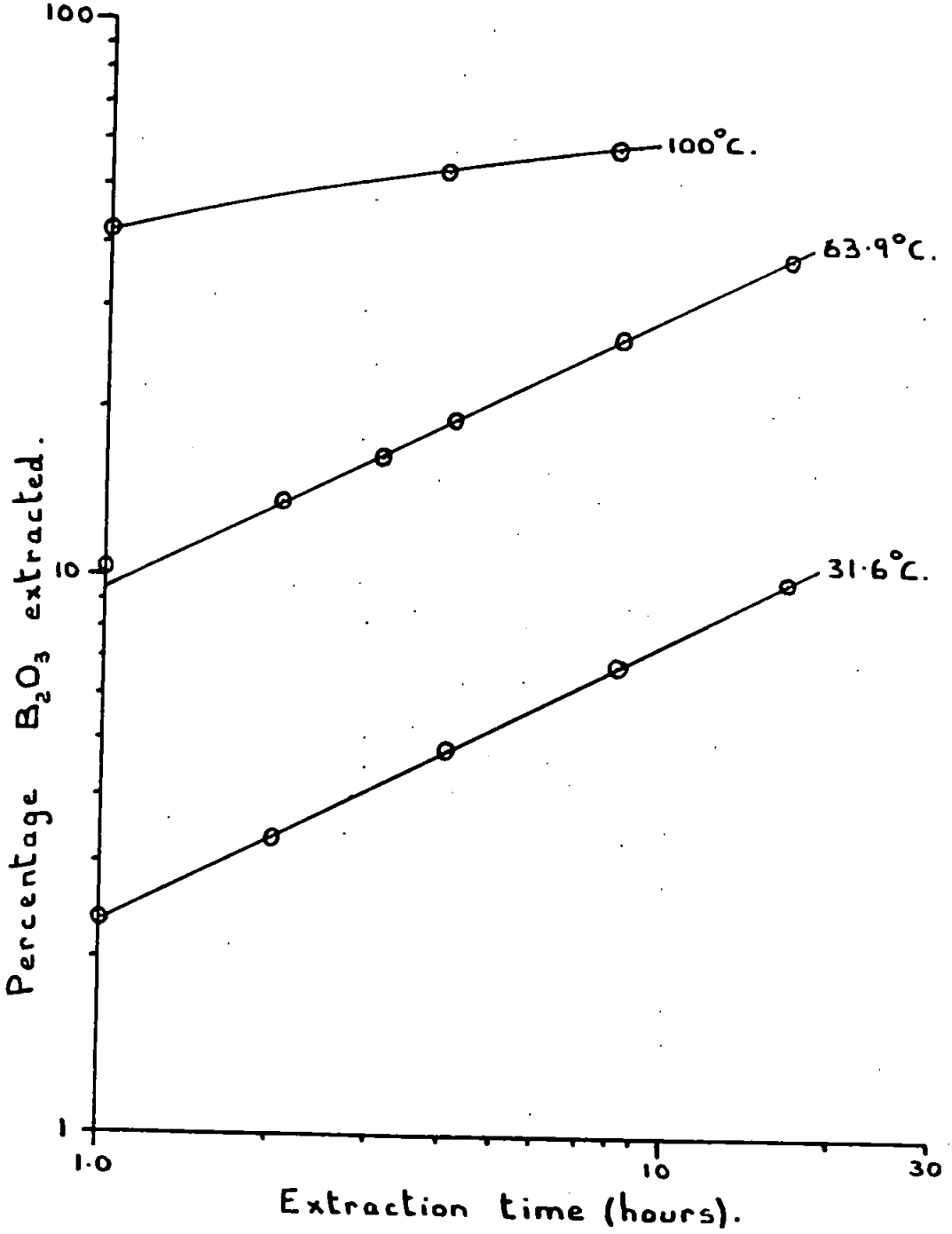

TABLE 34

Comparison of Extractability of Air Decomposed Schorl with that of Schorl Decomposed in Reducing Conditions.

In both sets of experiments the (100-300) mesh fraction was used.				
Extraction time (hours).	Schorl (8/2) 1 hour at 1200°C in Air; 5.00g. material with 100ml. boiling 0.5M.H_2SO_4, see Figures 9 and 11.		Schorl 1 hour at 1200°C in presence of activated charcoal; 1.00g. of material with 20ml. of boiling 0.5M.H_2SO_4.	
	Percentage of Species Extracted.			
	B_2O_3	Fe	B_2O_3	Fe
1	17.8	6.16	43.2	50.2
2	22.6	8.58	49.2	
4	36.6	12.3	55.5	55.2
8	50.6	17.8	60.0	58.7

TABLE 35

Extraction of Boric Oxide and Iron from Decomposed-Reduced Schorl as a Function of the Leaching Temperature.

	(8-100) mesh Schorl-Activated Charcoal heated for 1 hour at 1200°C, crushed, 1.00g. of (100-300) mesh material leached with 20ml. of 0.5M.H_2SO_4.					
Extraction time (hours).	Percentage boric oxide extracted.			Percentage iron extracted.		
	100°C	61.3°C	31.6°C	100°C	61.3°C	31.6°C
0.5	30.6			49.2		
1	43.2	10.0	2.33	50.2	57.2	45.9
2	49.2	13.2	3.25			
4	55.5	18.9	4.74	55.2	58.6	56.1
8	60.0	27.4	6.90	58.7	62.0	62.0
16		38.7	9.81			

At 61.3°C $(\%B_2O_3) = 9.26t^{0.51}$

At 31.6°C $(\%B_2O_3) = 2.32t^{0.50}$

In general the rate of extraction of boric oxide at 100°C did not obey a simple power law. This is probably due to the rapid depletion of the boric oxide present in the leachable amorphous phase, see section 1.1.1. However, the first two experimental values did obey the parabolic equation given below:-

At 100°C $(\%B_2O_3) = 43.2t^{0.50}$

The activation energy for the extraction of boric oxide from the amorphous phase was determined, by taking each time two of the rate constants from the three obtained and then calculating, from the total of three possible, the mean activation energy and the standard deviation. Using this technique the activation energy was found to be equal to 9.70± 0.17 kcal/mole.

This value is slightly higher than the activation energy for the extraction of boric oxide from air decomposed schorl, see section 1.2.1. However, the difference is only 1.7 kcal/mole which indicates that the reduction of about half the iron oxide present does not significantly affect the diffusion process controlling the extraction of boric oxide from the amorphous phase. The similarity between the two activation energies again provides indirect evidence that the amorphous phase contains a "sodium borate" microphase dispersed in a silica-iron oxide matrix. This is because the two activation energies would be expected to be similar if the boric oxide was not bonded to any great extent to the iron oxide.

(2.3) Extraction of Boric Oxide using various reagents.

To compare the extraction efficiency of various reagents 1.00g. of (100-300) mesh decomposed-reduced schorl was boiled for a given period of time with 20ml. of the reagent being investigated. The results obtained are given in tabulated form in Table 36.

The results obtained showed that the rate of boric oxide extraction is enhanced when the reagent used is either strongly acidic or strongly alkaline. When alkalis are used the boric oxide extracted is contaminated with dissolved alumina and when acids are used the main contaminant is iron. Therefore the boric oxide extracted by either type of reagent is contaminated and would require further processing before a pure product could be obtained.

(2.3.1.). X-ray Diffractometry of Solid Remaining after Alkali Leaching.

When the material remaining after acid leaching was examined by X-ray diffractometry no new crystalline product was found to be formed, see Table 32. However, when the material remaining after alkaline extraction was similarly examined several new interplanar spacings were obtained. To elucidate the nature of this new crystalline phase the simpler aluminosilicate "mullite ($3Al_2O_3 2 SiO_2$)" was boiled for 16 hours with M.NaOH. The powder remaining was then examined by X-ray diffractometry, see Chapter 9.3.2. The interplanar spacings obtained from the material formed by the alkali leaching of mullite ($3Al_2O_3.2SiO_2$) are compared in Table 37. with those obtained from the solid remaining after the alkali leaching of decomposed-reduced schorl.

TABLE 36

Extraction of Boric Oxide from (100-300) mesh Decomposed-Reduced Schorl using various Reagents.

Schorl decomposed for 1 hour at 1200°C in the presence of Activated Charcoal; 1.00g. boiled with 20ml. of reagent.		
Boiling time (hours).	Reagent.	Percentage extracted.
16	H_2O	1.90
16	0.5M.Na_2CO_3	7.20
16	M.NaOH	63.4
16	0.5M.H_2SO_4	65.3
8	M.NaOH	52.5
8	0.5M.H_2SO_4	60.2

TABLE 37

Interplanar spacings from Material formed by the Alkali Leaching of Mullite and Decomposed Schorl.

Spacings (Å) of material remaining after boiling with M.NaOH for 16 hours.									
Schorl		Mullite		Xal	Schorl		Mullite		Xal
I	d Å	I	d Å	species	I	d Å	I	d Å	species
2	7.0	1	7.0	S	2	2.170	5	2.190	M
2	5.32	1	5.32	M	3	2.090	8	2.111	M
1	4.97	1	4.94	S	5	2.030			Fe
5	4.10	3	4.05	S	3	1.815	3	1.829	M
3	3.34	10	3.38	M	3	1.668	4	1.690	M
10	3.17	4	3.14	S	1	1.581	2	1.588	M
		6	2.858	M	2	1.506	10	1.517	M
8	2.675	7	2.675	M	2	1.413	5	1.435	M
2	2.501	6	2.535	M	1	1.268	3	1.268	M
		4	2.416	M			3	1.260	M

Key:– I Relative Intensity; M Mullite; S New Crystalline species.

The similarity of the new spacings indicates that the new crystalline phase formed is the same and is almost certainly a sodium aluminium silicate. This compound is probably formed by the attack of sodium ions on the mullite crystals and was identified as a sodium aluminium silicate hydrate using the A.S.T.M. index (212). A comparison of the new interplanar spacings with those listed in the A.S.T.M. index (212) for sodium aluminium silicate hydrates is given in Table 38. All the silicates listed have a molar ratio of SiO_2 to Al_2O_3 considerably higher than that in either mullite or the boron containing mullite in decomposed schorl. The main reactions leading to the formation of the hydrated silicate phase are therefore:-

(i) The removal of the Al^{3+} ions by the following reaction:-

$NaOH + Al^{3+}$ Sol. $\longrightarrow$ Soluble sodium aluminate

(ii) Incorporation of Na^+ and OH^- ions into the disrupted mullite lattice.

The overall formation of one of the hydrated silicates listed in Table 38 is shown schematically below:-

$$2NaOH + 6(3Al_2O_3 2SiO_2) + H_2O \longrightarrow$$

$$\longrightarrow Na_2O.2Al_2O_3.12SiO_2.12H_2O + 32Al_2O_3 \text{ (Present as dissolved aluminate).}$$

(A.S.T.M. index No.12-687)

TABLE 38

Comparison of Interplanar Spacings of the New Crystalline Phase formed by the Alkali Leaching of Mullite or Decomposed Schorl with those listed in the A.S.T.M. index for Sodium Aluminium Silicates.

	Interplanar spacings (Å); with relative intensities in brackets.			
Schorl; 16 hrs. with boiling M.NaOH	7.0 (20)	4.97 (10)	4.10 (50)	3.17 (100)
Mullite; 16 hrs. with boiling M.NaOH	7.0 (10)	4.94 (10)	4.05 (30)	3.14 (100)
$Na_2O.Al_2O_3.5SiO_2.5.4H_2O$ (12-229)	6.85 (100)	5.00 (100)		3.43 (100)
$Na_4Al_2SiO_6O_{17}.H_2O$ (2-0577)	6.51 (70)	4.84 (70)		3.10 (100)
$NaAl_2Si_6O_{16}6H_2O$ (12-687)	7.10 (80)	5.74 (50)	4.08 (100)	3.16 (100)

(2.4) Mechanism of the Extraction Process.

The rate of acid leaching of boric oxide from the reduced decomposed schorl is faster than that from schorl decomposed in air, see Table 34. This is probably related to the faster rate at which the acid attacks the micro-crystals of iron present in the reduced material. This process would be expected to lead to a more porous material, thereby producing granules in which the boric oxide present would be more readily leachable. However, the extraction of boric oxide does not appear to be directly relatable to the rate of extraction of iron, because the activation energy for the extraction of boric oxide is equal to 9.70 ± 0.17 kcal/mole, whilst no significant variation

in the rate of extraction of iron was found with increase in the leaching temperature.

(3) Probable Mechanism of Heterogeneous Surface Reaction and General Discussion of the Liquid Extraction Experiments.

The most important quantitative kinetic data obtained from the liquid extraction studies are given below:-

(i) The activation energy for the extraction process from the amorphous phase in air decomposed schorl was found to be equal to:-

7.99 ± 0.19 kcal/mole for the extraction of B_2O_3

7.15 ± 1.04 kcal/mole for the extraction of Fe.

(ii) The activation energy for the extraction of boric oxide from the amorphous phase in decomposed-reduced schorl was found to be equal to 9.70 ± 0.17 kcal/mole.

(iii) The activation energy for the extraction process as a function of the schorl decomposition temperature was found to be equal to:-

19.2 ± 0.4 kcal/mole for the extraction of B_2O_3

10.9 ± 2.0 kcal/mole for the extraction of Fe.

The variation in the rate of extraction of boric oxide with schorl decomposition temperature was found to obey the exponential Arrhenius type function given below:-

Rate constant = A exp (-E/RT)

The increased rate of extraction with decomposition temperature was thought to be associated with the formation and growth of "sodium borate" microphases within the silica-iron oxide amorphous matrix. This diffusional growth would be expected to obey an activated Arrhenius type function (214) and was monitored in this investigation by following the increase in the rate of extraction of boric oxide with increase in decomposition temperature. The growth of such microheterogeneous regions within a sodium borosilicate glass has been investigated in detail by Kiyohisa et.al. (138) who found that the activation energy of the phase separation process was equal to 62 kcal/mole. The reason for the lower activation energy found in the present investigation may be due to:-

(1) The incomplete formation of a three dimensional lattice in the amorphous phase in decomposed schorl. The looser nature of this type of lattice would probably lead to a lower value for the activation energy of the diffusion process.

(2) The presence of Fe^{2+} ions in the amorphous phase. The presence of such ions may distort the amorphous silica lattice, thereby lowering the energy barrier of the diffusion process producing the phase separated regions.

The exact reason for the lower value for the activation energy found in the present investigation is not, however, known with certainty.

The increased extraction of iron with increase in decomposition temperature is possibly associated with the increased degree of distortion and disruption of the silica lattice as more Fe^{2+} ions are incorporated into the lattice. The increase could, however, be due to the formation and growth of microscopic regions within the

silica matrix containing mainly Fe^{2+} and O^{2-} ions. In view of the lack of relevant information no definite conclusions could be reached on the exact reasons for the increased rate of acid leaching of iron with increase in schorl decomposition temperature.

The activation energy for the leaching of normal glasses has been found to be close 20 kcal/mole, see Table 12. However, Kiyohisa et. al. (138) have found that the activation energy for the extraction of boric oxide and sodium oxide from a phase separated glass was equal to 6.9 kcal/mole. This value is close to the activation energy for the extraction of boric oxide and iron from decomposed schorl, indicating that the overall structure of the two amorphous materials are similar. These experiments therefore provide further indirect evidence that the amorphous phase in decomposed schorl contains microheterogeneous regions.

The extraction process was found in general to follow a parabolic law (1), indicating that the rate of leaching is controlled by some diffusion process:-

Rate of extraction $= kt^{0.5}$ ----(1)

Kiyohisa et. al. (138) thought that the rate controlling step was the diffusion of the B_2O_3–Na_2O phase through the porous silica membrane filled with acid. However, this was not thought to be the rate controlling process in the extraction of either boric oxide or iron from decomposed schorl because:-

(1) The rate of extraction of boric oxide was affected by the acidity and alkalinity of the leaching agent, see Table 36. If the diffusion of the B_2O_3–Na_2O phase controlled the rate of extraction, then the acidity or alkalinity of the leaching agent would not be expected to affect the leaching process.

(2) The diffusion of the liquid leaching agent would be expected to be much more rapid that that of the solid B_2O_3–Na_2O phase. The leaching agent will therefore diffuse to the reaction surface and dissolve a portion of the surface before the B_2O_3/Na_2O solid phase could diffuse.

The overall rate of extraction of boric oxide and iron from decomposed schorl is therefore controlled by one of the following processes:-

(1) Diffusion of active species to reaction surface. The rate of extraction of boric oxide, as a function of the acid concentration, was found to follow a Langmuir type adsorption function up to 0.5M.H_2SO_4, see section 1.3. Therefore the extraction process at low acid strengths is directly controlled by the availability of active species at the reaction surface. This indicates that the overall rate is controlled by the diffusion of active species to the reaction surface. At higher acid concentrations the increase in the rate of extraction is much smaller than the increase in availability of active species. The overall rate of extraction is then probably controlled by surface area considerations.

(2) Heterogeneous chemical reaction at reaction surface. Because of the low activation energy found for the extraction process this was not thought to be the rate controlling process. At higher acid concentrations where the overall rate of extraction is much smaller than the increase in the availability of active species, the extraction process does appear to be controlled by the heterogeneous chemical reaction. However, this is not necessarily true because even if the chemical reaction occurred instantaneously only a certain number of active species could be

adsorbed as a monolayer on the reactive surface. Therefore at high acid concentrations the overall rate of extraction appears to be limited by surface area considerations. The continuing slow increase in the rate of extraction at higher acid concentrations is probably controlled by the rate of multi-layer absorption of active species on the reaction surface of limited surface area.

(3) Diffusion of dissolved species from reaction surface through granules to surface. If this process was the rate controlling step the rate of extraction of boric oxide would not have obeyed the derived Langmuir adsorption isotherm, see section 1.3. Therefore in general this does not appear to be rate controlling process.

The overall extraction process can therefore be broken into the following elementary steps:-

(1) Diffusion of active species to granule surface. The active species are H^+ and SO_4^{2-} ions when sulphuric acid is used and Na^+ and OH^- ions when sodium hydroxide is used.

(2) Absorption of active species on granule surface.

(3) Diffusion of active species through granule to reaction surface. This is probably the rate controlling step.

(4) Activated bond breaking solid-liquid reactions at reaction surface, leading to the dissolution of B_2O_3, Na_2O and FeO when acids are used and B_2O_3, Al_2O_3 and some SiO_2 when alkalis are used.

(5) Diffusion of dissolved salts from reaction surface through granule to surface.

(6) Desorption of salts.

(7) Diffusion of dissolved salts away from granule surface.

The structure of the boron rich amorphous phase given below, was thought to be representative of the many possible considering the complexity of the system. The proportion

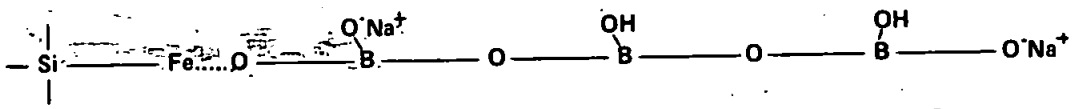

of the total boric oxide which is present in the amorphous phase of schorl decomposed at 1100°C was found to be 54%, see Table 31. Therefore the molar ratio of B_2O_3 to Na_2O in the amorphous phase is 1.5 to 1.0, instead of 3.0 to 1.0 in schorl itself. This ratio was used, in the partial structure given above, as it was representative of that in the amorphous phase of schorl decomposed between 900 and 1300°C. A Fe...O–B bond was included in the structure as it was thought that the boron rich microphase may be connected in some way to the silica-iron oxide lattice, however, this bonding does not affect the proposed leaching mechanism. The bonding could therefore be Si...O–B instead of the one given.

The heterogeneous reactions leading to the extraction of boric oxide by acidic reagents probably proceeds by the following series of elementary steps:-

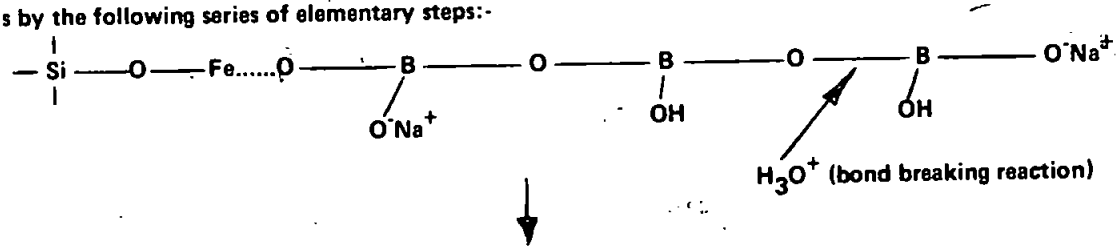

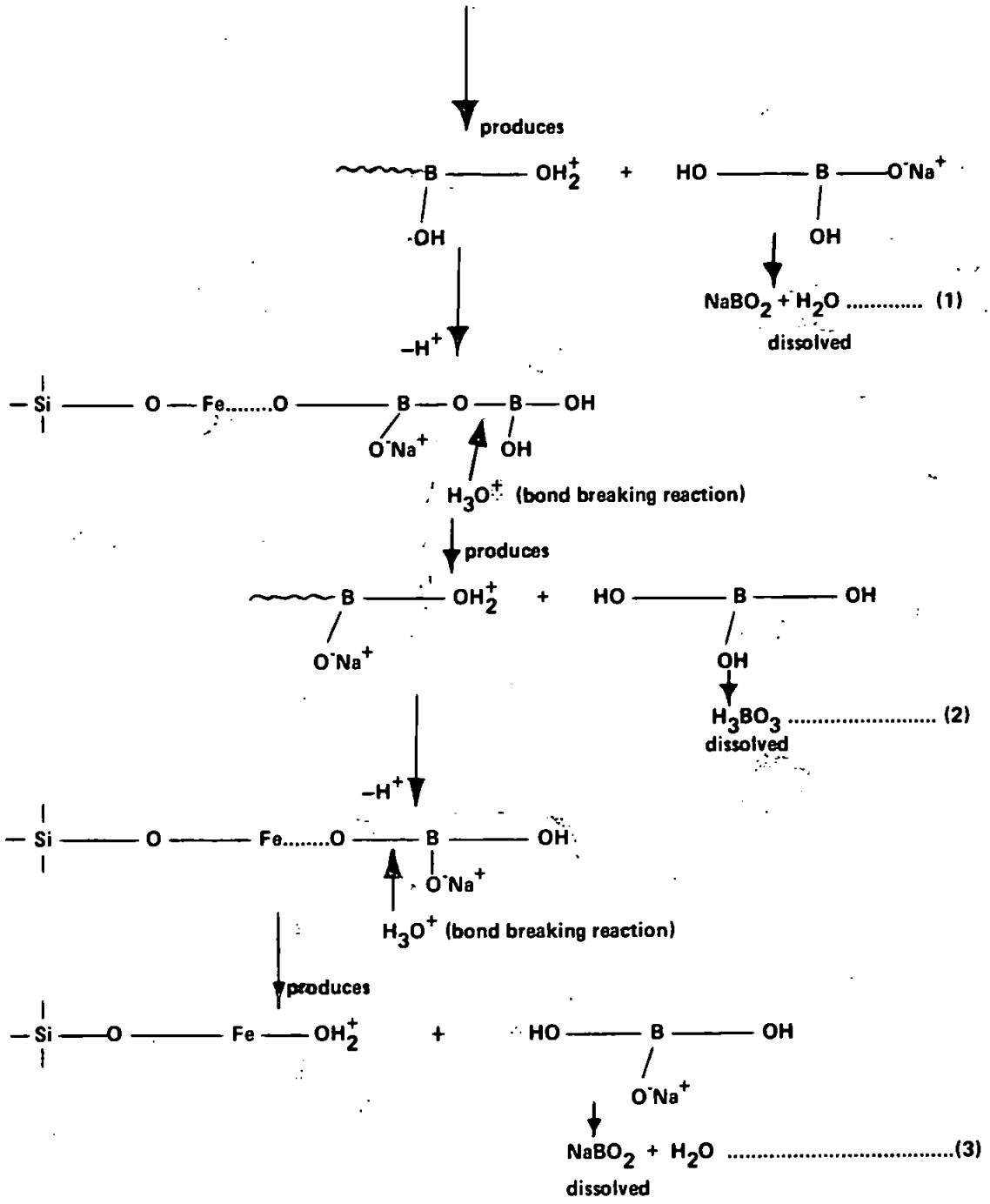

When alkalis are used as leaching agents the extraction of boron oxide probably proceeds by the following series of elementary steps:-

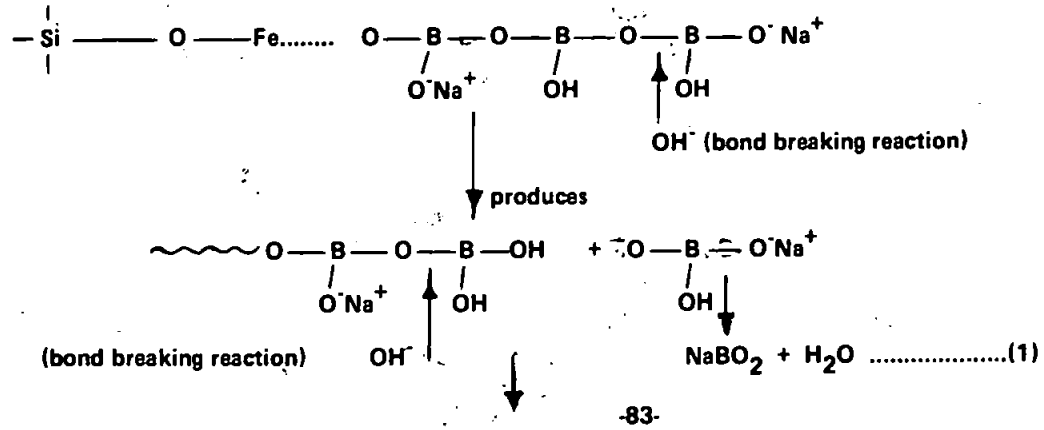

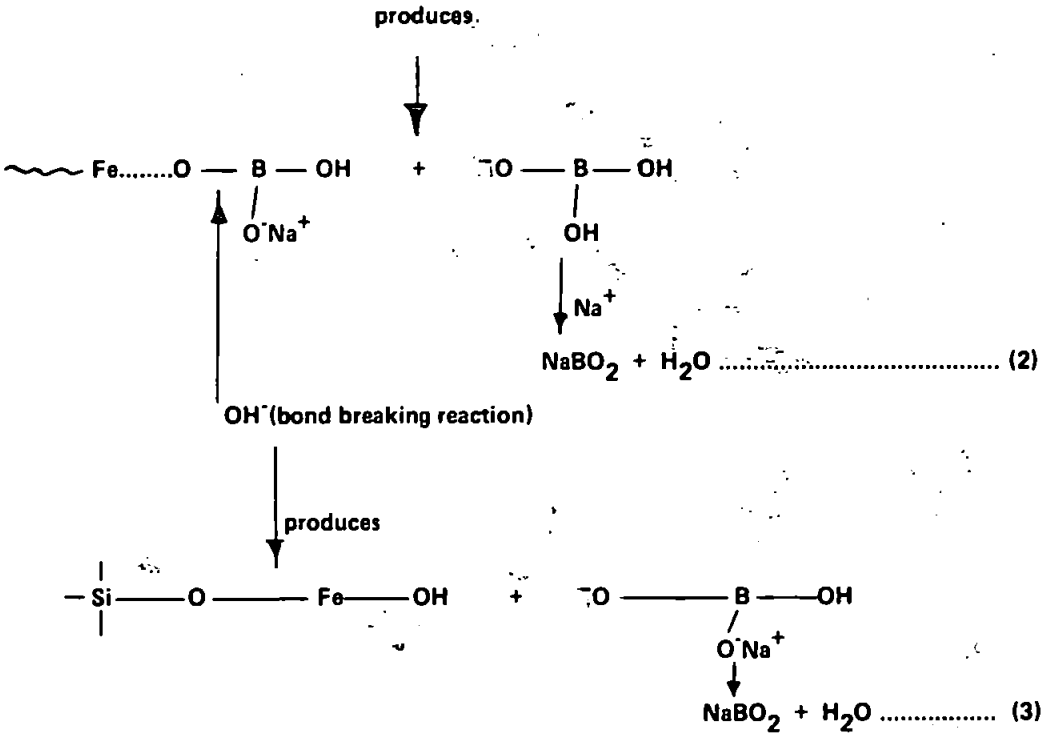

The structure of the silica-iron oxide amorphous phase is probably similar to that shown schematically below:-

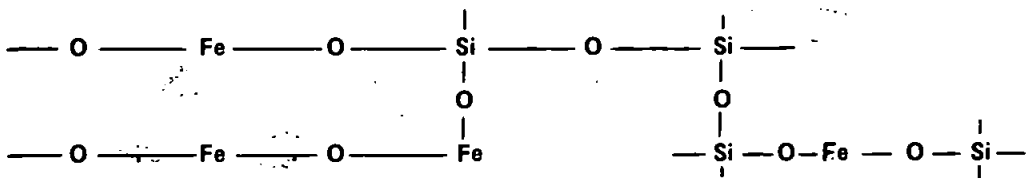

The heterogeneous reactions leading to the extraction of iron from this type of lattice can be envisaged to proceed as follows:-

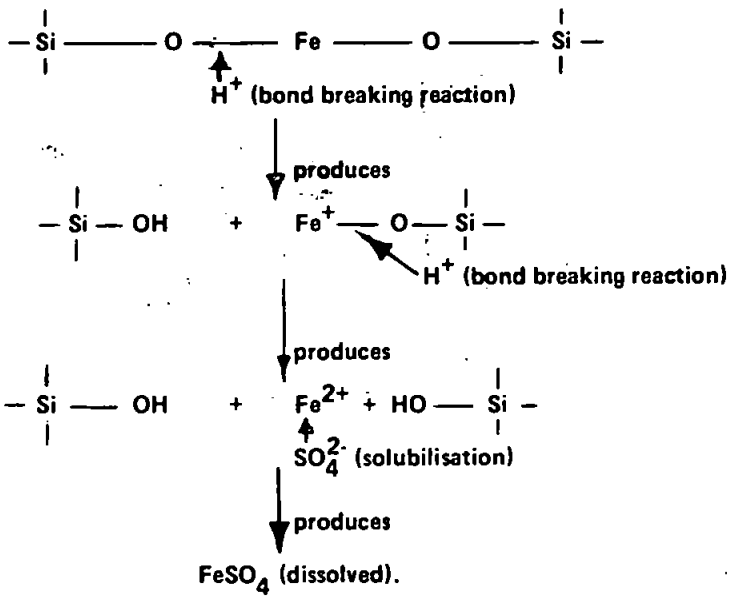

Even if the degree of phase separation is much smaller than in the structures proposed previously, a similar type of activated bond breaking process can be envisaged. The acid leaching of boric oxide and iron from a lattice in which the boric oxide is bonded to the silica-iron oxide matrix would probably proceed by the following series of elementary steps:-

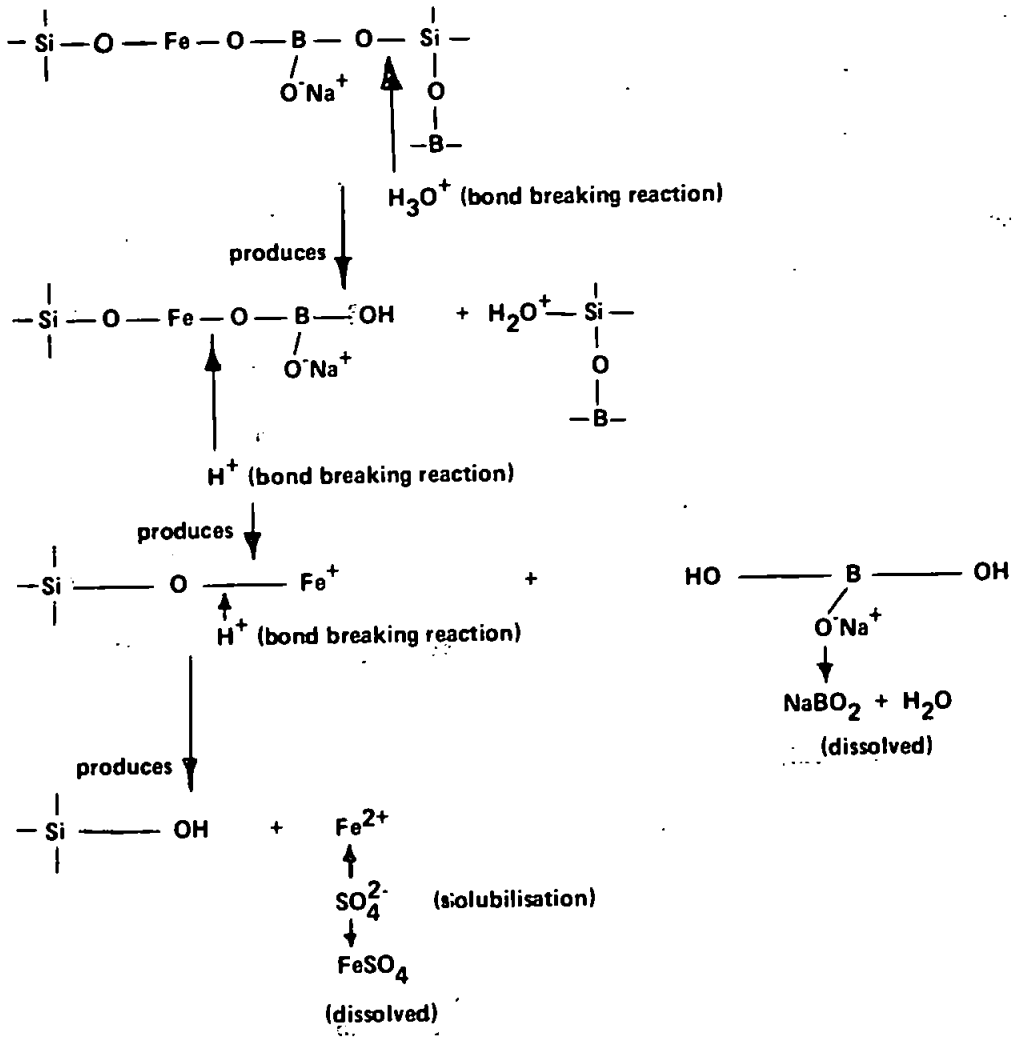

These "ion-molecule" type heterogeneous reactions would be expected to be fast and to have low activation energies, indicating that the rate controlling process is not the heterogeneous reaction.

CHAPTER 17

Pyrohydrolysis Experiments.

(1) Introduction.

Previous investigations have shown that it is possible to extract the boric oxide present in certain glasses and borate ores, by passing water vapour over the materials at high temperatures, see Chapter 5. It was therefore thought probable that the boric oxide present in tourmaline could be similarly extracted. If successful this technique would have the distinct advantage over acid or alkali extraction methods because only boric oxide would be removed by the water vapour.

(2) Preliminary Experiments.

In this section the first preliminary results obtained using the pyrohydrolysis method are described. In the first experiment the (100-300) mesh size fraction from schorl (8/1) decomposed for 1 hour at 1300°C, was used, see Chapter 11.2. 1.000g. of this powder was poured into an alumina boat, which was then introduced into the tube furnace prior to passing steam over the sample, see Chapter 13. The amount of boric oxide extracted was determined as a function of the pyrohydrolysis time. The results obtained are presented in tabulated form in Table 38 and in graphical form on a log-log scale in Figure 16.

If the extraction of boric oxide follows a simple power law of the type (1), then a straight line of slope (n) is obtained when the percentage boric oxide extracted as a function of time is plotted directly on log-log graph paper. The experimental curve obtained, however, is not a straight line but a curve with a continuously decreasing slope. This change in slope indicates that the mechanism of extraction from a powdered material is quite complex.

$$(B_2O_3) = kt^n \quad \ldots\ldots\ldots\ldots\ldots\ldots (1)$$

Sintering of the powder is probably one of the most important processes which leads to the slowing down of the rate of extraction. The importance of sintering was evident by the observation that the material remaining in the boat at the end of the experiment was no longer a powder but a hard compacted solid. A short discussion on sintering of powders at elevated temperatures is given in Appendix 1.

(2.1) Importance of sintering.

The experiments described in this section were designed to investigate the effect of sintering on the extraction process.

In the first control experiment a know weight of (100-300) mesh schorl (8/1) was poured into a mullite boat. This boat was then pushed into the centre of the tube furnace prior to reconnecting the steam supply, see Chapter 13. The rate of extraction of boric oxide by passage of water vapour over the sample was determined. The results obtained are presented in tabulated form in Table 39.

In the next experiment the same weight of (100-300) mesh schorl (8/1) was poured into a mullite boat having the same dimensions as the one used in the control experiment. The powder was then sintered in an oven furnace at 1310°C for a period of 1 hour. The boat was then introduced into the tube furnace and the rate of extraction of boric oxide was determined using the same experimental conditions as those used in the control

FIGURE 16.

Extraction of B_2O_3 by pyrohydrolysis of decomposed schorl (preliminary experiment).

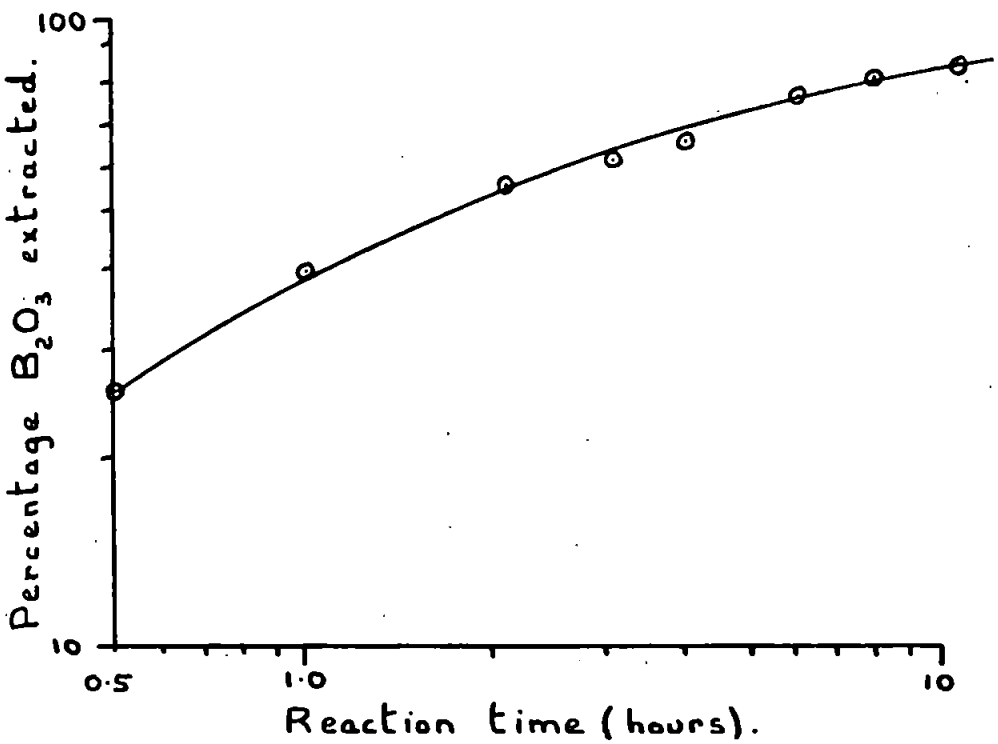

TABLE 38

First Preliminary Experiment to test the feasibility of Extracting Boric Oxide from Tourmaline by passing Water Vapour over the mineral.

(8-100) mesh schorl (8/1) heated for 1 hr. at 1300°C; sintered material crushed and (100-300) mesh fraction used.

Weight of sample 1.000g.
Temperature of preheater 1050°C
Temperature of tube furnace 1260°C
Weight of water passed over sample 1.31 ± 0.08 g./min.

Time steam passed (hours).	Titre of M/20 NaOH	mg. of B_2O_3 extracted	Per cent of B_2O_3 extracted
0.50	13.62	23.7	26.1
1.0	7.16	36.2	39.8
2.0	6.00	46.6	51.2
4.1	8.82	58.4	64.2
6.0	4.52	69.7	76.7
8.0	2.40	74.1	81.4
11.0	2.29	78.0	85.8

TABLE 39

Effect of Sintering on the Rate of Pyrohydrolysis of Boric Oxide from Powdered Schorl.

(100-300) mesh Schorl (8/1)

Wt. of powder in each experiment was 0.531g.

Wt. of water passing in each expt. 3.2 ± 0.1 g/min.

Temperature of tube furnace 1240°C.

Time water passed (min).	Control exptt per cent B_2O_3	Schorl (8/1) 1 hr. at 1310°C. per cent B_2O_3
5	13.6	4.92
10	23.6	9.01
20	37.1	14.4
40	49.2	20.1
60	54.8	23.5
120	61.6	29.3
240	65.5	35.8
300	66.5	38.4

experiment. The results obtained are presented in tabulated form in Table 39 and compared with those obtained in the control experiment in Figure 17.

These experiments were both carried out using the same experimental conditions and with the same geometrical surface area of sample exposed to the water vapour. The reduced rate of extraction in the second experiment can therefore probably be related to the decrease in the specific surface, due to the powder sintering when heated at 1310°C prior to beginning the pyrohydrolysis experiment. Therefore sintering is an important factor influencing the rate at which boric oxide can be extracted from powdered tourmaline.

(2.2) Optimum Particle Size.

Sintering has been found to be an important factor influencing the extraction process. It was therefore thought useful to investigate the effect of particle size on the rate of extraction of boric oxide.

In these experiments three ranges of particle size were used; namely (8-100) mesh, (100-300) mesh and less than 300 mesh respectively. In each experiment the same weight of powder was poured into similar alumina boats, thereby standardising the external surface area of sample exposed to the water vapour. The results obtained are presented in tabulated form in Table 40 and in graphical form on a log-log scale in Figure 18.

A comparison of the results obtained shows that in general the rate of extraction is faster the larger the particle size. This surprising result can be probably explained by considering that the finer powder was sintering much more rapidly than the coarser material and that the corresponding decrease in surface area is faster than the increased rate of pyrohydrolysis from the originally finer powder. The overall effect would then be a reduction in the amount of boric oxide extracted with decrease in particle size.

(2.3) Attempted Determination of the Activation Energy of Pyrohydrolysis.

An attempt was made to determine the activation energy of pyrohydrolysis by determining the rate of extraction of boric oxide from (100-300) mesh schorl at two reaction temperatures. In both experiments the same weight of powder was poured in two similar alumina boats. The pyrohydrolysis experiments were carried out at 1240°C and 1300°C respectively, using the same rate of flow of water vapour.

The percentage of boric oxide extracted as a function of time in both experiments is shown in Figure 19. The curves obtained are clearly of no value in determining the activation energy of the process as any value calculated using the Arrhenius equation (1) would varying with the reaction time.

$$k = A \exp(-E/RT) \quad \ldots\ldots\ldots\ldots (1)$$

(2.4) Conclusions.

The results obtained using powdered samples show that pyrohydrolysis can be used to extract pure boric oxide from tourmaline, although temperatures above at least 1000°C are required to obtain any significant extraction. A systematic study of the extraction process using powdered tourmaline was not undertaken due to the added complication of sintering of the powder.

(3) Systematic Investigations.

(3.1) Introduction.

FIGURE 17.

Effect of sintering on the rate of extraction of B_2O_3 from powdered schorl.

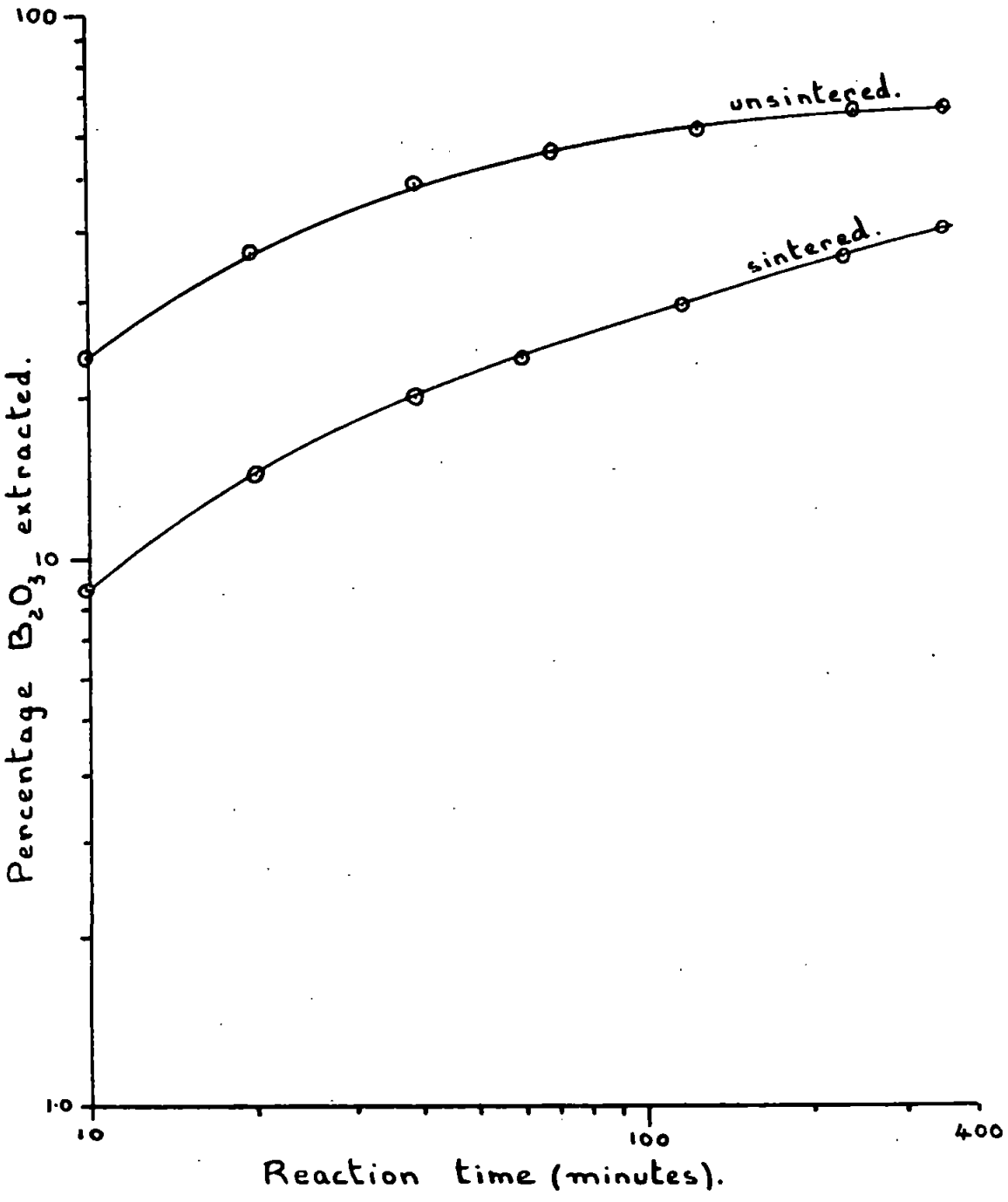

TABLE 40

Effect of Particle Size on the Rate of Extraction of Boric Oxide by Pyrohydrolysis.

Wt. of sample used in each experiment 1.142 g.			
Wt. of water flowing	1.2 ± 0.2 g/min.		
Temperature of furnace	1230 ± 10°C.		
Time water passed (minutes).	Percentage boric oxide extracted from schorl (8/1) of size:-		
	(8-100) mesh	(100-300) mesh	300 mesh
5	8.75	13.6	5.92
10	19.20	23.9	8.31
20	38.6	37.1	11.2
40	57.6	49.4	14.5
60	67.0	54.6	16.7
100	75.0	60.0	20.6
160	80.0	63.8	25.1
240	84.0	66.3	28.5

Due to the difficulties experienced with the use of powdered tourmaline a great deal of effort was expended in trying to overcome the sintering of the powdered samples.

The method thought most likely to overcome this was by heating the schorl granules for a certain period of time at a higher temperature than that at which the pyrohydrolysis experiments are carried out.

The first experiment carried out using this technique involved heating ten separate lumps of (3/16–5) mesh schorl (8/1). Each of these lumps was stuck onto small alumina chips using "durofix" adhesive, to prevent the lumps rolling around whilst being pushed into the tube furnace for the preheat treatment discussed above. The schorl lumps were then sintered for 1 hour at 1390°C. The rate of extraction of boric oxide was then determined using a pyrohydrolysis temperature of 1350°C. The results obtained are presented in tabulated form in Table 41 and in graphical form on a log-log scale in Figure 20.

The curve obtained consisted of two separate straight lines both obeying a simple power law of the type:-

$$(B_2O_3) = kt^n$$

A value of 0.71 for n was found to be valid up to 22 per cent boric oxide extracted when the process was found to continue at a slower rate, a value for n of 0.50 was then found to be valid. The two rate equations

FIGURE 20.

Rate of extraction of B_2O_3 from heat-treated (3/16-5) mesh schorl granules.

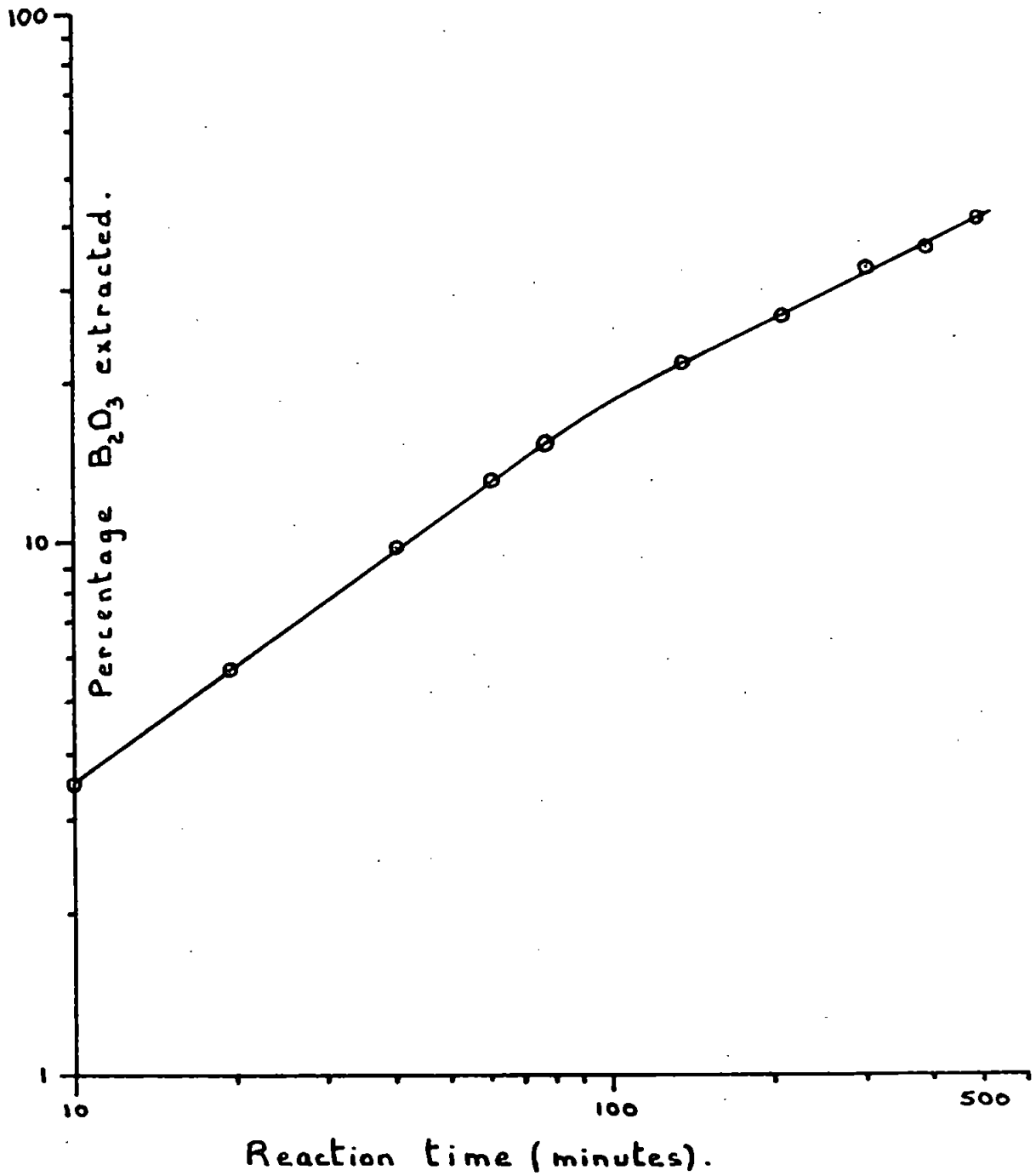

calculated are given below:-

(1) Valid up to 22 per cent B_2O_3 extracted.

$$B_2O_3 = k_1t^{0.71}$$

(2) Valid above 22 per cent B_2O_3 extracted up at least 45 per cent.

$$B_2O_3 = k_2t^{0.50}$$

Although the mechanism of the extraction process is not apparently the same throughout the whole range, at least the individual portions obey similar rate equations as those used in previous heterogeneous reaction studies, see Chapter 7.

This investigation clearly shows that the prior heating of the sample at a temperature above that at which the pyrohydrolysis experiment is carried out has reduced further sintering of the sample during the pyrohydrolysis experiment to a negligible amount.

(3.2) Activation Energy of Pyrohydrolysis from Schorl.

In view of the success of the technique described in the previous section it was thought probable that by using this method that the activation energy for extraction of boric oxide from schorl (8/1) by pyrohydrolysis could be determined. To determine the activation energy it is necessary to also have the same effective surface area of sample exposed to the water vapour at all the temperatures used. This was achieved in the first determination using approximately 1 $cm.^3$ cubes of schorl (8/1) cut from a large lump of tourmaline using a rock cutting machine, see Chapter 8.2. In a second determination (5-8)mesh schorl (8/1) lumps were used.

Another possible variable that may influence the pyrohydrolysis extraction process is the change that was shown to occur in the nature of the amorphous phase when tourmaline is heated at different temperatures. This change was exhibited by the greater extractability of the boric oxide present as the schorl decomposition temperature was increased, see Chapter 16.1.1. This change was thought to be due to the growth of micro-regions of a "sodium borate" phase within the amorphous silica-iron oxide matrix. The prior heating of the schorl at a temperature above those at which the pyrohydrolysis experiments are carried out, would probably reduce any further growth of such regions during the pyrohydrolysis experiments to a negligible amount. The activation energy calculated can therefore then be related to the actual energy barrier of the extraction process and not complicated by other effects.

(3.2.1) Using 1 $cm.^3$ cubes.

The $1cm.^3$ cubes were each placed on a small weighed alumina chip and heated for 1 hour at 1300°C in the oven furnace. All of the cubes were then weighed and paired up in such a way that the total weight of all the pairs were equal to within 0.25%. It was therefore thought probable that the effective surface area of all the paired cubes are equal to within 1%.

In these experiments every effort was made to standardise the experimental conditions. In all the experiments the same rate of flow of water vapour was used and at each temperature the cooling effect of the water vapour was checked using a platinum/13% rhodium-platinum thermocouple placed at the centre of the tube furnace. Only with the tube furnace temperature at 1390°C was there a significantly greater temperature

TABLE 41

Pyrohydrolysis of Powdered Schorl that has been Sintered prior to passing the Water Vapour.

(3/16-5) mesh schorl lumps heated for 1 hr. at 1390°C.

Total weight of 10 lumps 1.1561 g.

Temperature of tube furnace with water passing 1350°C.

Rate of flow of water 2.61 ± 0.06 g/min.

Time water passed (mins.)	Per cent B_2O_3 extracted	Time water vapour passed (mins.)	Per cent B_2O_3 extracted
5	1.84	150	23.1
10	3.49	180	25.4
15	4.73	210	27.5
20	5.72	270	30.9
30	7.54	330	33.7
45	10.2	390	36.2
60	12.7	450	39.1
75	14.8	510	42.2
90	16.6	570	45.1
120	20.2		

decrease than the approximate 5°C variation in the furnace temperature that occurred throughout the day. Therefore when the experiment was carried out at this temperature only 1 minute was allowed between introducing the two cubes and reconnecting the steam supply. At all the other temperatures used 2 minutes was allowed for the cubes to attain the equilibrium furnace temperature prior to starting the pyrohydrolysis experiment by reconnecting the steam supply.

The extraction of boric oxide as a function of the pyrohydrolysis time at each of the five temperatures used is presented in graphical form on a log-log scale in Figure 21. At all the temperatures used the rate of extraction was found to obey a simple power law of the type (1):-

$$(\%B_2O_3) = kt^n \quad \ldots\ldots\ldots\ldots (1)$$

The value of the rate constant (k) and the exponent (n) were calculated from the curves drawn for each of the experimental temperatures and presented in tabulated form in Table 42.

The rate of extraction of boric oxide at 1370°C was not consistent with the rate constants calculated for the extraction process at the other temperatures. The reason for this is not known with certainty but may be related to the observation that one of the cubes was found to have completely disintegrated when examined

FIGURE 21.

Rate of extraction of B_2O_3 from 1 cm^3 cubes of schorl as a function of the pyrohydrolysis temperature.

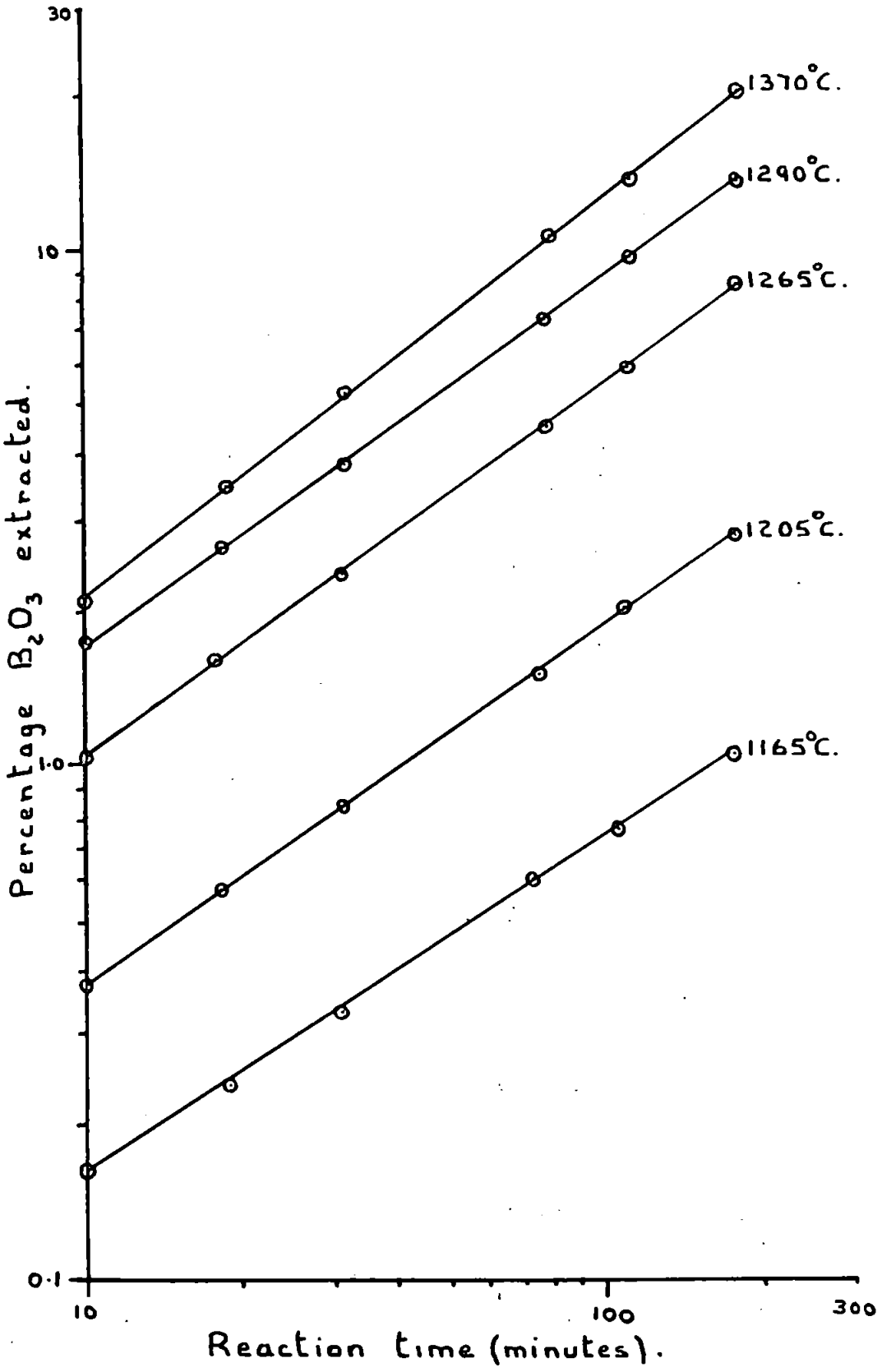

TABLE 42

Extraction of Boric Oxide from 1 $cm.^3$ cubes of Schorl as a Function of Pyrohydrolysis Temperature.

Tube furnace temperature (°C)	1 cm^3 cubes of Schorl (8/1) heated for 1 hour at 1300°C. Weight of two cubes 4.432g (to within 0.25%). Rate of flow water 2.44 ± 0.08 g/min.		
	Pyrohydrolysis temperature (± 5°C)	Rate constant k	Exponent n
1390	1370	0.305	0.827
1300	1290	0.324	0.732
1270	1265	0.179	0.755
1215	1210	0.0759	0.697
1165	1165	0.0336	0.680

at the end of the experiment. Another interesting observation was that the other, still intact cube, was found when broken in half to contain large voids, reminiscent of the appearance of materials such as coke or lava formed at high temperatures in the presence of a gas.

The mean value of the exponent with the standard deviation was calculated using the values listed in Table 42, apart from the one obtained at 1370°C, and found to be equal to 0.71 ± 0.03. The extraction of boric oxide by pyrohydrolysis from 1 cm^3 cubes of schorl was therefore found to obey the following power law (2):-

$$(\%B_2O_3) = kt^{0.71 \pm 0.03} \quad \ldots\ldots\ldots\ldots (2)$$

The acrivation energy of the extraction process was calculated using the Arrhenius equation (3):-

$$k = A.\exp(-E/RT) \quad \ldots\ldots\ldots\ldots (3)$$

The percentage of boric oxide extracted after 100 minutes in each experiment was taken as the relative rate constants in the determination of the activation energy instead of the constants calculated, see Table 42. This was because there seemed to be an increase in the value of the exponent with increase in pyrohydrolysis temperature. This increase is probably related to abnormally low percentage extraction at short reaction times due to the cubes not quite attaining the equilibrium furnace temperature at the higher temperatures within the 2 minutes allowed between introducing the cubes and reconnecting the steam supply. Therefore the percentage of boric oxide extracted after a reaction time of 100 minutes was used, as it was thought that after this period of time such errors would be minimal. The percentage of boric oxide extracted after 100 minutes at each of the pyrohydrolysis temperatures is listed in Table 43.

An Arrhenius plot of $\log_{10}$ (percentage B_2O_3 extracted after 100 mins.) against the reciprocal of the

TABLE 43

Percentage of Boric Oxide Extracted after 100 minutes from

1 cm.^{3} cubes of Schorl as a Function of the Pyrohydrolysis Temperature.

1 cm.^{3} cubes schorl heated for 1 hr. at 1300°C.	
Pyrohydrolysis temperature (°C)	Per cent B_2O_3 extracted after 100 mins.
1290	9.45
1265	5.85
1210	1.88
1165	0.77

pyrohydrolysis temperature (degrees absolute)is shown in Figure 22.

A value of 89 ± 7 kcal/mole for the activation energy was calculated from the slope obtained. The error given was obtained by drawing maximum and minimum slopes through the experimental points and then recalculating the activation energy from the slopes obtained.

(3.2.2) Using (5-8) mesh Schorl (8/1).

Because of the extremely high value found for the activation energy in section (3.2.1), it was thought desirable to redetermine the activation energy at lower pyrohydrolysis temperatures using schorl granules of smaller size.

In these and other experiments a new type of boat was used to contain the samples. Two such boats were made approximately 10 cm. long and 2 cm. wide from a sheet of a high temperature Ni/Cr alloy. These boats had the great advantage in that they were flat bottomed and could be used repeatedly, as the sintered schorl granules were easily removed at the end of each experiment.

To prevent the granules rolling around, whilst the boats are pushed into the tube furnace, the surface of each was covered with a thin film of "durofix" glue. The same known weight of (5-8) mesh schorl granules was then carefully sprinkled over the surfaces in such a way that each granule was separate from the others. Because the same weight and size distribution of schorl granules was sprinkled into each boat the total effective surface area of each sample was the same. To complete the sintering of the small tourmaline crystals within the (5-8) mesh granules each boat was introduced into the tube furnace and left for 10 minutes at 1350°C.

In these experiments a smaller rate of flow of water was used as compared to those used previously and when combined with the lower experimental temperatures it was found possible to maintain the pyrohydrolysis temperature to within ± 3°C.

The rate of extraction of boric oxide at the two pyrohydrolysis temperatures is presented in tabulated

FIGURE 22.

Arrhenius plot of the rate of extraction of B_2O_3 as a function of the pyrohydrolysis temperature.

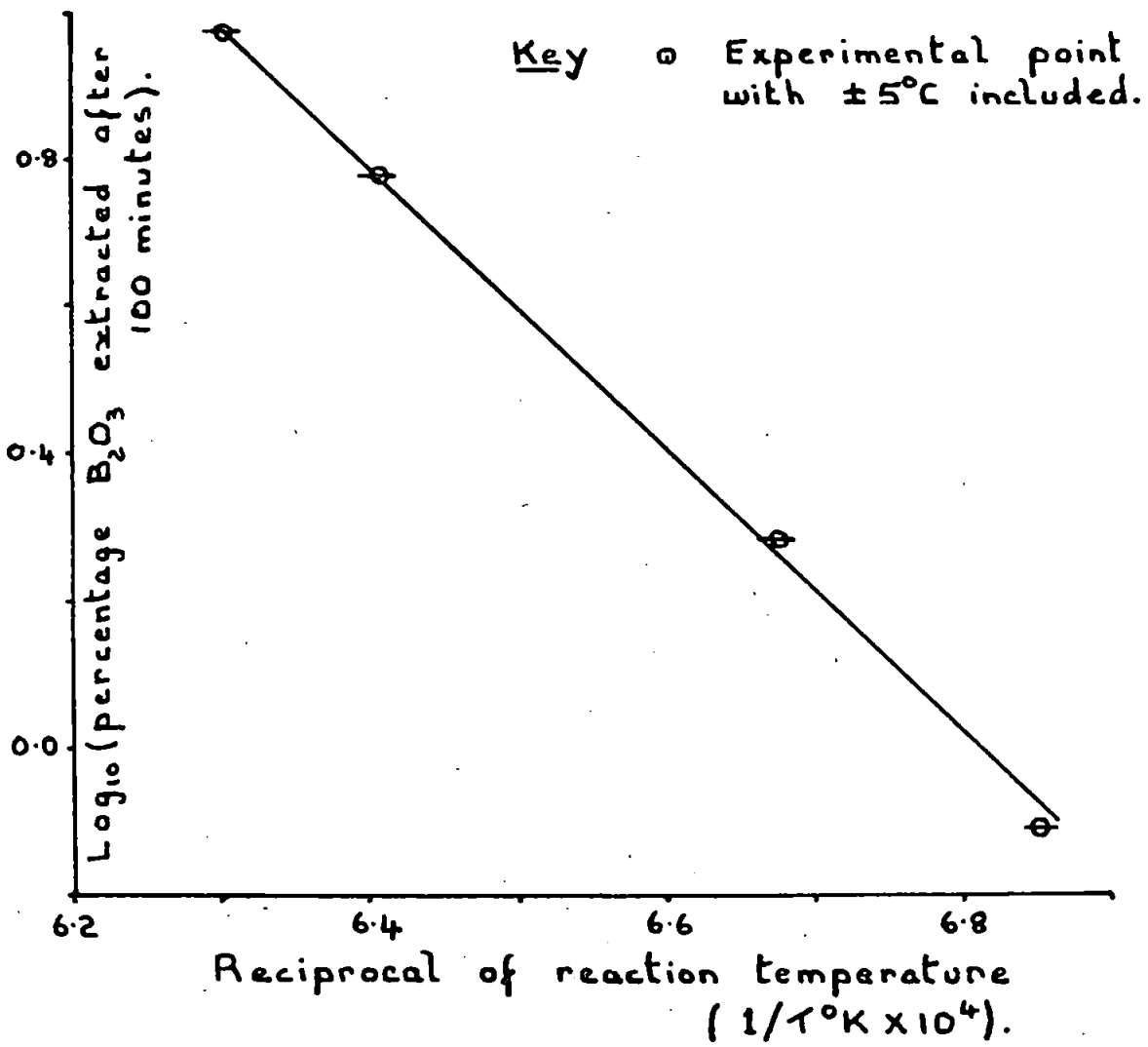

form in Table 44 and in graphical form on a log-log scale in Figure 23. The two rate equations calculated from the log-log curves are included in Table 44.

The activation energy (E) for the pyrohydrolysis of boric oxide from schorl was calculated from the two experimental rate constants given in Table 44 using the Arrhenius equation:-

$$k = A \exp (-E/RT)$$

A value for the activation energy of 81 ± 9 kcal/mole was obtained and the error included was calculated on the assumption that the maximum temperature variation during each experiment was ± 3^0C.

TABLE 44

Extraction of Boric Oxide from (5-8) mesh Schorl as a Function of Pyrohydrolysis Temperature.

(5-8) mesh schorl (8/1) granules heated for 10 mins. at 1350°C.		
Time water vapour passed. (minutes).	Total weight 1.153 g. Rate flow water 0.69 ± 0.02 g/min. Temperature 1158 ± 3°C.	Total weight 1.134 g. Rate flow water 0.89 ± 0.05 g/min. Temperature 1100 ± 3°C.
	Percentage B_2O_3 extracted.	Percentage B_2O_3 extracted.
10	10.8	3.15
20	14.5	4.69
30	18.3	5.65
45	23.1	6.84
60	26.5	7.90
90	31.7	10.0
120	36.1	11.2
180	44.1	13.4
Rate Equations calculated:- (1) 1100°C (% B_2O_3) = $1.03t^{0.50}$ (2) 1158°C (% B_2O_3) = $3.34t^{0.50}$		

(3.3) Conclusions and possible mechanisms of Pyrohydrolysis.

The activation energy of pyrohydrolysis from schorl was found in two completely separate experiments

FIGURE 23.

Rate of extraction of B_2O_3 from (5-8) mesh schorl granules as a function of the pyrohydrolysis temperature.

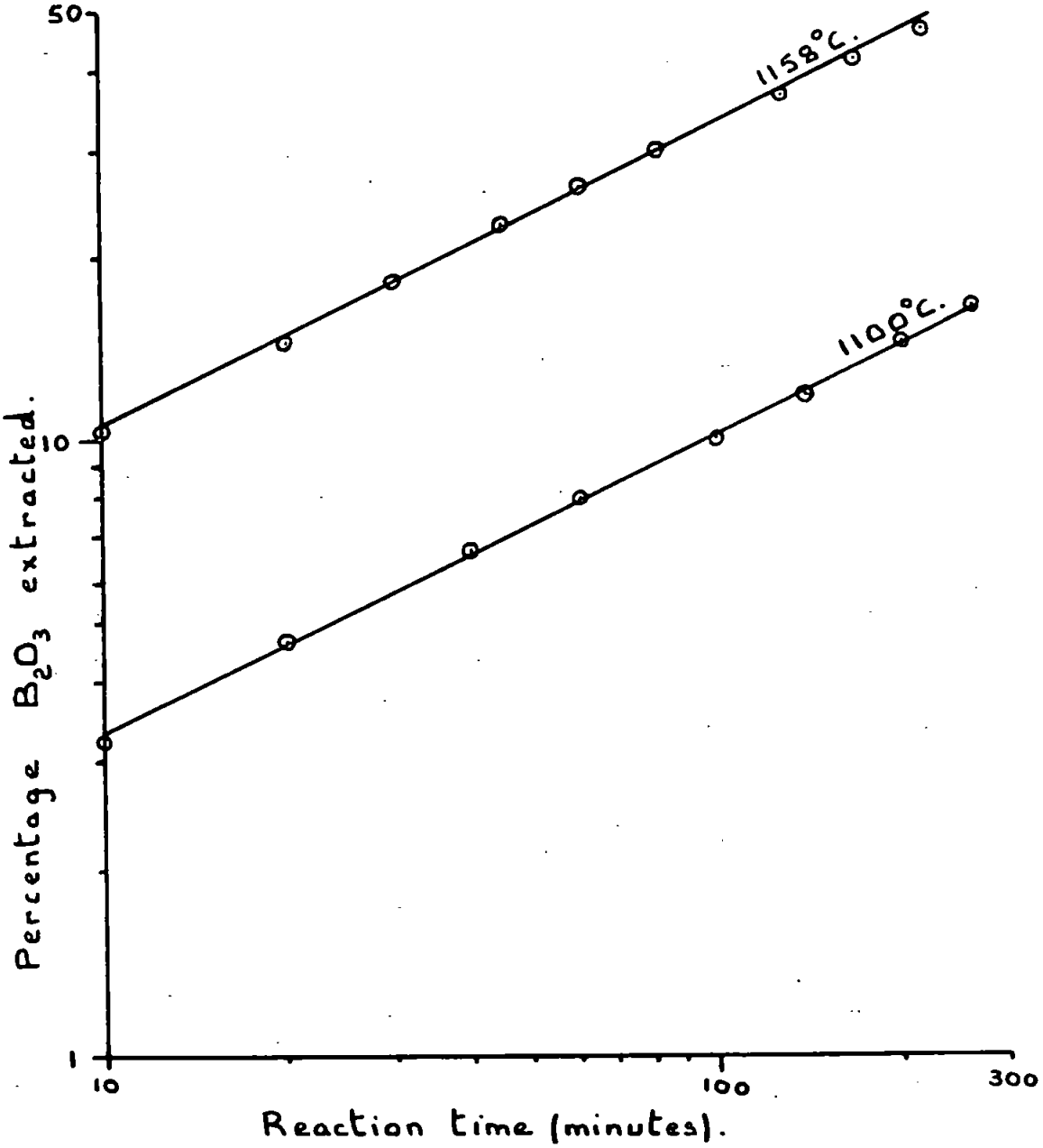

to be the same within the probable experimental error. The mean value calculated was 85 ± 8 kcal/mole and this was taken to be the most probable value for the activation energy of pyrohydrolysis from schorl.

The rate of extraction of boric oxide from the 1 cm.^{3} cubes of decomposed schorl was found to follow the rate equation (1), whilst a parabolic rate equation (2) was found to be obeyed when (5-8) mesh decomposed schorl granules were used.

$$(\% B_2O_3) = kt^{0.71} \quad \ldots\ldots\ldots\ldots (1)$$

$$(\% B_2O_3) = kt^{0.50} \quad \ldots\ldots\ldots\ldots (2)$$

It was thought that the larger value of the exponent found when the 1 cm.^{3} cubes were used could be related to the volatilisation of some boric oxide from the surface layers during the heating period of 1 hour at 1300^{0}C. This process would be expected to lead to the initial percentages of boric oxide extracted being lower than expected. To check this possibility several 1 cm.^{3} cubes of schorl were heated at 1300^{0}C for 1 hour to determine the percentage loss in weight. The mean weight loss using six 1 cm.^{3} cubes was 3.67 ± 0.01 per cent. The tourmaline (8/1) used was found previously to have a composition close to $Na_2O.6FeO.6Al_2O_3.3B_2O_3.12SiO_2.4H_2O$, see Chapter 14. If the lattice water was completely volatilised then the theoretical weight loss would be 3.41 per cent. The weight loss from the 1 cm.^{3} is 0.26 per cent greater than this. The difference may be due to the volatilisation of boric oxide from the surface layers of the cubes.

If it is assumed that the 0.26 per cent is entirely due to the volatilisation of boric oxide then this loss would represent approximately 3.5 per cent of the total boric oxide present in each cube. This figure may be significant in view of the small percentages of boric oxide extracted from the 1 cm.^{3} cubes, see Figure 21.

The basic extraction process therefore obeys a parabolic rate equation (2), indicating that the extraction of boric oxide is controlled by some diffusion process, see Chapter 7.

$$(\% B_2O_3) = kt^{0.50} \quad \ldots\ldots\ldots\ldots (2)$$

This diffusion process controlling the rate of reaction could be either:-

(1) The diffusion of water vapour through the silica-iron oxide amorphous matrix to the continuously contracting boric oxide containing reaction surface. Meschi et. al. (130) found that reaction (1) was the main heterogeneous reaction between boric oxide and water vapour between 800 and 1200^{0}C.

$$B_2O_3\,(l) + H_2O\,(g) = 2HBO_2\,(g) \quad \ldots\ldots\ldots\ldots (1)$$

(2) The diffusion of boric oxide through the granules to the surface leading to a homogeneous gas phase reaction (2):-

$$B_2O_3\,(g) + H_2O\,(g) = 2HBO_2\,(g) \quad \ldots\ldots\ldots\ldots (2)$$

In a study of the heterogeneous reaction between boric oxide and water vapour Meschi et. al. (130) found that this homogeneous reaction (2) became of greater relative importance as the reaction temperature increased, see Table 11. Hildenbrand et. al. (77) found that the heat of vapourisation of boric oxide was equal to 93 kcal/mole. The similarity between this and the activation energy of pyrohydrolysis from schorl would seem to support this

type of mechanism. However, further pyrohydrolysis experiments using "pyrex" glass and dravite (8/4) did not support this mechanism. These experiments are described in detail in the following two sections.

(3.4) Activation Energy of Pyrohydrolysis from "pyrex" glass.

Because of the extremely high value obtained for the activation energy of pyrohydrolysis from decomposed schorl it was thought necessary to determine the activation energy for extraction of boric oxide by pyrohydrolysis, from a completely different boron containing system. The borosilicate glass with the brand name "pyrex" was chosen mainly because of its availability. The composition of glass, given in Table 45, was taken from a catalogue supplied by J. A. Jobling and Co. Ltd.

Two short lengths, about 4 cm. long, were cut from a length of 6 mm. diameter "pyrex" rod. The weighed pieces of rod were placed in two similar alumina boats of dimensions 5 cm. long and 1.4 cm. wide. The glass was then heated for 1 hour at 1200°C to minimise any changes occurring, such as the growth of microheterogeneous regions within the glass during the pyrohydrolysis experiments, see Chapter 6. The rate of extraction of boric oxide was then determined at two different temperatures using the technique described in Chapter 12. The results obtained are presented in tabulated form in Table 46 and in a graphical form on a log-log scale in Figure 24.

The rate equations calculated from the two curves obtained are:-

(1) At 980°C

$$(\text{mg. } B_2O_3) = 0.0225t^{0.675}$$

(2) At 1090°C

$$(\text{mg. } B_2O_3) = 0.0469t^{0.675}$$

The activation energy for the extraction of boric oxide from "pyrex" glass was found to be equal to 22 ± 1 kcal/mole using the two rate constants given above. The error was calculated on the assumption that the maximum variation in the experimental temperatures was ± 3°C. This value for the activation energy is very close to that of 20 ± 4 kcal/mole, obtained by Charles (156), for the activation energy of the attack by water vapour on soda-lime glass. The similarity of the two values indicates that the extraction process from either glass is controlled by a similar mechanism.

(3.5) Activation energy of Pyrohydrolysis from Dravite.

The activation energy of pyrohydrolysis from the decomposed magnesium tourmaline, dravite (8/4) was determined because of the basic similarity between the nature of decomposed iron and magnesium tourmalines. The main decomposition product, in either, was found to be a boron containing mullite embedded in a boron containing amorphous matrix, see Chapter 15.1.4. It was therefore thought that the determination of the activation energy of pyrohydrolysis from dravite would help in the elucidation of the mechanism by which the extraction process proceeds.

The percentage of boric oxide present in dravite (8/4) was found to be equal to 9.60% using the technique described in Chapter 10.1.2.

FIGURE 24.

Rate of extraction of B_2O_3 from "pyrex" glass as a function of the pyrohydrolysis temperature.

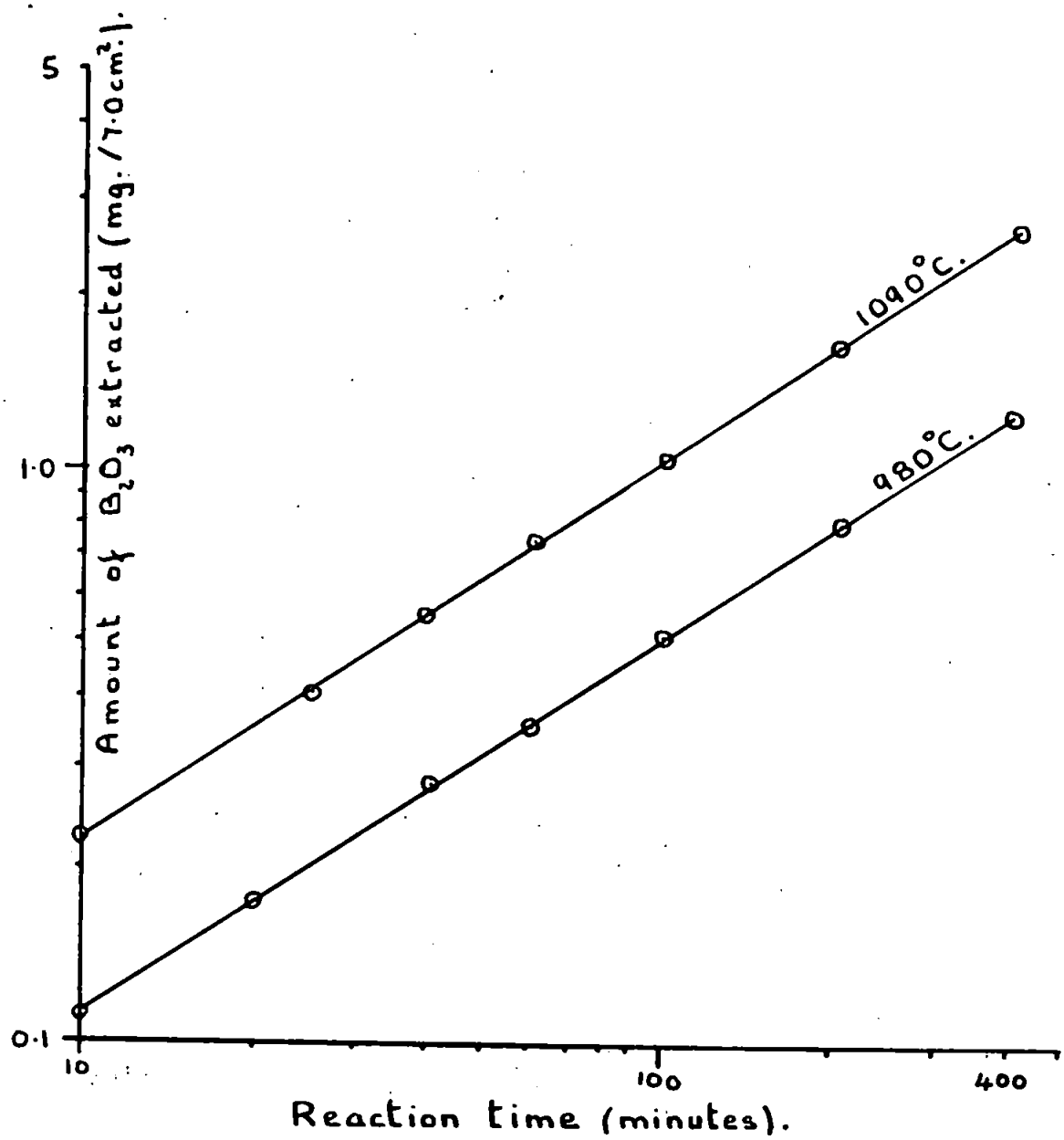

In determination of the activation energy (5-8) mesh dravite (8/4) granules were used. The experimental technique used was the same as that described in section 3.2.2, when a similar determination using

TABLE 45

Composition of "pyrex" Glass.

Oxide	Per cent.	Oxide	Per cent.
SiO_2	80.6	Al_2O_3	2.2
B_2O_3	12.6	CaO	0.05
Na_2O	4.2	Fe_2O_3	0.04

TABLE 46

Extraction of Boric Oxide from "pyrex" Glass as a Function of the Pyrohydrolysis Temperature.

Pyrex rods heated 1 hr. at 1200°C.		
Pyrohydrolysis time (minutes).	Temperature 980 ± 3°C. Rate flow water 1.03 g/min. mg. B_2O_3 extracted.	Temperature 1090 ± 3°C. Rate flow water 0.98 g/min. mg. B_2O_3 extracted.
10	0.104	0.216
30	0.226	0.470
60	0.360	0.745
120	0.571	1.22
180	0.759	1.56
300	1.058	2.24
Wt. of rods 3.86 g. in each expt. Surface area of molten pyrex 7.0 cm^2.		

(5-8) mesh schorl (8/1) granules was undertaken.

The experimental results obtained using two pyrohydrolysis temperatures are presented in tabulated form in Table 47 and in graphical form on a log-log scale in Figure 25. The rate equations calculated from the two log-log curves are also given in Table 47.

The rate of extraction of boric oxide from dravite was found to follow the same rate equation (1) as was established previously in the case of the extraction of boric oxide from (5-8) mesh schorl, see section 3.3.

$$(\%\ B_2O_3) = kt^{0.50} \quad \ldots\ldots\ldots\ldots (1)$$

FIGURE 25.

Rate of extraction of B_2O_3 from (5-8) mesh dravite as a function of the pyrohydrolysis temperature.

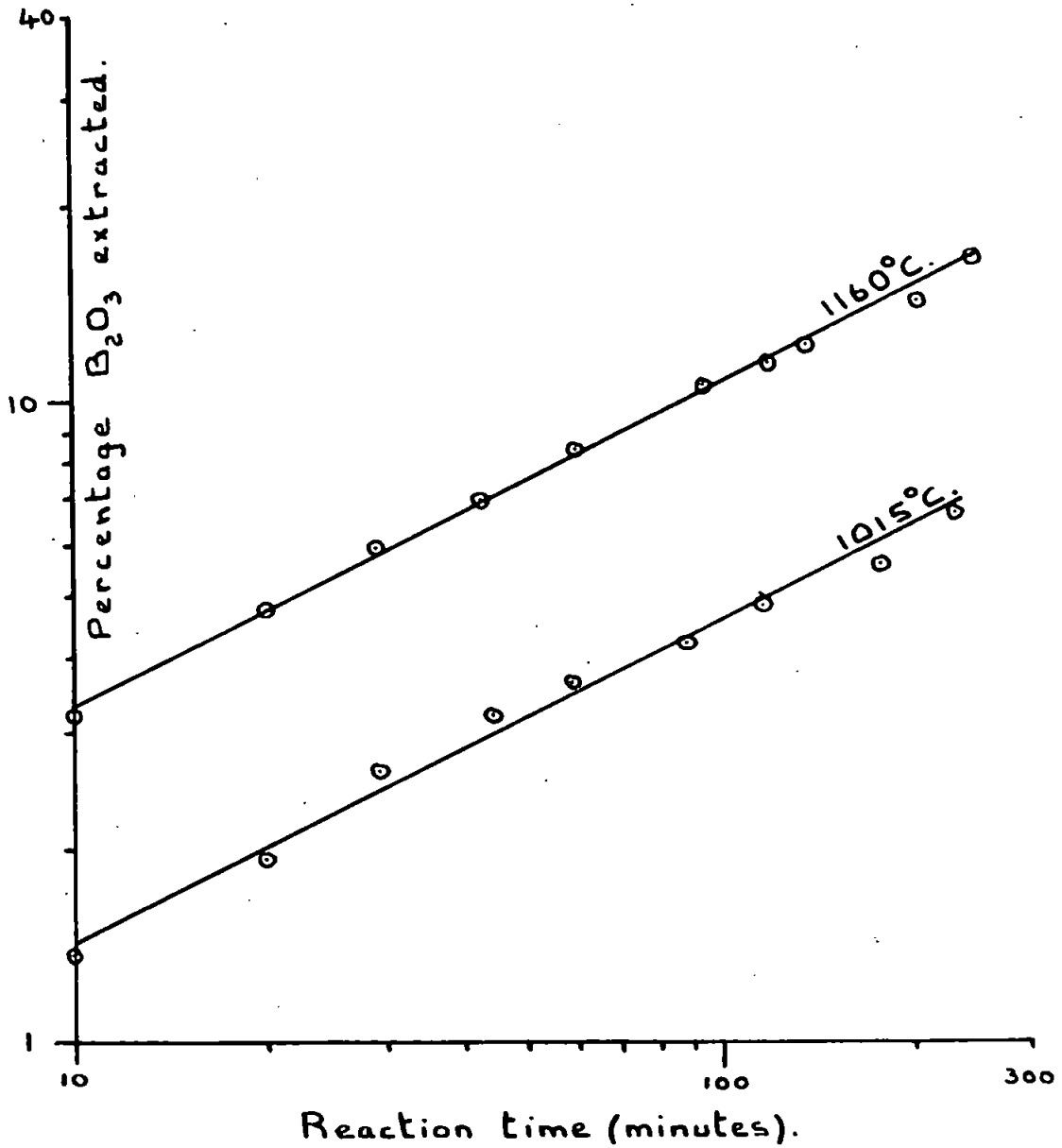

The activation energy for the extraction of boric oxide from decomposed dravite (8/4) was found to be equal to 22± 1 kcal/mole using the two rate equations given in Table 47. The error included was calculated on the assumption that the maximum variation in the experimental temperatures was ± 3°C.

TABLE 47

Extraction of Boric Oxide from Dravite as a Function of the Pyrohydrolysis Temperature.

(5-8) mesh Dravite (8/4) heated for 30 mins. at 1225°C.
Wt. of samples 0.983 g. in each experiment.
Rate of flow water 1.00 ± 0.05 g/min.

Pyrohydrolysis Time (minutes).	Temperature of experiment	
	1015 ± 3°C	1160 ± 3°C
	Per cent B_2O_3 extracted.	Per cent B_2O_3 extracted.
10	1.02	3.03
20	1.92	4.73
30	2.63	5.94
60	3.64	8.48
90	4.22	10.2
120	4.72	11.8
200	6.35	15.1

Rate equations calculated:-

(1) 1015°C $(\%\ B_2O_3) = 0.444\ t^{0.50}$

(2) 1160°C $(\%\ B_2O_3) = 1.04\ t^{0.51}$

(3.6) Activation Energy of Pyrohydrolysis from Liquid Boric Oxide.

The activation energy of removal of boric oxide by pyrohydrolysis from liquid boric oxide was determined to establish whether or not there is a significant energy barrier for the heterogeneous reaction (1):-

$$B_2O_3\ (l) + H_2O\ (g) = 2HBO_2\ (g) \quad \text{.....(1)}$$

Approximately 0.5 g. of boric oxide was weighed out each time into two similar mullite boats of cross-sectional area 4.1 ± 0.1 $cm.^2$ The powder was then melted at 500°C prior to beginning the pyrohydrolysis experiments. The results obtained using two pyrohydrolysis temperatures are presented in graphical form on a log-log scale in Figure 26.

The rate equations calculated from the curvesobtained are equal to:-

FIGURE 26.

Rate of extraction of B_2O_3 from liquid boric oxide as a function of the pyrohydrolysis temperature.

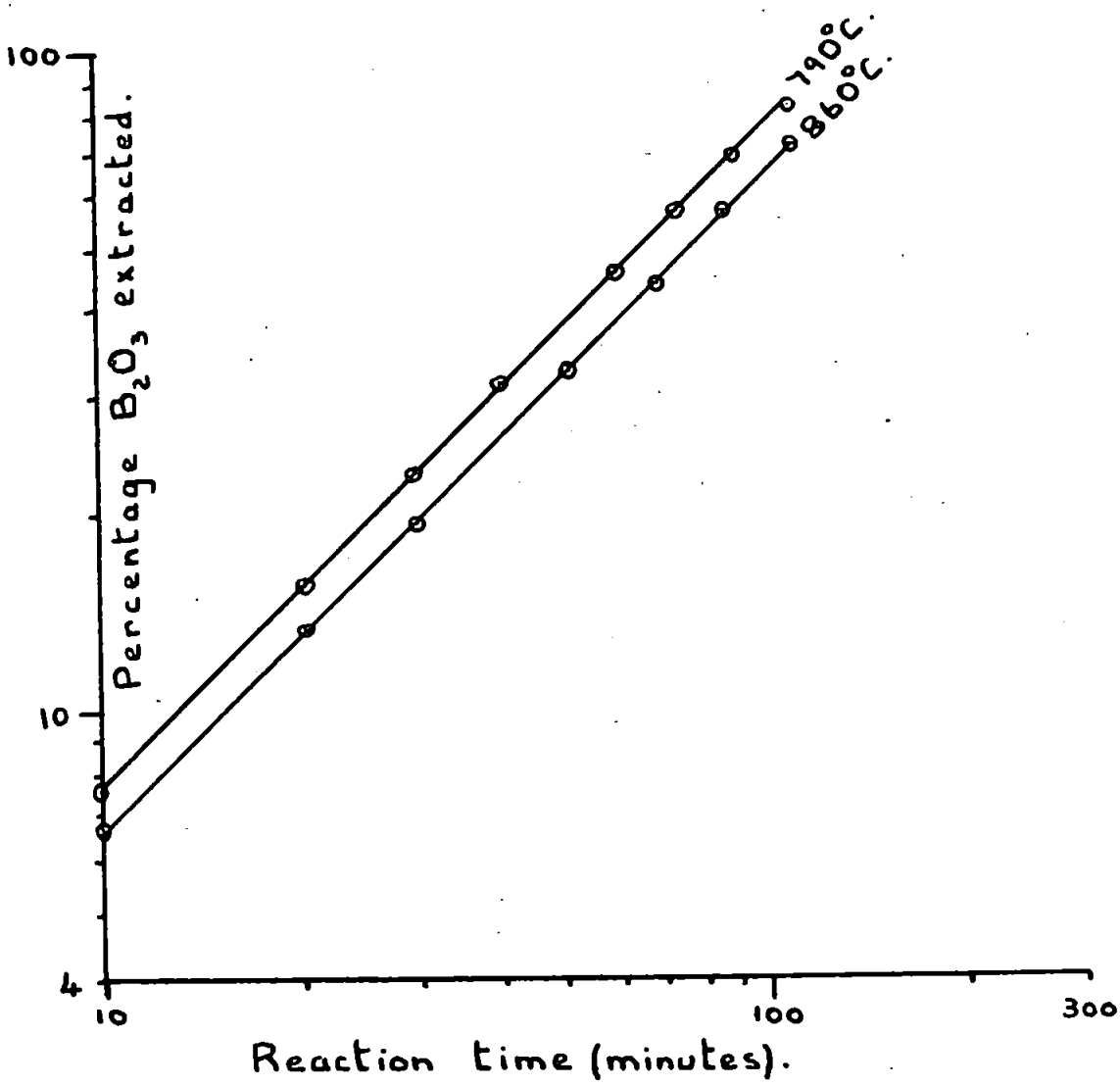

(1) At 760°C.

(% B_2O_3) = 0.77 t

(2) At 860°C

(% B_2O_3) = 0.66 t

The rate of extraction is therefore a linear function of the pyrohydrolysis time (t mins.), as would be expected for a surface reaction (1) where the surface area does not change with reaction time.

$$B_2O_3\,(l) + H_2O(g) \longrightarrow 2HBO_2\,(g) \quad \ldots\ldots\ldots (1)$$

The activation energy for the extraction process was calculated using the two rate constants given above, and found to equal to -3 6 kcal/mole. This surprising negative value would mean, if real, that the rate of extraction is slower the higher the reaction temperature.

This negative value can possibly be accounted for by the change with temperature of one or more of the transport properties of water vapour. One of the transport properties most likely to affect the heterogeneous surface reaction is viscosity. The temperature coefficient of viscosity for most gases has been found to obey Sutherlands equation (218). A derived form of this equation is given below:-

$$\eta_1/\eta_2 = (T_1/T_2)^{1/2} \times \frac{(1 + C/T_2)}{(1 + C/T_1)} \quad \ldots\ldots\ldots (1)$$

Where C is Sutherlands constant and η and T the viscosity and temperature (°K) respectively. The value of C for water vapour is 650(218). Using equation (1) and this value for C the differential increase in viscosity (η_1/η_2) between the two pyrohydrolysis temperatures was found to be equal to 1.09. If it is assumed that the thickness of the boundary layer at the reaction surface increases linearly with viscosity and that the rate of volatilisation is partially controlled by this boundary layer then the rate constant at 860°C must be increased by the factor of 1.09. The new rate constant at 860°C is now equal to 0.70 instead of 0.66.

The activation energy for the volatilisation process using this new value for the rate constant at 860°C was found to have increased to -1.32 kcal/mole. There is no direct evidence that the increase in viscosity with temperature has any effect on the volatilisation process, however, these calculations do at least produce a value for the activation energy which is more realistic in that it is closer to zero or a small positive value.

The extraction of boric oxide from the borosilicate systems studied have activation energies much greater than that for the primary heterogeneous reaction (1). The extraction of boric oxide from such systems is therefore

$$B_2O_3\,(l) + H_2O\,(g) = 2HBO_2\,(g) \quad \ldots\ldots\ldots (1)$$

not controlled by the actual reaction between the oxide and water vapour but by some other probably diffusional process.

(3.7) Effect of Particle Size.

To investigate the extraction process in greater detail the effect of particle size on the rate of extraction was investigated In this series of experiments two different temperatures were used for the prior heat treatment.

(3.7.1) Prior heating for 1 hour at 1070°C.

In this set of experiments three ranges of granule size of schorl (8/1) were used, these being (3/16 -5) mesh, (12-16) mesh and (18-25) mesh respectively. A known weight of schorl (8/1) granules was each time carefully sprinkled on to the surface of a Ni/Cr alloy boat as described in section 3.2.2, prior to being heated at 1070°C for 1 hour. The results of the three pyrohydrolysis experiments carried out at 1000°C are given in tabulated form in Table 48. The calculated rate equation for each of the three samples used is also included in this table.

TABLE 48

Effect of Particle Size on the Rate of Extraction of Boric Oxide from Schorl which had been heated for 1 hour at 1070°C before beginning the Pyrohydrolysis Experiments.

Schorl (8/1) granules heated 1 hr. at 1070°C. Pyrohydrolysis experiments carried out at 1000 ± 5°C.			
Pyrohydrolysis time (minutes).	(3/16 - 5) mesh mean diameter 4.02 mm.	(12-18) mesh mean diameter 1.20 mm.	(18-25) mesh mean diameter 0.725 mm.
	Percentage boric oxide extracted.		
10	3.24	3.89	4.25
20	4.60	5.78	5.90
45	7.01	8.69	9.00
60	8.10	9.98	10.1
100	10.3	12.8	13.6
180	13.6	16.8	17.4
300	17.1	21.2	21.6
Weight of sample.	0.916 g.	0.830 g.	0.844 g.
Rate flow water.	1.99 g/min.	2.03 g/min.	1.98 g/min.

Rate Equations:-

(1) (3/16 - 5) mesh $(\% B_2O_3) = 1.04\, t^{0.50}$

(2) (12-18) mesh $(\% B_2O_3 = 1.27\, t^{0.50}$

(3) (18-25) mesh $(\% B_2O_3) = 1.35\, t^{0.50}$

Ratio of surface areas per unit weight:-

1/4.02 : 1/1.20 : 1/0.725

or 1 : 1.66: 5.58

Although the ratio between the geometrical surface areas per unit weight is equal to 1.00: 1.66: 5.58, the ratio in the rate constants is only 1:1.22:1.30. It would appear from these results that the rate of extraction is almost independent of the size of the schorl. The probable explanation for this apparent independence is given in the section 3.7.3.

(3.7.2) Prior heating for 10 minutes at 1350°C.

In this set of experiments (3/16 - 5) mesh, (5 - 8) mesh and (12 -16) mesh granules of schorl (8/1) were used. A known weight of sample was each time carefully sprinkled onto the surface of a Ni/Cr alloy boat as described in section 3.2.2 and then heated for 10 minutes at 1350°C to complete the sintering process. The results obtained using a pyrohydrolysis temperature of 1100°C are given in tabulated form in Table 49. The calculated rate equation form each of the three samples used is also included in this table.

TABLE 49

Effect of Particle Size on the Rate of Extraction of Boric Oxide from Schorl which had been heated for 10 minutes at 1350°C before beginning the Pyrohydrolysis Experiments.

Schorl granules heated for 10 mins at 1350°C. Pyrohydrolysis experiments carried out at 1100 ± 5°C.			
Pyrohydrolysis time (minutes).	Percentage boric oxide extracted		
	(3/16 - 5) mesh	(5 - 8) mesh	(12 - 16) mesh
10	1.61	3.20	5.31
20	2.32	4.58	7.50
45	3.41	7.00	11.4
90	5.08	9.80	16.4
150	6.40	12.7	21.5
250	8.36	16.2	27.0
Wt. of sample	2.001 g.	1.1068 g.	0.578 g.
Rate of flow water (g/min.)	0.66	0.89	0.40
Mean diameter of granules (mm).	4.02	2.70	1.20
Rate equations:-			Ratio of rate constants:-
(1) 3/16 - 5 mesh	$\%B_2O_3 = 0.527\ t^{0.50}$		1:1.94:3.11
(2) 5 - 8 mesh	$\%B_2O_3 = 1.02\ t^{0.50}$		Ratio of surface areas per unit mass:- 1/4.02:1/2.70:1/1.20
(3) 12 - 16 mesh	$\%B_2O_3 = 1.69\ t^{0.50}$		= 1:2.25: 3.35

The ratio of the surface areas of the three sets of granules used is equal to 1:2.25:3.35, whilst the ratio of the rate constants is 1:1.94:3.11. The rate of extraction is therefore to within experimental error directly proportional to the effective surface area of the schorl granules. This result is in agreement with the suggestion that the diffusion of reactive species to the contracting boron containing surface is the rate controlling step, see section 3.3

The experimental ratios are slightly lower than that theoretically expected by the relative increase in surface area. This could be due to a small portion of the granule sintering to the alloy boat. The lowering of the effective surface area would become of greater relative importance as the granule size decreases; thereby leading to the slightly lower ratios found experimentally.

(3.7.3) Conclusions.

The apparent discrepancy between the results obtained using granules of schorl (8/1) that had been heated for 1 hour at 1070^{o}C with those obtained using granules that had been heated for 10 minutes at 1350^{0}C can probably be explained as follows.

The granules of schorl (8/1) used although of differing geometric size are actually composed of small crystals of schorl which adhere together forming the massive tourmaline rock from which the samples were obtained.

If the prior heating and pyrohydrolysis temperatures are low only slight sintering of these, now decomposed "crystals" within the granules may occur. Such granules would therefore be expected to be quite porous and the rate of extraction would then be controlled by the actual size of these "crystals" and not by the external geometrical surface area.

This could be the possible explanation of the approximate independence in the rate of extraction with granule size from the material that had been heated for 1 hour at 1070^{o}C, see Table 48. At this temperature only slight sintering of the decomposed "crystals" making up the granules has occurred, the effective surface area would then be similar leading to approximately the same rate of extraction whatever granule size is used until this is smaller than the "crystals" which make up the composite granules.

This explanation is in agreement with the approximate Tammann temperature for schorl (8/1) of 1140 ± 50^{o}C, see Appendix 1. Below this temperature the rate of sintering of the schorl granules would be extremely slow. This explanation is also consistent with the higher temperature experiments where complete sintering of the granules has occurred leading to the rate of extraction being directly proportional to the surface area of the granules.

The size of the " crystals" present in the composite granules can be calculated since the rate of extraction from sintered granules of known surface area has been determined, see Table 49. The rate equation obtained using the (3/16 - 5) mesh sintered granules was used as this was thought the most accurate since only a small proportion of the total surface area was rendered ineffective due to sintering of the granules to the alloy boat.

The rate equation was determined at a reaction temperature of 1100^{o}C, the rate at 1000^{o}C can, however,

be calculated by using the activation energy of 85 kcal/mole for the extraction process in combination with the Arrhenius equation (1):-

$$\log k_1 - \log k_2 = \frac{E}{R}\left(\frac{1}{T_2} - \frac{1}{T_1}\right) \quad \text{.....(1)}$$

At 1100°C the rate equation was found to be equal to:-

$(\% B_2O_3) = 0.537\, t^{0.50}$ (Table 49)

The derived rate equation for a reaction temperature of 1000°C was found to be equal to:-

$(\% B_2O_3) = 0.047\, t^{0.50}$

The rate equation obtained at 1000°C using (18-25) mesh granules of schorl which been heated for 1 hour at 1070°C wasfound to be equal:-

$(\% B_2O_3) = 1.04\, t^{0.50}$ (Table 48)

The two rate constants for a reaction temperature of 1000°C were then compared to determine the approximate size of the "crystals" present within the schorl granules:-

$$\frac{\text{Surface area per unit mass (2)}}{\text{Surface area per unit mass (1)}} = \frac{\text{Rate constant (2)}}{\text{Rate constant (1)}} \quad \text{.....(2)}$$

$$\frac{\text{Diameter (1)}}{\text{Diameter (2)}} = \frac{0.047}{1.04}$$

$$\frac{d_1}{4.02} = \frac{0.047}{1.04}$$

$$d_1 = 0.18 \text{ mm.}$$

The "crystals" within the granules are therefore approximately 0.18 mm. in diameter. This result is in agreement with the visual observation that the massive schorl (8/1) rock was mainly made up of crystals less than 0.5 mm. in diameter.

(3.8) Effect of rate of flow water.

The effect of the rate of flow of water vapour on the extraction process was studied using flow rates varying from 1.13 g/min. to 5.08 g/min. In each of the experiments the same weight of (3/16 - 5) mesh schorl granules were carefully sprinkled over the surface of the Ni/Cr boat. The granules were then heated for 1 hour at 1010°C before beginning the pyrohydrolysis experiments. The results obtained using three different flow rates are presented in tabulated form in Table 50.

The rate of extraction of boric oxide is therefore independent of the mass rate of flow of water vapour over the sample.

This is not surprising in view of the fact that the most concentrated solution obtained was only 0.428 mg. B_2O_3 per 1 ml. of water. Within the experimental conditions used the basic heterogeneous reaction (1) is pseudo first order. The rate of reaction is therefore simply related to the concentration of boric oxide.

$$B_2O_3\,(l) + H_2O\,(g) = 2\,HBO_2\,(g) \quad \text{..... (1)}$$

The equilibrium concentration of metaboric acid (HBO_2) which could be obtained from this reaction at

1000°C was calculated from the thermodynamic data obtained by Meschi et. al. (130), see Table 11.

TABLE 50

Effect of Mass Rate of flow of Water Vapour on Extraction of Boric Oxide.

(3/16 - 5) mesh Schorl (8/1) heated for 1 hr. at 1010°C.

Wt. of sample used 1.643 g. in each experiment.

Temperature used 1000 ± 5°C.

	Percentage of Boric Oxide extracted.			
Pyrohydrolysis time (minutes).	Rate flow H_2O 1.13 g/min.	Rate flow H_2O 2.05 g/min.	Rate flow H_2O 5.08 g/min.	mg. of B_2O_3 extracted.
10	2.81	2.46	2.60	4.28
30	5.27	5.14	5.39	7.48
60	7.26	7.62	7.65	11.0
90	8.62	9.56	9.49	13.6
180	11.6	13.7	13.0	17.8

At 1000°C the equilibrium constant (K_p) was found to be equal to 1.86×10^{-3} for the heterogeneous reaction (1). The equilibrium constant (K_c) in terms of molar concentration is related to the pressure equilibrium

$$\tfrac{1}{2} B_2O_3 (l) + \tfrac{1}{2} H_2O (g) = HBO_2 (g) \quad \ldots\ldots\ldots\ldots (1)$$

constant (K_p) by the equation (2), see reference (219), where Δn is the number of moles of products less that of reactants in the stoichiometric equation for the reaction. In the heterogeneous reaction being considered the vapour pressure of liquid boric oxide is extremely small and has therefore been neglected in the determination of the equilibrium constant (K_p). The change in the number of moles (Δn) can, therefore be taken as being equal

$$K_c = \frac{K_p}{(RT)^{\Delta n}} \quad \ldots\ldots\ldots\ldots (2)$$

$$K_p = \frac{P(HBO_2)}{P(H_2O)^{\frac{1}{2}}} = 1.86 \times 10^{-3} \text{ (ref. 130)}$$

to ½.

The equilibrium constant in terms of molar concentrations is therefore:-

$$K_c = \frac{1.86 \times 10^{-3}}{(RT)^{\frac{1}{2}}}$$

In the experiments described in this thesis the water vapour pressure used was one atmosphere, the molar concentration is therefore equal to (1/RT) moles per litre. The concentration of metaboric acid is therefore equal to:-

$$n(HBO_2) = K_c \times (n(H_2O))^{\frac{1}{2}}$$

$$= \frac{1.86 \times 10^{-3}}{(RT)^{\frac{1}{2}}} \times \frac{1}{(RT)^{\frac{1}{2}}} \text{ moles per litre.}$$

The maximum boric acid concentration at 1000°C is therefore:-

$1.86 \times 10^{-3} \times (1/RT)$ moles HBO_2 per $(1/RT)$ moles H_2O.

This molar concentration is equal to a weight concentration of 0.45 g. of HBO_2 per 100 g. H_2O.

By using the data obtained by Meschi et. al. (130) for a reaction temperature of 1200°C the weight concentration theoretically possible was found to have increased to 7.3 g. HBO_2 per 100 g. H_2O. The actual equilibrium concentration of boron containing species in the vapour phase is slightly higher than the above value because the following reactions were found to begin to become measurable at temperatures above about 1100°C.

$$\tfrac{1}{2}B_2O_3\,(g) + \tfrac{1}{2}H_2O\,(g) = HBO_2\,(g)$$

$$3/2\,B_2O_3\,(l) + 3/2\,H_2O\,(g) = (HBO_2)_3\,(g)$$

The solubility of boric acid at 20°C is equal to 4.88 g. per 100 g. H_2O (86), therefore these equilibrium calculations indicate that at reaction temperatures close to 1200°C it is theoretically possible to obtain a saturated solution of boric acid, if the volatilised "boric oxide" is condensed to room temperature. However, in view of the dilute solutions obtained experimentally, due to the slow rate of extraction, a recycling process would probably have to be evolved before an efficient extraction process could be achieved.

(3.9) Effect of Adding Uranium Oxide (U_3O_8).

The addition of certain compounds to powdered borosilicate glasses has been found to accelerate the extraction of boric oxide. For example, Williams et. al. (121) have found that the addition of uranium oxide (U_3O_8) accelerated the rate of volatilisation of boric oxide from silicate glasses, see Chapter 5.2.1. It was therefore thought possible that the addition of this oxide to powdered schorl (8/1) may similarly accelerated the extraction process.

The effect of addition was investigated by comparing the rates of extraction of boric oxide from powdered schorl (8/1) and a powdered schorl (8/1) - uranium oxide mixture.

In the control experiment a known weight of less than 300 mesh schorl (8/1) was poured into a mullite boat and then heated for 1 hour at 1200°C prior to beginning the pyrohydrolysis experiment.

To study the effect of adding uranium oxide a mixture of this oxide and < 300 mesh schorl (8/1) powder was made up in the weight ratio of 1 to 2. This mixture was poured into a mullite boat having the same dimensions as the one used in the control experiment. This mixture was then heated for 1 hour at 1200°C, to complete any possible reaction between the two solids prior to beginning the pyrohydrolysis experiment.

The results obtained are presented in tabulated form in Table 51 and in graphical form on a log-log scale in Figure 27. The two rate equations calculated from the two log-log curves were found to be equal to:-

(1) Schorl (8/1)

$$(\%\,B_2O_3) = 0.97\,t^{0.50} \quad \ldots\ldots\ldots\ldots (1)$$

(2) Schorl (8/1) - U_3O_8 mixture.

$$(\%B_2O_3) = 0.51t^{0.50} \quad \ldots\ldots\ldots\ldots (2)$$

FIGURE 27.

Effect of adding uranium oxide to powdered schorl on the rate of extraction of B_2O_3.

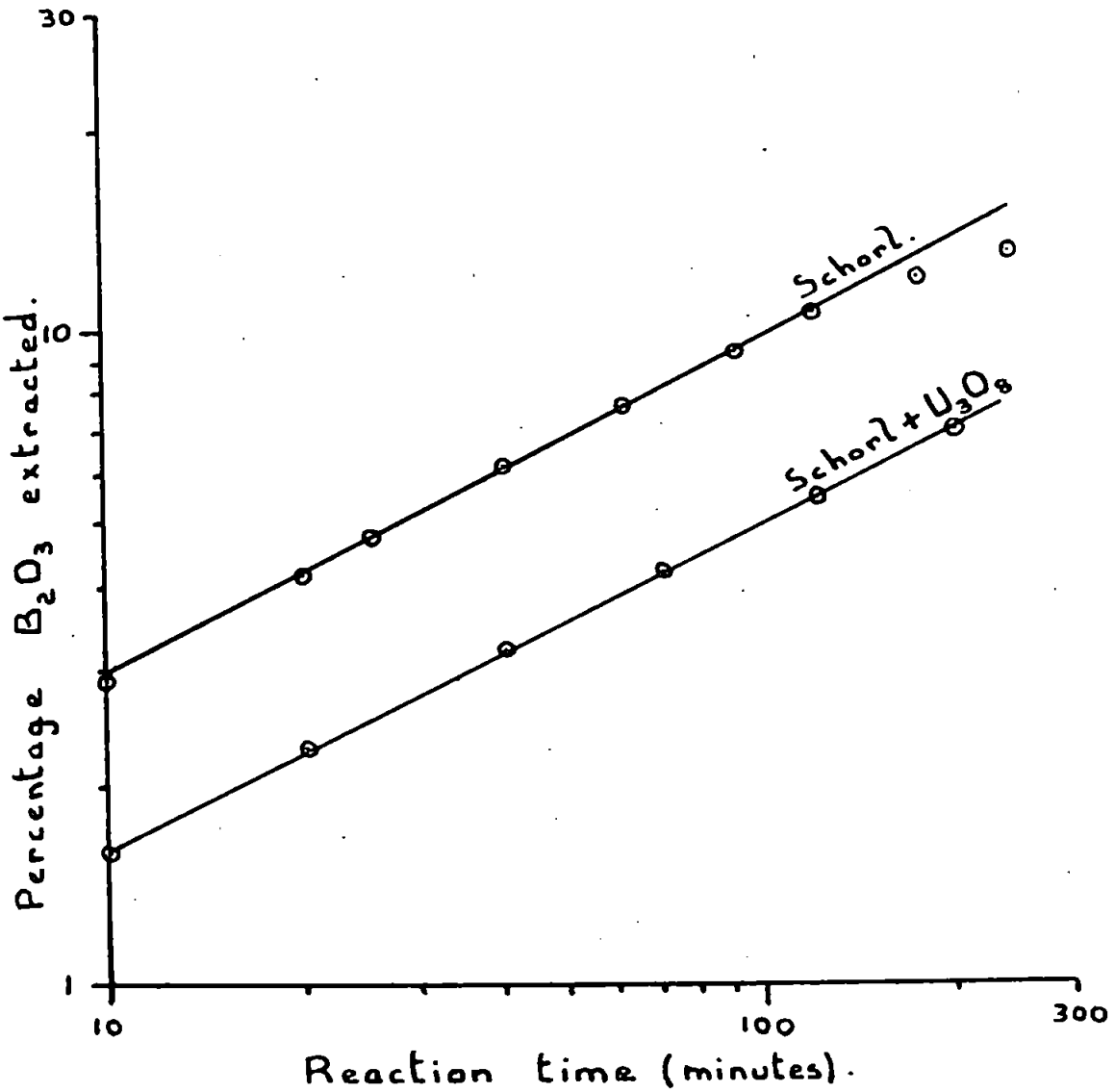

The addition of uranium oxide apparently reduces the rate of extraction of boric oxide , however, this may not be necessarily true, because there could be a difference in the effective surface area of schorl exposed to the water vapour in control experiment as compared to that in the mixture experiment. No realistic calculation of this difference could be undertaken because the size distribution of the uranium oxide and the schorl granules were unknown. However, even without such calculations these experiments clearly indicate that the addition of uranium oxide does not significantly increase the rate of extraction of boric oxide from schorl.

TABLE 51

Effect of Adding Uranium Oxide on the Rate of Extraction of Boric Oxide from Decomposed Schorl.

Samples heated for 1 hour at 1200°C prior to pyrohydrolysis experiments.
Pyrohydrolysis temperature 1025 ± 5°C.
Weight of schorl used in each experiment 1.500 g.
Rate of flow water 1.26 ± 0.02 g/min.

Pyrohydrolysis time (mins.)	Percentage B_2O_3 extracted from schorl.	Percentage B_2O_3 extracted from (schorl + U_3O_8).
10	2.79	1.58
40	6.38	3.24
60	7.93	3.94
90	9.50	4.68
120	10.5	5.37
240	14.8	7.86

(3.10) Probable Mechanism of Heterogeneous Surface Reaction and General Discussion of Pyrohydrolysis Experiments.

The most important quantitative kinetic results obtained in the present investigation on the pyrohydrolysis of boric oxide are:-

(1) The activation energy for the pyrohydrolysis of boric oxide from decomposed schorl was found to be equal to 85 ± 8 kcal/mole.

(2) The activation energy for the pyrohydrolysis of boric oxide from decomposed dravite was found to be equal to 22 ± 1 kcal/mole.

(3) The activation energy for the pyrohydrolysis of boric oxide from "pyrex" glass was found to be equal to 22 ± 1 kcal/mole.

(4) The activation energy for the pyrohydrolysis of boric oxide from liquid boric oxide was found to be very small, probably less than 1 kcal/mole.

The basic rate of extraction of boric oxide from decomposed tourmaline was found to obey a parabolic rate equation (1). This type of time dependent process has been found to be followed by a number of

$$(B_2O_3) = k^{0.50} \quad \ldots\ldots\ldots (1)$$

heterogeneous reactions in which diffusion is the rate controlling process, see Chapter 7.

The activation energy of extraction of boric oxide from schorl was found to be 85 ± 8 kcal/mole, whilst the heat of vapourisation of boric oxide was found by Hildenbrand et. al. (77) to be equal to 93 kcal/mole. The similarity of these values would seem to indicate that the extraction process may be controlled by the volatilisation of boric oxide from the interior of the granules to the gas phase leading to the homogeneous gas reaction (2). However, this type of volatilisation mechanism was not thought to be the basic rate controlling

$$B_2O_3\,(g) + H_2O\,(g) = 2HBO_2\,(g) \quad \ldots\ldots\ldots (2)$$

process, because if the extraction process was controlled by such a mechanism the rate of removal of boric oxide would obey a linear equation, instead of the parabolic type function (1) obtained experimentally, because the number of molecules in the gas phase at any time would then be directly proportional to the vapour pressure of boric oxide at that reaction temperature.

The only difference between composition of decomposed schorl and decomposed dravite is the presence of iron in schorl. Therefore the increased value for the activation energy of pyrohydrolysis of boric oxide from decomposed schorl must be due to the presence of iron oxide in the amorphous phase of the decomposed mineral.

The similarity between the activation energy of extraction from "pyrex" and dravite would indicate that the Mg^{2+} ions present in the decomposed mineral does not affect the basic structure of the amorphous silica lattice.

The difference between the effect of Fe^{2+} and Mg^{2+} ions on the silica lattice in decomposed schorl and dravite respectively may be associated with the large difference in the melting points of the two oxides. The melting points of which are given below together with their respective Tamman temperatures (half the melting point in degrees absolute). Above this temperature it has been found that rapid migration of ions through solids can take place, see Appendix 1.

	Melting Point (220)	Tamman Temperature (221)
MgO	$2800^{o}C$	$1270^{o}C$
FeO	$1420^{o}C$	$580^{o}C$

The temperatures used for the heat treatment of the samples prior to beginning the pyrohydrolysis experiments were all either below or close to the Tamman temperature for MgO, but at least $700^{o}C$ higher than the Tamman temperature for FeO. Therefore considerable diffusion of Fe^{2+} ions could occur during the heat treatment time, leading to extensive incorporation of Fe^{2+} ions into the silicate lattice. However, when MgO is considered only slight diffusion of Mg^{2+} ions would occur during the heat treatment time. The positions of these ions are possibly controlled by the limitations imposed by the crystallographic structure of dravite in relation to the microscopic mechanism by which the lattice breaks down.

The structure of the amorphous matrix in decomposed schorl is therefore probably close to that of an "iron silicate", whilst that in decomposed dravite is probably similar to silica with the Mg^{2+} ions filling the vacancies in the lattice (222).

The exact nature of the boron containing reaction surface is not known with certainty, but it probably has a structure close to one of the following proposed models:-

(1) The reaction surface could be basically homogeneous in nature containing borate, Na^+, Mg^{2+} or Fe^{2+} (not present in pyrex) ions bonded to an amorphous silicate lattice, forming a continuous but irregular network. This type of model is similar to that proposed by Zachariasen (132) for the structure of glass. The structure of this model would be the same as that drawn in Chapter 16.3 for the acid leaching of a non-phase separated amorphous system. The basic two dimensional structure of the amorphous phase in decomposed schorl would, on this model, be similar to that drawn below:-

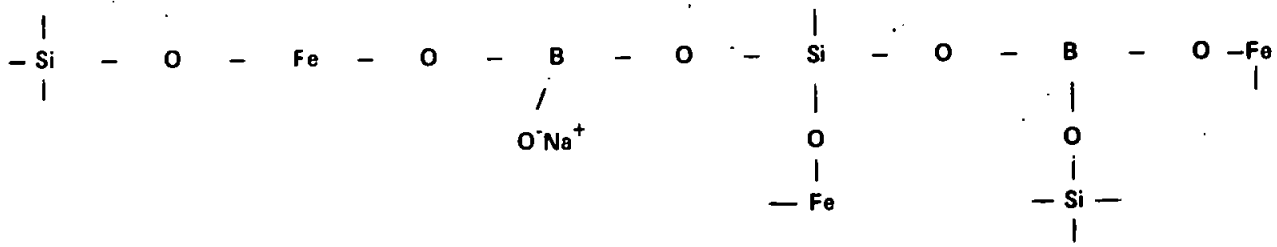

(2) The reaction surface could be built up of two phases, the main one being a silica-metal oxide amorphous matrix in which micro-regions of a "sodium borate" phase are embedded. A model of this type was proposed earlier in this thesis to account for the variability in the rate of acid extraction of boric oxide with schorl decomposition temperature, see Chapter 16.1.1.1.1. This type of structural model was first proposed by Lebedev (131) and expanded upon by later investigators, see Chapter 6. The structure of the boron rich phase separated regions has been discussed in some detail in Chapter 16.3. The proposed structure of this boron rich micro-phase in decomposed schorl is shown below:-

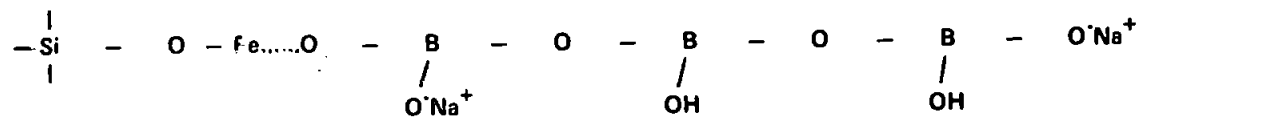

The removal of boric oxide from the amorphous phase in decomposed schorl would probably involve the same two elementary steps which-ever of the two structures is correct. These two steps are:-

(1) Diffusion of water vapour through amorphous phase to boron containing reaction surface.

(2) Heterogeneous surface reaction involving a (B—O) bond breaking step.

The (B—O) bond breaking step can be envisaged to proceed via the following elementary steps in the case of the removal of boric oxide from liquid boric oxide:-

(1) Initial formation of hydrogen bond between boric oxide and water molecules.

(2) Formation of four-centred transition complex.

(3) Bond breaking step proceeding via rearrangement of bonds in complex.

(4) Formation of products.

These elementary steps leading to the formation of gaseous metaboric acid (HBO_2) are shown schematically below:-

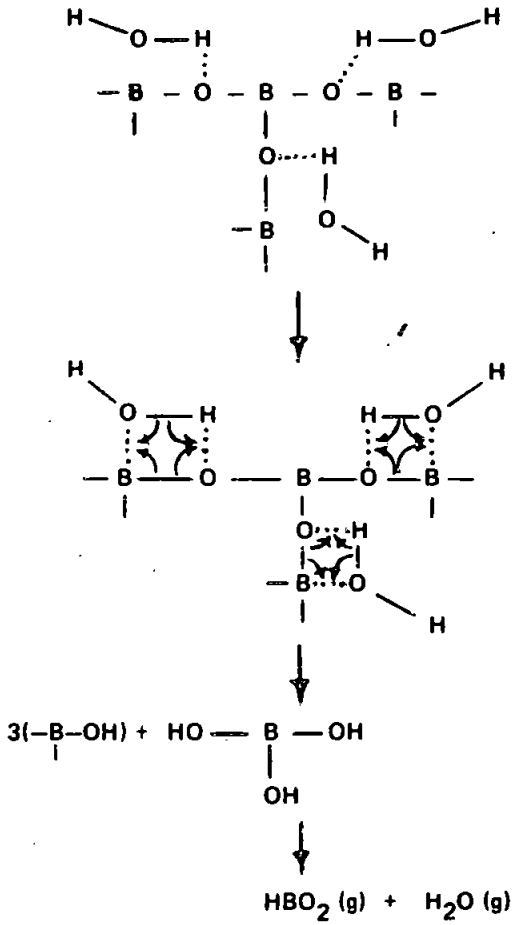

The activation energy for the removal of boric oxide from liquid boric oxide by pyrohydrolysis was found to be very small. However, the activation energies for the pyrohydrolysis of boric oxide from the borosilicate systems investigated are all greater than 20 kcal/mole. Therefore the main heterogeneous (B—O) bond breaking process that must occur at the reaction surface before boric oxide can be extracted from such systems does not appear to be the rate controlling step.

Thus even for a completely homogeneous boron containing lattice the basic bond breaking process will almost certainly be of the same type as that described for the extraction of boric oxide from liquid boric oxide. A structure for this type of lattice in decomposed schorl was proposed earlier in this section, when the Zachariasen (132) concept of the structure of glass was utilised. The extraction of boric oxide from this fully bonded boron containing surface can be envisaged to proceed as follows:-

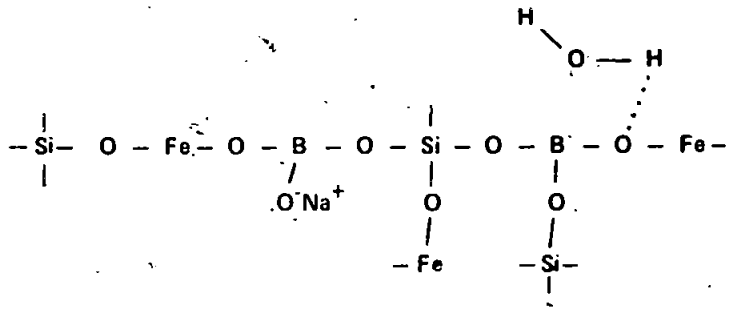

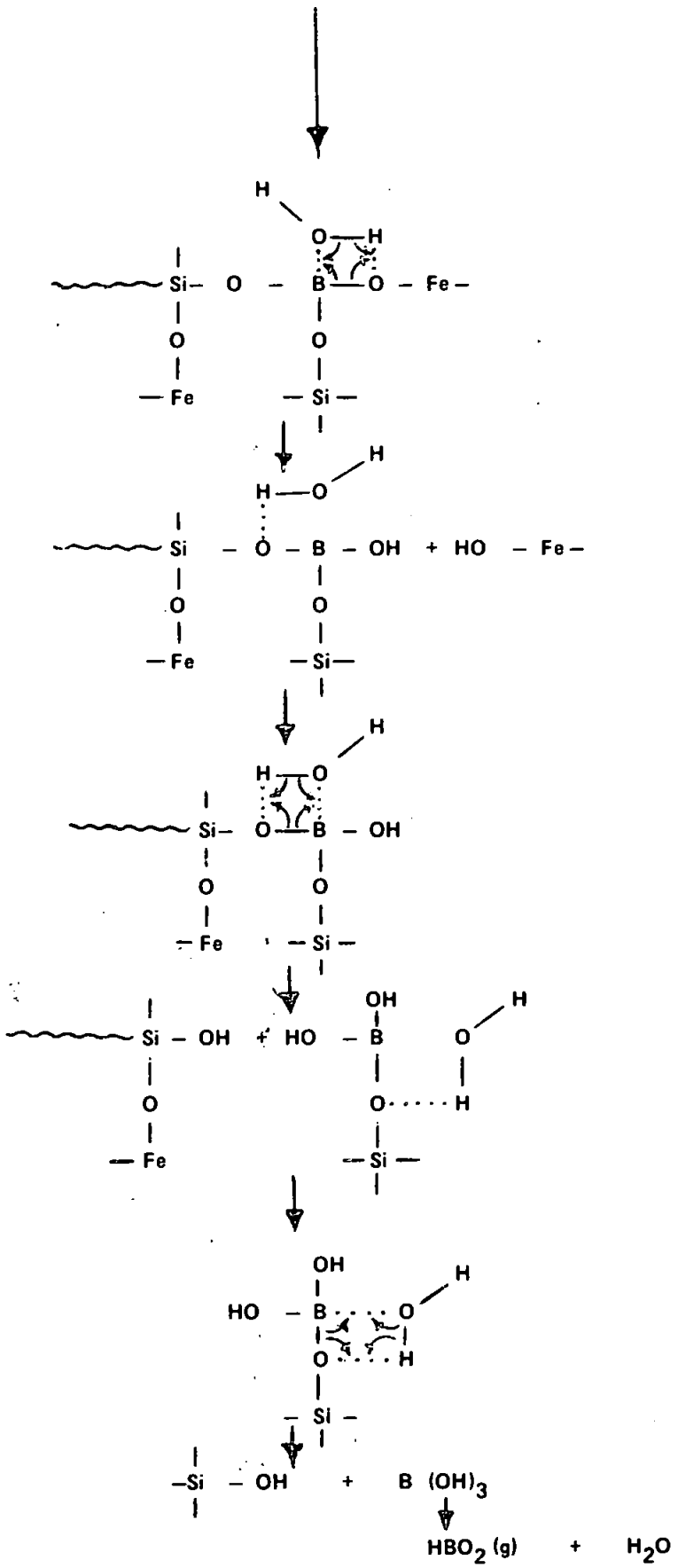
H
O — H
Si – O – B — O – Fe –
O
O
— Fe
— Si —
H — O
H
Si – O – B – OH + HO – Fe –
O
O
— Fe
— Si —
H
H — O
Si – O — B – OH
O
O
— Fe
— Si —
OH
H
Si – OH + HO – B
O
O · · · · · H
O
— Fe
— Si —
OH
H
HO – B · · · O
O · · · H
— Si —
–Si – OH + B (OH)3
HBO2 (g) + H2O

The extraction of boric oxide from this fully bonded borosilicate system therefore proceeds via the same type of bond breaking process as occurs in the extraction of boric oxide from liquid boric oxide. The activation energies found for extraction process from the borosilicate systems studied are considerably greater than for the extraction of boric oxide from liquid boric oxide. Therefore the rate controlling step for the pyro-hydrolysis of boric oxide from the borosilicate systems investigated is not the heterogeneous surface reaction, but most probably the diffusion of water vapour through the amorphous matrix to the boron containing surface.

The difference in the activation energy for the pyrohydrolysis of boric oxide from decomposed schorl, compared to that for the pyrohydrolysis of boric oxide from either decomposed dravite or "pyrex" glass, must therefore be due to the iron oxide in the amorphous phase affecting in some way the energy barrier of the diffusion process.

The relatively low Tamman temperature for iron oxide of 580°C indicated that extensive incorporation of Fe^{2+} ions into the amorphous silica lattice would probably occur during the preheat treatment of the schorl samples. This process would probably alter considerably the properties of the amorphous silica phase in decomposed schorl compared to that in decomposed dravite or "pyrex" glass. This change apparently manifests itself in the increase in the activation energy for the diffusion of water vapour through the amorphous lattice.

Most of the experimental evidence obtained in recent studies on the structure of complex glasses (135-138) and the more indirect results obtained by acid leaching of decomposed schorl, support the view that thermally treated borosilicate systems contain boron rich phase separated micro-regions. The extraction of boric oxide by pyrohydrolysis from such phase separated regions, having the same structure as the one proposed in Chapter 16.3, would probably proceed by a similar type of (B–O) bond breaking process as was described in the case of the extraction of boric oxide from liquid boric oxide:-

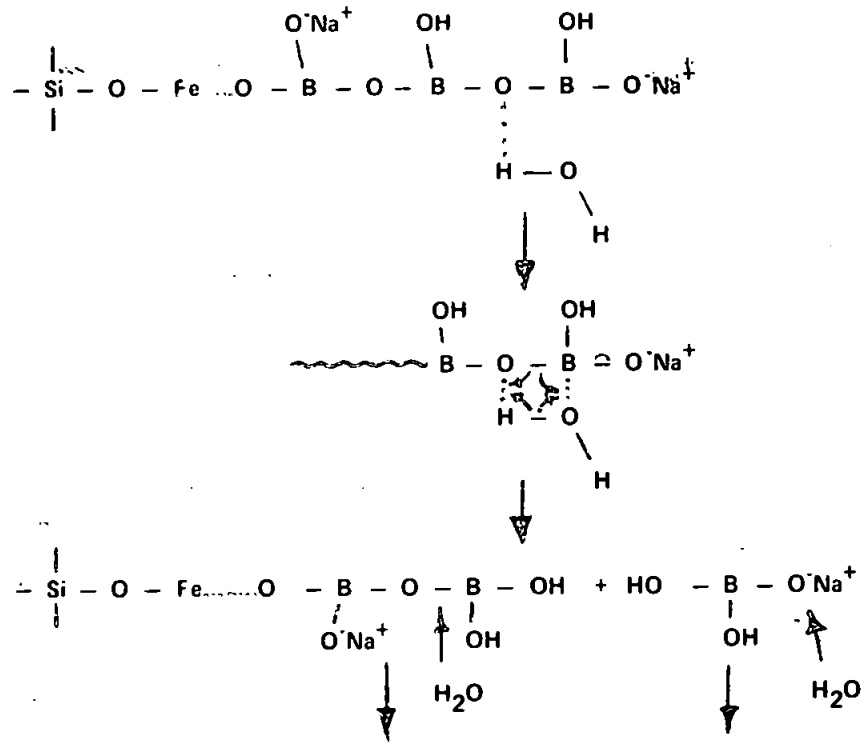

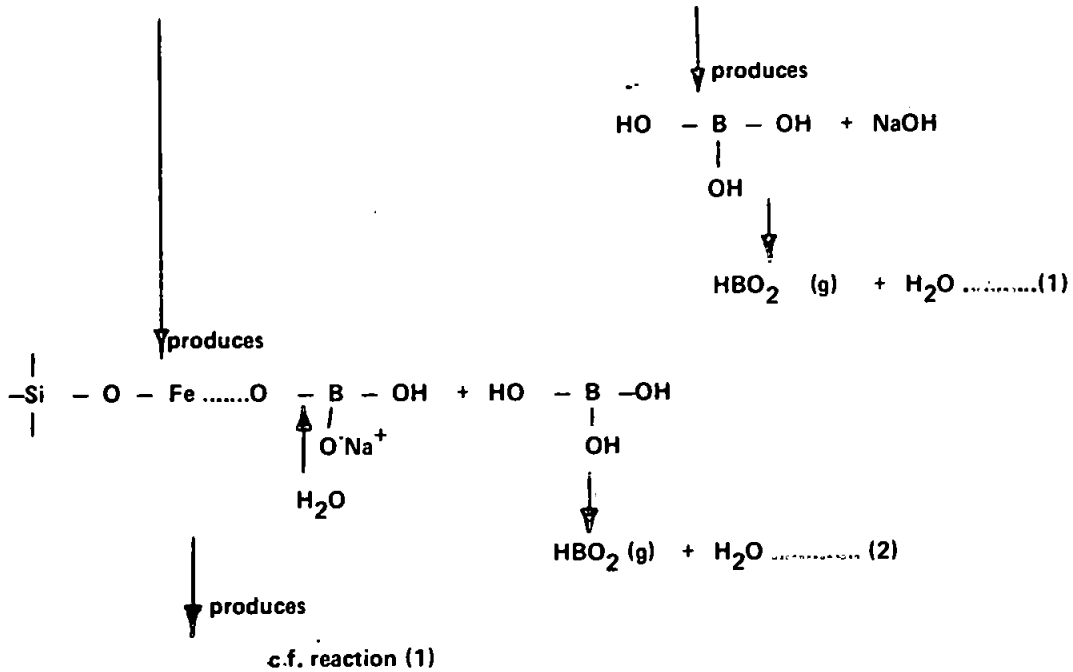

The process by which the extraction of boric oxide proceeds can therefore probably be broken into the following elementary steps:-

(1) Diffusion of water vapour to granules surface.

(2) Adsorption of water vapour on surface.

(3) Diffusion of water vapour through the silica-metal oxide amorphous matrix to the boron containing reaction surface.

(4) Heterogeneous surface reaction between water vapour and the boron rich reaction surface.

(5) Diffusion of metaboric acid (HBO_2) gas through amorphous matrix to surface.

(6) Desorption of metaboric acid.

(7) Diffusion of metaboric acid away from surface.

(8) Condensation of metaboric acid in the stream of water vapour leading to formation of dilute solution of orthoboric acid:- $H_2O + HBO_2 = H_3BO_3$.

(3.11) Calculation of General Rate Equation.

An approximate overall rate equation can be derived by combining the activation energy found for the extraction process with the pyrohydrolysis results listed in Table 49 using 17 lumps of (3/16 - 5) mesh "sintered" schorl. The rate equation calculated from the results obtained using (3/16 - 5) mesh granules and a pyrohydrolysis temperature of 1100°C was found to be equal to:-

$$(\% B_2O_3) = 0.53\, t^{0.5} \quad \ldots\ldots\ldots\ldots (1)$$

The generalised rate equation for granules of any size can be deduced as follows:-

The weight (W) of n spherical granules of radius (r) and density (d) equals:-

$$W = 4/3\, \pi r^3\, nd.$$

The total surface area (S_n) of n such granules is equal to:-

$$S_n = 4\pi r^2 n.$$

$$\therefore S_n = \frac{4 r^2 \pi 3W}{4\pi r^3 d}$$

$$\therefore S_n = \frac{3W}{rd}$$

The surface area per unit weight (S_o) is therefore equal to:-

$$S_o = \frac{3}{rd}$$

The mean radius of the (3/16 - 5) mesh schorl granules is equal to 0.203 cm.

The rate equation (1) can therefore be reduced to the rate of extraction of boric oxide from a surface of unit area by dividing by S_o as follows:-

$$(\% B_2O_3) \text{ /unit area} = \frac{0.53 t^{0.50}}{S_o}$$

$$= 0.53 \times 0.203 \frac{d}{3} t^{0.50} \quad \ldots\ldots\ldots\ldots\ldots (3)$$

Since the rate of extraction has been found to be proportional to the surface area of the schorl granules, see section 3.7, this equation (3) can be used to calculate the rate of extraction of boric oxide from schorl granules of any radius by multiplying by S_o:-

$$(\% B_2O_3) = 0.53 \times 0.203 \times \frac{d}{3} \cdot \frac{3}{rd} t^{0.50}$$

$$\therefore (\% B_2O_3) = \frac{0.11 t^{0.50}}{r}$$

This equation can be generalised to calculate the rate of extraction of boric oxide from schorl at any temperature by combining this equation with the activation energy for the pyrohydrolysis reaction as follows:-

$$(\% B_2O_3) = 0.11 t^{0.5} \exp [((85000 \pm 8000)/2)(1/1373 - 1/T)] /r$$

Where r is the mean radius of granules used.

T is the pyrohydrolysis temperature (degrees absolute).

The percentages of boric oxide extracted from schorl granules of various sizes at pyrohydrolysis temperatures of 1100 and 1200^{o}C are listed in Table 52.

Because of the temperatures and sample sizes used in the systematic pyrohydrolysis studies the maximum percentage to which the process could be followed was approximately 50 per cent, therefore no restriction was put on the percentage boric oxide extractable in the general rate equation given above. The maximum percentage of boric oxide easily extractable by acid leaching was found to be about 50 - 70 per cent, see Chapter 16. The subsequent fall off in the rate was thought to be due to the depletion of the boric oxide present in the amorphous phase. A similar fall off in the rate of extraction using the pyrohydrolysis technique will therefore almost certainly

occur once the boric oxide present in the amorphous phase is removed.

TABLE 52

Theoretical Calculation of Percentage of Boric Oxide Extracted as a Function of Particle Size, Time and Pyrohydrolysis Temperature.

Schorl granules		Temperature 1100°C Reaction time (mins).		Temperature 1200°C Reaction time (mins).	
Mesh Size.	Radius (cm).	1	10	0.1	1
		% B_2O_3	% B_2O_3	% B_2O_3	% B_2O_3
5	0.168	0.67	2.1	1.8	1.8
16	0.050	2.2	7.0	5.7	18
52	0.015	7.5	24	20	62
100	0.0075	15	47	40	125

The results listed in Table 52 are therefore probably only valid up to approximately 50 - 70 per cent boric oxide extracted. However, they do show that for the process to be reasonably efficient very small granules are required combined with a reaction temperature of at least 1100°C. In this temperature range sintering of the powder would occur especially if a large quantity was used. One technique that could possibly overcome this tendency is Fluidisation (223, 224). Assuming that it is possible to fluidise powdered schorl at temperatures close to 1100°C, this method, in conjunction with a recycling technique to increase the total reaction time would seem to be the most fruitful large scale approach to evolving an efficient extraction process.

CHAPTER 18

Suggestions for Further Work.

(1) Basic Chemistry.

The structure of the amorphous phase (s) present in decomposed tourmaline could be elucidated by the use of such techniques as low angle X-ray diffraction (225, 226), infra-red spectroscopy (133) and electron microscopy (134), although this would be extremely difficult in view of the complexity of the system. Sensitive Differential Thermal Analysis equipment may also be of use in detecting the minute variations in the structure of the amorphous phase, that were postulated to occur as the temperature at which the mineral was decomposed is raised.

The decomposition process could be investigated in greater detail by the use of a high temperature X-ray camera. Any changes in the cell dimensions of the mineral with thermal treatment could then be easily determined, and a detailed investigation into the decomposition process could also be undertaken.

A more accurate determination of the cell dimensions of the boron containing mullite microcrystals would be desirable. These parameters could then be compared with the accurate cell dimensions of boron containing mullites of know composition. The compositions of these microcrystals and the variation with decomposition temperature could then be determined precisely. If the accurate relative intensities of the reflections from these boron containing mullite microcrystals were compared with those obtained from mullite ($3Al_2O_3.2SiO_2$) itself, it may be possible using a Fourier summation (226) to determine the lattice positions occupied by the boron atoms.

Further acid and alkali extraction investigations would be useful in determining the rate of sodium and aluminium extraction by acid and silicon by alkali as none of these elements were studied in the present investigation. A study of the effect of the rate of cooling the thermally treated schorl on the rate of acid extraction of boric oxide and iron oxide may be useful in correlating the results obtained in the present investigation on the acid leaching of decomposed schorl with those obtained by Matsaberidze et. al. (25).

(2) Industrial Chemistry.

An investigation into the possibility of fluidising powdered tourmaline in an air-water vapour mixture in the temperature range above 1000°C would seem worthwhile. However, the probable temperature at which the rate of sintering begins to increase rapidly is approximately 1100°C, see Appendix 1. It would therefore seem unlikely that the powder could be fluidised unless each granule is coated by a thin layer of a porous high melting material such as alumina. This could be undertaken by washing the powder in a dilute aluminium chloride solution followed by a roasting at 1000°C. If this technique was successful a further investigation from a large scale industrial point of view may be useful.

REFERENCES

REFERENCES

(1) Vinogradov, A.P. Pedology (USSR) 1945, 348.

(2) Dana E.S. The System of Minerology, Chapman and Hall Ltd 7th Ed. 1957.

(3) Hanson, C. and Murthy, S.L.N. Chem. and Ind. 1969, 21, 677.

(4) Clarke, F.W. and Washington, H.S. Proc. Natl. Acad. Sci. 1922, 8, 108.

(5) Samsonov, G.V. Markovskii, L. Ya. Zhigach, A.F. and Valyashko, M.G.
Boron, it's Compounds and Alloys, Acad. Sci. Ukr. SSR. Kiev 1960 USAEC Translation 1961 No. 5032.

(6) Adams R.M. (Editor) Boron, Metallo-Boron Compounds and Boranes. Interscience, 1964.

(7) Schaller, W.G. US Geol. Sar. Bull. 1936, 871, 99.

(8) Gale, H.S. ibid. 1914, 580 - L.

(9) Whitney, J.D. Geology 1865, 1, 97.

(10) Foshag, W.F. Econ. Geol. 1921, 16, 199.

(11) Gale, H.S. Calif. J. Mines Geol. 1946, 42, 325.

(12) Mining Mag. Supplement, 1969, 121, No. 3.

(13) Mineral Trade Notes 1946, 58, 2.

(14) Wamsley, W.H. ibid. 1957, 43, 60.

(15) Hellmers, H.D. Pacific Chem. Met. Ind. 1938, 9, 2.

(16) Havighorst, C.R. Chem. Eng. 1963, 70, 228.

(17) Klopfenstein, R.K. J. of Metals, 1966, 18, 1193.

(18) Albright, H.M. Mining Contgr. J. 1956, 42, 55.

(19) Samsonov, G.V. c.f. ref. 5 p.29.

(20) Banateanu, Gh., Totoescu, D. et. al.(CA63: 7927g). Studii Cercetari Chem. 1965, 14, 379.

(21) Nagai,S.J. Japan Ceram. Assoc. 1944,52,87.(CA.45:7311f).

(22) Kamiko. M.J. J.Japan Cer. Assoc. 1944, 52, 131. (CA 45: 7323d).

(23) Karashima, Y. et. al. (CA46: 2671f). Japan Patent 173, 829, Oct. 9. 1946.

(24) Hatoga, T. Japan Pat. 174, 835, Feb.27, 1948.(CA.48:7200f).

(25) Matsaberidze, T.G., Voitsekhouskaya, N.F., Lominadze, D.L., Dolendzhishvili, Ts. G. Tr. Tbibis. Gos. Univ. 1968, 126, 149. (CA. 73: 47103h).

(26) Penfield, S.L. and Foote, H.W. Amer.J. Sci. 1899, 7, 97.

(27) Kunitz, W. Chemie der Erde 1929, 4, 208.

(28) Machatschki F. Zeit. Krist. 1929, 70, 211, and 1929 71, 45.

(29) Ward G.W. Amer. Min. 1931, 23, 607.

(30) Donnay, G. and Buerger, M.J. Acta. Cryst. 1950, 3, 379.

(31) Ito, T. and Sadanaga, R. Ibid. 1951, 4, 385.

(32) Deer, W.A. Howie, R.A. and Zussman. J. Rock Forming Minerals (Vol. 1) Longmans, 1962.

(33) Mason, B., Donnay, G. and Hardie, L. A. Sci. 1964 144, 71.

(34) Frondel, C., Biedl, A. and Ito, J. Amer. Min. 1966, 51, 1501.

(35) Power, G.M. Min. Mag. 1968, 36, 1078.

(36) Kulaszewski, C. Abhandl. Math-phys. kl. sachs. Akad. Wiss. Leipzig 1921, 38, MA 2 -15.

(37) Buerger, M.J. and Parrish, W. Amer. Min. 1937, 22, 1139.

(38) Epprecht, W. Schweiz. Min. Petr. Mitt. 1953, 33, 481.

(39) Hamburger, G. E. and Buerger, M.J. Amer. Min. 1948, 33, 532.

(40) Belov, N.V. and Belova, E.N. Doklady Acad. Sci. 1949, 69, 185 (CA: 45: 7475c).

(41) Belov, N.V. and Belova, E.N. Doklady Acad. Sci. 1950 75, 807 (CA:45:8944c).

(42) Ito, T. X-ray Studies on Polymorphism. Maruzen Co.Ltd. 1950 p.134.

(43) Handbook of Chemistry and Physics. The Chemical Rubber Co. 49th ed. 1968-69 p.B.334.

(44) Lowenstein, W. Amer. Min. 1956, 41, 349.

(45) Kurylenko, C. Mineral Sbornik, L'vov. Geol. Obshchestvo, L'vov. Gosudarst. Univ. im I Franko. 1957. 11, 19. Russ. Trans. Prog. 5019 yr.1969.

(46) Buerger, M.J., Burham, C.W. and Peacor D.R. Acta. Cryst, 1962, 15, 583.

(47) Donnay, G. and Barton, R. Abs. GSA Annual Meeting, San Francisco 1966.

(48) Barton, R. Acta. Cryst. 1969, 25B, 1524.

(49) Frondel, C., Hurlbut, C.S. and Collette, R.C. Amer. Min. 1947, 32, 480.

(50) Michel-Levy, M. Compt. Rend. Acad. Sci. Paris 1949 228, 1814.

(51) Michel-Levy, M. Bull. Soc. franc. Min-Christ, 1953 76, 237.

(52) Smith F.G. Econ. Geol. 1949, 44, 186.

(53) Frondel. C. and Collette, R.L. Amer. Min. 1957, 42, 754.

(54) Taylor, A.M. and Terrell, B.C. J. Cryst. Growth 1967, 1, 238.

(55) Quensel, P. and Gabrielson, O. Geo. For. Forh. Stockholm, 1939, 61, 63.

(56) Slivoko, M.M. The Study of Tourmalines, from certain localities in the USSR. Publ. L'vov. Univ. 1955.

(57) Bradley, J.E.S. and Bradley, O. Min. Mag. 1953, 30, 26.

(58) Wilkins, R.W.T., Ferrell, E.F. and Naiman, C.S. J. Phys. Chem. Solids 1969, 30, 43.

(59) Addison, W.E. and Sharp, J.H. Clays, Clay minerals 11th. conf. 1963, p.95.

(60) Manning, P.G. Can. Mineral, 1969, 10, 57.

(61) Machatschki, T. Zentr. Min. Geol. A 1941, 135.

(62) Kurylenko, C. Bull. Doc. franc. min. 1950, 73, 49.

(63) Kurylenko, C. Compt. rend. Acad. Sci. Paris 1951, 232, 2109.

(64) Kurylenko, C. Compt. rend. Acad. Sci. Paris 1953, 237, 735.

(65) Korzhinskii, A.F. Pretrog. Acad. Nauk. SSR. Inst.Khim. Silikatov. Leningrad 1958, 1956, 97(CA 54: 19322c).

(66) Tsu-Min Fuh. Sci. Rept. Taiwan Univ. 1st. ser. 1956, 11, 21, (CA 65: 10343g).

(67) Muetterties, E.L. The Chemistry of Boron and it's Compounds. John Wiley and Sons, 1967.

(68) Strong, S.L. and Taplow, R. Acta. Cryst. 1968, B24, 1032.

(69) Prewitt, C.T. and Shannon, R.D. Acta. Cryst. 1968, 1324, 869.

(70) Krogh-Moe, J.J. Non-Cryst. Solids, 1969, 1, 269.

(71) White, D., Mann, D. E. Walsh, P.N. and Sommer, A. J. Chem. Phys. 1960, 32, 481.

(72) Hanst, P.L. and Early, V.H. Phys. 1965, 42, 1097.

(73) Sommer, A., White, D., Linevsky, M.J. and Mann, D.E. J. Chem. Phys. 1963, 38, 87.

(74) Akishin, P. A., and Spiridonov, V.P. Dokl. Akad. Nauk. SSR 1960, 131, 557. Transl. Proc. Acad. Sci. USSR. 1960. 131. 255.

(75) Kracek, F. C., Morey, G.W. and Merwin, H.E. Am. J. Sci. 1938 35A. 143.

(76) Mackenzie, J.D. J. Phys. Chem. 1959, 63, 1875.

(77) Hildenbrand, D.L. Hall, W.F. and Potter, N.D. J. Chem. Phys. 1963. 39, 296.

(78) Green, T. and Margrave, J.L. J. Phys. Chem 1966, 70, 2112.

(79) Cousen, A. and Turner, W.E.S. J. Chem. Soc. 1928, 2654.

(80) Heinrich, E. W. Am. Min. 1946, 31, 71.

(81) Mackenzie J. D. J.Am. Ceram. Soc. 1961, 44, 79.

(82) Li, D.C. Ghose, A.C. and Su. G. J. ibid 1962, 45, 83.

(83) Li, D.C. Ghose, A.C. and Su. G. J. ibid 1962, 45, 89.

(84) Zachariasen, W.H. Z. Krist, 1934, 88, 150.

(85) Evans, W.H., Posen, E. J. and Wagman, D. D. "Thermochemistry and Thermodynamic Function of some boron compounds" in Thermodynamic and Transport properties of Gases, Liquids and Solids. Am.Soc. Mech. Engrs. McGraw-Hill New York, 1959, p.226.

(86) Blasdale W.C. and Slansky, C.M. J.Am.Chem. Soc. 1939 61, 917.

(87) Manov, G. G., Delollis, N.J. and Acree, S.F. J. Res. Natl. Bur. Std. 1944. 33. 287.

(88) Zachariasen, W.H. Acta. Cryst. 1954, 7, 305.

(89) ibid ibid 1952, 5, 68.

(90) ibid ibid 1963, 16, 380.

(91) Hendricks, S. B. J. Wash. Acad. Sci. 1944, 34, 241.

(92) Parsons, J.L. Silver, A.H. and Milberg, M.E. J. Chem. Phys. 1961, 34, 2192.

(93) Bleininger, A. V. and Teetor, P. Trans. Am. Ceram. Soc. 1912, 14, 210.

(94) Morey, G. W. and Ingerson, E. Am. Mineralogist 1937 22, 37

(95) Morey G. W. J. Soc. Glass, Technol. 1951, 35, 270.

(96) Englert, W.J. and Hummel, F.A. ibid 1955, 39, 121.

(97) Jenckel, E. Glastech Ber. 1938, 16, 191.

(98) Dimbleby, V., Hodkin, F. W. Parkin, M., and Turner, W.E.S. J.Soc. Glass Technol. 1923, 7, 57.

(99) Cousen, A. and Turner, W.E.S. J. Soc. Glass Technol. 1928, 12, 169.

(100) Rockett, T.J. and Foster, W.R. J. Am. Ceram. Soc. 1965, 48, 75.

(101) Zhdanov, S.P. Doklady Akad. Nauk. SSR. 1953, 92, 597.

(102) Aramaki, S. and Roy, R. J. Am. Ceram. Soc. 1959, 42, 644.

(103) Dietzel, A. and Scholze, H. Glastechn. Ber. 1955 28, 47.

(104) Gelsdorf, G. Mueller-Hesse, H. and Schwiete, H.E. Arch. Eisenhuttenwes 1958, 29, 513.

(105) Letort, Y. Intern. Ceram. Conf. Paris 1952, 19.

(106) Gielisse, P.J. and Foster, W. R. Ohio State Univ. Research Foundation, report 931-9. AD. 266889 1961.

(107) Baumann, H. N. and Moore, C.H. J. Amer. Ceram. Soc. 1942. 25, 391.

(108) Scholze , H. Z.anorg. allgem. chem. 1956, 284, 272.

(109) Gielisse, P.J. and Foster, W.R. Nature 1962, 195, 69.

(110) Schairer, J. F. and Yagi, K. Am.J. Sci. Bowen Vol. (pt 2) 1952, 471.

(111) Fischer, W.A. and Hoffmann. Arch. Eisenhuttenw, 1956, 27, 343.

(112) Block, S., Burley, G., Perloff, A. and Mason, R.D. J. Res. Natl. Bur. Std. 1959, 62, 95.

(113) Bernal, I., Struck, C.W. and White, J.G. Acta. Cryst. 1963, 16, 849.

(114) Nuan, A. Trans. Am. Inst. Mining Met. Engrs. 1955, 203, 965.

(115) Harrington, D.E. and Dorsett, R. S. A.E.C. Accession No. 12765 Report No. DP - 1004, 1965.

(116) Warf, J.C., Cline, W. D. and Tevebaugh, R.D. Anal Chem 1954, 26, 342.

(117) Powell, R. H. and Menis, O Anal Chem. 1958, 30, 1546.

(118) Susano, C.D., White, J.C. and Lee, J.E. Anal. Chem 1955, 27, 453.

(119) Myasnikov, Ye. G. and Bogachev, G.N. Tr. Ural Nauh-Issled Khim Inst. 1968, 17, 27.(CA 70: 81346n).

(120) Mikhailov, M.A. and Sklyadnev, Yu, N. Inu. Sib. Otd. Akad. Nauk. SSR. Khim. Nauk. 1968, 5, 40, (CA 70: 61553z).

(121) Williams, J.P. Campbell, E.E. and Magliscca, T.S. Anal, Chem. 1959, 31, 1560.

(122) Wiederkehr, V.R. and Goward, G.W. ibid 1959 31. 2102.

(123) Harman C.G. U.S. Patent 2,898, 192. Aug.4,1959.

(124) Mikhailov, M.A. USSR Patent 117, 373, Feb. 6, 1959. (CA 53: 18414e).

(125) Mikhailov, M.A. Vedernikova, T.I. Ozhigov, E.P. Izvest. Siber. Otdel. Akad. Nauk. USSR. 1961, 2, 68, (CA 55: 16314a).

(126) Stackelberg, M., Quatram, F. and Dressel, J. Z. Electrochem. 1937. 43, 14.

(127) Margrave, J.L. and Damron, T. J. Phys. Chem. 1956, 60,715.

(128) Randell, S.P. and Margrave, J.L. J. Inorg. Nucl. Chem. 1960, 16, 29.

(129) Margrave, J.L. Univ. of Wisconsin Rept. to Gallery Chem. Co. No.CCC - 1024 - TR - 231.

(130) Meschi, D.J., Chupka, W.A. and Berkowitz, J. J.Chem.Phys. 1960, 33, 530.

(131) Lebedev, A.A. Rev. D'Optique Theor-et instr.1926, 5, 4.

(132) Zachariasen W.H. J. Amer. Chem. Soc. 1932, 54, 3841.

(133) Acad. of Sci. USSR. The Structure of Glass.
Vol. 1. Proc. of second conf. Leningrad 1953.
Vol. 2. Proc. of third conf. Leningrad 1959.
Consultants Bureau, New York, and Chapman Hall Ltd., London.

(134) Skatulla, W., Vogel, W. and Wessel, H. Silikattechnik 1958, 9, 323.

(135) Makishima, A. and Sakaino, T. I. Amer Ceram Soc. 1970, 53,64.

(136) Haller, W., Blackburn, D.H., Wagstaff, F.E. and Charles, R.I. I. Amer Ceram Soc. 1970, 53, 34.

(137) Cordelier, I.F. Verres. Refract. 1970, 24, 113.

(138) Kiyohisa,E., Kenji, T. and Shuji,F.
Yogyo Kyokai Shi 1969, 77, 301,(CA.71:116043m).

(139) Gregg, S.J. The Surface Chemistry of Solids, Chapman and Hall Ltd. 2nd. Ed. 1961, p. 369.

(140) Nernst, W. Z. Phys. Chem. 1904, 47, 52.

(141) Karstein, O. Z. anorg. Chem. 1954, 276, 247.

(142) Kilpatrick, M. and Rushton, J.A. J. Phys. Chem. 1934, 38, 269.

(143) King, C.V. and Lia, C.L. J. Am. Chem. Soc. 1933, 55, 1928.

(144) Palmer, W.G. and Clark, R.E.D. Proc. Roy Soc. A. 1935, 34, 14.

(145) Moore, W.J. Physical Chemistry. Longmans 3rd. Ed. 1960, p. 581.

(146) Gregg, S.J. The Surface Chemistry of Solids. Chapman and Hall Ltd. 2nd. Ed. 1961, p. 363.

(147) Galwey, A.K. Chemistry of Solids. Chapman and Hall Ltd. 1967, p. 189.

(148) Roy, D.M. and Osborn, E.F. J.Am. Ceram. Soc. 1953, 36, 149.

(149) Greig, J.W. Am. J. Sci. 1927, 13, 133.

(150) Webb, W.W. Norton, J.T. and Wagner, C. J. Electrochem. Soc. 1956, 103, 108.

(151) Moore, W.J. and Lee, J.K. Trans. Fara. Soc. 1952, 48, 916.

(152) Beattie, L.R. J. Soc. Glass, Technol. 1952, 36, N.

(153) Morey, G.W. The Properties of Glass. 2nd. Ed. 1954, p. 101. Reinhold Publ. Corp. New York.

(154) Shand, E.B. Glass Engineering Handbook. McGraw Hill, London 1958.

(155) Holland, L. The Properties of Glass Surfaces. Chapman and Hall, London 1964.

(156) Charles, R.J. J. Appl. Phys. 1958, 11, 1549.

(157) Lyle, A.K. J. Amer. Ceram. Soc. 1943, 26, 206.

(158) Douglas, R.W. and Isard, J.O. J. Soc. Glass Technol. 1955, 204, 20.

(159) Kuehne, K. Z. Phys. Chem. 1955, 204, 20.

(160) Jones, F.L. and Homer, H.J. J. Opt. Soc. Amer. 1941, 31, 34.

(161) Berger, E. J. Soc. Glass Technol. 1936, 20, 257, T.

(162) Geffcken, W. and Berger, E. Glasstechn. Ber. 1955, 28, 299.

(163) Hubbard, D. and Hamilton, E.H. J. Res. Nat. Bur. Stan. 1941, 27, 143.

(164) Chilton, J.P. Principals of Metallic Corrosion. RIC. monograph No. 4. 1961.

(165) Kingery, W.D. Introduction to Ceramics. John Wiley and Sons. Inc. 1960, p. 162.

(166) Berthold, R. and Trost, A. Z. Scheizer Archiv. 1952, 9, 18.

(167) Brentano, J.C.M. Proc. Phys. Soc. 1925, 37, 184.

(168) Bunn, C.W. Chemical Crystallography. Oxford at Clarendon Press 2nd. Ed. 1963.

(169) Scherrer, P. Gottinger Nachrichten 1918, 2, 98.

(170) Alexander, L.E. and Klug, H.P. X-ray Diffraction Procedures. Wiley (New York) 1954 Chapt. 9.

(171) Warren, B.E. and Averbach, B.L. J. Appl. Phys. 1952, 23, 297.

(172) British Standards 3406 (Pt. 4); 3625, 1963.

(173) Roberts-Austen,J. Proc. Inst. Mech. Engrs. (Lon) 1899, 35.

(174) Burgess, G.K. Nat. Bur. Stan. Tech. News Bull. 1908-9, 5, 199.

(175) Grimshaw, R.W. Heaton, E. and Roberts, A.L. Trans. Ceram. Soc. 1949, 44, 76.

(176) Kodama, K. Methods of Quantitative Inorganic Analysis Interscience, 1963.

(177) Wilson, C.L. and Wilson, D.W. Comprehensive Analytical Chemistry (1^{c}) Elsevier, 1962.

(178) Furman, N.H. Standard Methods of Chemical Analysis (Vol. 1) D. Van Nostrand 1962.

(179) Charlot, G. Colourimetric Determination of Elements, Elsevier, 1964.

(180) Martin, J.R. and Hayes, J.R. Anal. Chem. 1952, 24, 182.

(181) Kramer, H. Anal. Chem. 1955, 27, 144.

(182) Wolszon, J.D. and Hayes, J.R. Anal. Chem. 1957, 29, 829.

(183) Schutz, E. Mitt. Gebiete Lebensm.u.Hyg. 1952, 44, 231.

(184) Samuelson, O. Ion Exchangein Analytical Chemistry, Wiley, New York. 1953, p. 169.

(185) Hazel, W.M. and Ogilvie, G.H. Anal. Chem. 1950, 22, 692.

(186) Fresenius, W. and Gander, G. Handuch der analytischem. Chemie Teil III, Quant. Analyse, 1942.

(187) Hollander, M. and Rieman, W. Ind. Eng. Chem. 1946, 18, 788.

(188) Ellis, G.H., Zook, E.G. and Baudisch, O. Anal. Chem. 1949, 21, 3145.

(189) Silverman, L. and Trego, K. Anal. Chem. 1953,25, 1246.

(190) Callicoat, D.L. and Wolszon, J.D. Anal. Chem. 1959, 31, 1434.

(191) Henly, W.B. Anal. Chem. 1951, 23, 1716.

(192) Carlson, R.M. and Pual, J.L. Anal. Chem. 1968, 40, 1292.

(193) Lewis, D.T. Analyst 1956, 81, 531.

(194) Shalgosky, H.I. Analyst 1957, 82, 648.

(195) Manning, D.C. Atomic Absorption Newsletter. 1966, 5, 127.

(196) Abresch, K. and Classen, I. Coulometric Analysis. Chapman and Hall Ltd. 1965, p. 192.

(197) Hollingshead, Oxime and it's Derivatives. Butterworths, London, 1954, Vol. 1. p. 180.

(198) Mehlig, J.P. and Hullett, H.R. Ind. Eng. Chem. Anal. Ed. 1942, 14, 869.

(199) Yoe, J.H. and Harvey, A.E. J. Am. Chem. Soc. 1948, 70, 648.

(200) Sen, D.C. J. Indian, Chem. Soc. 1948, 25, 473.

(201) Vogel, A.L. Quantitative Inorganic Analysis, Longmans 1962.

(202) Bragg, L. The Crystalline State (Vol. 1.) G.Bell and Sons Ltd. 1966, p. 196.

(203) Bragg, L. p. 191.

(204) Hartshorne, N.H. and Stuart, A. Crystals and the Polarising Microscope. Arnold, London, 3rd. Ed. 1960.

(205) Brown, G. X-ray Indentification and Crystal Structures of Clay minerals. Min. Soc. London 1961.

(206) Brindley, G.W. and Ali, S.Z.Acta. Cryst. 1950, 3, 25.

(207) Henry, N.F.M., Lipson, H. and Wooster, W.A. The Interpretation of X-ray Diffraction Photographs, Macmillan and Co. Ltd 2nd. Ed. 1960.

(208) Brindley, G.W. and Nakahira, M. Nature, 1958,818,133.

(209) Kingery, W.D. Introduction to Ceramics. J.Wiley and Sons, Inc. 1960.

(210) Vegard, L. Z. Phys. 1921, 5, 393.

(211) Pines, B. Ya. ZhETF. 1941, 11, 147.

(212) A.S.T.M. index (Inorganic) to the Powder Diffraction File 1963. Amer. Soc. for Testing and Materials.

(213) Krause, O. and Tiel, W. Ber. Deutsch. Keram. Ges. 1934, 104, 169.

(214) Helvesy, G. and Groh, J. Ann. d. Phys. 1920, 63, 85 and Ann. d. Phys. 1921, 65, 216.

(215) Borom, M.P. U.S. At. Energy Comm. UCRL - 16232, 1965.

(216) Von-Name, and Edgar. J.Amer. Chem. Soc. 1916, 38, 253.

(217) Moore, W.J. Physical Chemistry. Longmans 3rd. Ed. 1960, p. 515.

(218) Partington, J.R. An Advanced Treatise on Physical Chemistry. Vol.1, p. 864-:

(219) Denbigh, K. The Principals of Chemical Equilibrium, Cambridge University Press.

(220) Handbook of Chemistry and Physics. The Chemical Rubber Co. 49th. Ed. 1968 - 69.

(221) Tamman, G. Z. anorg. Chem. 1928, 176, 47.

(222) Kingery, W.D. Introduction to Ceramics, John Wiley and Sons. 1960, p.147.

(223) Kirk-Othner. Encyclopedia of Chemical Technology, Vol. 9. Interscience 2nd. Ed. 1965. p. 398 -

(224) Cremer, H. W. Chemical Engineering Practice (Vol. 6 pt. 11) Butterworths, 1958 p. 169 -

(225) Peiser, H. S. Rooksby, H.P. and Wilson, A. J. C. X-ray Diffraction of Polycrystalline Materials. Chapman and Hall Ltd. 1960 p. 232 -

(226) Brown, G. The X-ray Identification and Crystal Structures of Clay Minerals. Min. Soc.(London) 1961.

(227) Budnikov, P.P. and Ginstling, A.M. Principals of Solid State Chemistry, Translated by K. Shaw. Maclaren & Son Ltd. 1968, p. 58-

(228) Gregg, S. J. The Surface Chemistry of Solids. Chapman and Hall Ltd. 1961, p. 149 -

(229) Rouse P. Private communication

(230) Tazaki, H. J. Sci. Hiroshima Univ. 10A, 55, 1940 (CA 34:4318).

APPENDICES

Appendix 1.

Sintering.

The introductory discussion of sintering which follows has been mainly taken from books by Budnikov and Ginstling (227) and Gregg (228).

The adhesion of particles of a solid to form aggregates at elevated temperatures is known as sintering. The term is a broad one and difficult to define exactly, but it always involves a reduction in the specific surface of the solid and a shrinkage in the overall dimensions of the compact, brought about by heating to temperatures below the melting point of the solid. Surface energy considerations alone show that small particles of solid will always have some tendency to agglomerate into larger units.

The mechanism of sintering has been considered from two basic points of view. The first considers the process on a macroscopic scale by relating the rate of sintering to the viscosity or plasticity of the solid (227, 228). The second approach considers the process on a microscopic scale by relating the rate of sintering to the surface and volume diffusion of ions in the solid(227).

It has been found experimentally that the rate of sintering of many powdered metals, oxides and nitrides, etc (228) increases rapidly within a narrow range of temperatures close to 0.5 T_m (T_m ^oK is the melting point of the solid). This temperature is often known as the Tamman temperature (228). However, in the case of certain silicates this rapid increase in the rate of sintering does not occur until a temperature close to 0.9 T_m ^oK is reached (227).

Using high temperature Differential Thermal Analysis the melting point of schorl (8/1) has been found to be close to 1300 ± 50^oC (229). The rate of sintering of this silicate would therefore be expected to increase rapidly at temperatures close to 1140 ± 50^oC (0.9 T_m ^oK).